Distribution Agreement

In presenting this thesis or dissertation as a partial fulfillment of the requirements for an advanced degree from Emory University, I hereby grant to Emory University and its agents the non-exclusive license to archive, make accessible, and display my thesis or dissertation in whole or in part in all forms of media, now or hereafter known, including display on the world wide web. I understand that I may select some access restrictions as part of the online submission of this thesis or dissertation. I retain all ownership rights to the copyright of the thesis or dissertation. I also retain the right to use in future works (such as articles or books) all or part of this thesis or dissertation.

Signature:

_____ _____

Marta D'Elia Date

Assimilation of velocity data into fluid dynamic simulations,
an application to computational hemodynamics

by

Marta D'Elia
Doctor of Philosophy

Mathematics and Computer Science

Alessandro Veneziani, Ph.D.
Advisor

Michele Benzi, Ph.D.
Committee Member

James Nagy, Ph.D.
Committee Member

Accepted:

Lisa A. Tedesco, Ph.D.
Dean of the James T. Laney School of Graduate Studies

Date

Assimilation of velocity data into fluid dynamic simulations,
an application to computational hemodynamics

By

Marta D'Elia
M.S. in Mathematical Engineering, Politecnico di Milano, 2007
B.S. in Mathematical Engineering, Politecnico di Milano, 2005

Advisor: Alessandro Veneziani, Ph.D.

An abstract of
A dissertation submitted to the Faculty of the
James T. Laney School of Graduate Studies of Emory University
in partial fulfillment of the requirements for the degree of
Doctor of Philosophy
in Mathematics and Computer Science
2011

Abstract

Assimilation of velocity data into fluid dynamic simulations,
an application to computational hemodynamics
By Marta D'Elia

Cardiovascular applications recently fostered the development of numerical methods for fluid dynamics. Furthermore, thanks to new precise measurement devices and efficient image processing techniques, medicine is experiencing a tremendous increment of available data, inevitably affected by noise. Beyond validation, these data can be combined with numerical simulations in order to develop mathematical tools, known as data assimilation (DA) methods, of clinical impact. In the context of hemodynamics, accuracy and reliability of assimilated solutions are particularly crucial in view of possible applications in the clinical practice. Hence, it is fundamental to quantify the uncertainty of numerical results.

In this thesis, we propose a robust DA technique for the inclusion of noisy velocity measures, collected from magnetic resonance imaging, into the simulation of hemodynamics equations, namely the incompressible Navier-Stokes equations (NSE). The technique is formulated as a control problem where a weighted misfit between velocity and data is minimized under the constraint of the NSE; the optimization problem is solved with a discretize then optimize approach relying on the finite element method. The control variable is the normal stress on the inflow section of the vessel, which is usually unknown in real applications. We design deterministic and statistical estimators (the latter based on a Bayesian approach to inverse problems) for the estimation of the blood velocity and its statistical properties and of related variables of medical relevance, such as the wall shear stress. We also derive conditions on data location that guarantee the existence of an optimal solution.

Numerical simulations on 2-dimensional and axisymmetric 3-dimensional geometries show the consistency and accuracy of the method with synthetic noise-free and noisy data. Simulations on 2-dimensional geometries approximating blood vessels demonstrate the applicability of the approach for hemodynamics applications.

Assimilation of velocity data into fluid dynamic simulations, an application to computational hemodynamics

By

Marta D'Elia
M.S. in Mathematical Engineering, Politecnico di Milano, 2007
B.S. in Mathematical Engineering, Politecnico di Milano, 2005

Advisor: Alessandro Veneziani, Ph.D.

A dissertation submitted to the Faculty of the
James T. Laney School of Graduate Studies of Emory University
in partial fulfillment of the requirements for the degree of
Doctor of Philosophy
in Mathematics and Computer Science
2011

Acknowledgements

I begin by thanking my advisor, Alessandro Veneziani, aka *the boss*. Thank you because actually you were not a boss; because you shared with me your love for applied mathematics; because sometimes we did not agree; because you challenged me, studied and learned with me. Grazie perché ci hai insegnato che non è importante giocare in panchina con la Juventus ma in campo con l'Atalanta e che non c'è gusto a vincere facile.

Thank you to my committee members, Michele Benzi and Jim Nagy, not only because you took time to read my thesis and provide me with advice and suggestions; thank you for being a guide during these four years. Your doors were always open for me anytime I was looking for scientific (and non-scientific) answers.

Thank you to Eldad Haber, I have learned so much from you. You showed me that the world does not have to be discretized by finite elements and you passed on your passion for scientific computing, optimization and inverse problems. Thank you to Max Gunzburger because you got interested in my work as soon as we met and you kept on advising me whenever I needed suggestions and alternative points of view. Your brilliant and challenging ideas inspired me during this work.

Special thanks to Tiziano and Umberto, because life(V) would not have been so easy without you. To Marina, BB, aka LucaB, and GG, aka LucaG, because life(V?) is not easy at all, but you made it fun. To N404 inhabitants and ex-inhabitants, best office mates ever. To Valen and don Pie because it was like having you here; inevitabilmente, immancabilmente ed instancabilmente presenti. To Gio and Marci because you always knew that I could have made it, even when I did not believe so; this work is dedicated to you.

And thank you, Mauro, because all this could not have been possible without you ♡

to Gio and Marci

Contents

List of Figures

List of Tables

Glossary

BE Backward Euler. 31, 110, 115, 133

BS Boundary sites. 58, 61, 64, 67

DA Data assimilation. 2–4, 13, 14, 16, 17, 19, 28, 30, 42, 43, 54, 61, 63–65, 70, 71, 77, 105, 108, 120, 123, 131, 132

DO Discretize then optimize. 30, 32–34, 41, 44, 47, 110, 111, 120, 132

DOF Degree of freedom. 25, 26, 45, 46, 49–53, 57, 62, 66, 81, 88–91, 95, 97, 99, 103–105, 110

DP Discrepancy principle. 45, 52, 54, 63, 115, 116

DR Dynamic relaxation. 27, 30–33

FE Finite element. 22, 44, 45, 49, 50, 54–57, 61, 63, 65, 66, 69, 70, 92, 93, 101, 110, 115, 120, 131

GCV Generalized cross validation. 115, 116

GMRES Generalized minimal residual. 36, 54, 56, 59, 62, 92, 94, 119

IC Incomplete Cholesky. 118–120

IS Internal sites. 58, 59, 61, 67, 93

MAP Maximum a posteriori. 14, 17, 78, 85–87, 91, 123

ML Maximum likelihood. 17, 78, 85, 86, 91, 93, 101, 102, 123, 124

MU Matrix updating. 30–32

NSE Navier-Stokes equations. 14, 16, 17, 19, 41, 42, 51, 65, 78, 81, 84, 87, 91, 96, 108, 129

OD Optimize then discretize. 30, 32, 33, 133

PCD Pressure convection diffusion. 55, 92, 131

PCG Preconditioned conjugate gradient. 119, 120

PDE Partial differential equation. 8, 11, 13, 14, 34, 49, 63, 87, 92, 113, 132

PDF Probability density function. 17, 77–79, 81–83, 86, 87, 90

SNR Signal to noise ratio. 29–31, 34, 36, 37, 57, 58, 62, 65, 67, 69–74, 93–100, 104, 115, 124, 126, 130

WSS Wall shear stress. 66, 70–73, 78, 91, 100, 102–105, 130

1 Introduction

Reliability of numerical methods and simulations is becoming a crucial issue as scientific computing has an increasing role in different fields of engineering, science and, more generally, society. The quality of numerical results needs to be certified not only for the mathematical investigation of the different methods, but also for assessing its impact in practice (see [1, 2]). As a matter of fact, scientific computing is extensively used beyond traditional engineering studies (civil, aerospace, automotive), in geophysics, sport, finance, medicine. A careful analysis of the impact of errors and uncertainties is therefore not only needed for a theoretical understanding (and ranking) of the methods but also for the reliability of numerical simulations as a tool for supporting, for instance, the decision making of a medical doctor.

More specifically, in the last 20 years numerical methods for incompressible fluid dynamics have been fostered by applications to the cardiovascular system (see e.g. [3, 4, 5]). Mathematical and numerical models have been progressively used as a tool for supporting medical research in the cardiovascular science. In this particular field, whose social relevance is testified by the impact of cardiovascular diseases in the industrialized Countries[1], numerical simulations are increasingly considered as a valuable tool for investigating physio-pathological dynamics or even designing therapies [3, 4, 6, 7, 8, 9]. *In silico* experiments can provide remarkable insights into a physio-pathological process completing more traditional *in vitro* and *in vivo* investigations. Numerical models have been playing the role of “individual based" simulators, able to

[1] According to the statistics reported by the Center for Disease Control `www.cdc.gov/nchs/data/nvsr/nvsr55/nvsr55_19.pdf`.

give a dynamical representation of the biology of a specific patient as a support to the prognostic activity.

At the same time, the need for quantitative responses for diagnostic purposes has strongly stimulated the design of new methods and instruments for measurements and imaging. On the one hand, we can simulate large 3-dimensional portions of the cardiovascular system of a real patient properly including simplified models for the peripheral sites (see e.g. [3, 5, 6, 7, 8]). On the other, images and measures nowadays provide doctors and bioengineers with a huge amount of data. As an example, Figure 1.1 shows an MRI [10] of the ascending aorta where blood velocity measurements have been collected. Obviously these data offer new possible benchmarks for the numerical simulations (see e.g. [11]). However, beyond the validation, it is possible to merge simulations and measures by means of more sophisticated numerical techniques. A strong integration of data and numerical modeling is expected to bring a great benefit to the development of mathematical and computational tools with a clinical impact. This procedure is called *data assimilation* (DA) (see e.g. [12]). With this name we mean the ensemble of methods for merging observed (generally sparse and noisy) information into a numerical model based on the approximation of physical and constitutive laws. In other words, the goal of DA is to merge together heterogeneous (in nature, quality, and density) sources of information in order to retrieve a consistent state for phenomena of interest. In particular, in hemodynamics, numerical simulations are improved by the merging of data that allow to include effects otherwise difficult to model (at the qualitative or quantitative level), such as the presence of tissues surrounding an artery or the motion of the heart affecting the aortic dynamics. Also, since measures are in general affected by noise, the assimilation based on physical and constitutive laws introduces a sophisticated filter, forcing the consistency with basic principles. Even though the term DA has often been used for time dependent phenomena, in this thesis (as done in [11]) we consider also stationary phenomena and we refer to DA also as a

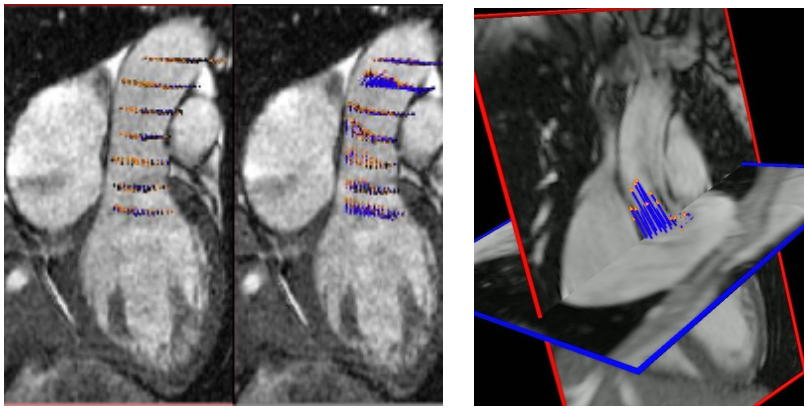

Figure 1.1: View of blood measured velocities in MRIs of the ascending aorta.

technique for the inclusion of data which are sparse in space and collected at the same instant of time. In the next sections we present a brief history of DA for fluid geophysics applications (oceanography and meteorology) mainly based on the excellent review by Blum et al. in [12] and we summarize the state of the art of DA in hemodynamics applications.

1.1 Methods for DA in fluid geophysics

The mathematical modeling of geophysical flows has experienced a tremendous development during the last decades, mainly due to the growth of the available computing resources and to the improvement of networks of observations. Therefore, it is clear that modeling and simulating have to take into account observations; these are irregularly distributed in space and time, and they have different structures of random error. Errors arise from various sources such as instrumental noise, environmental noise, sampling, and interpretation of sensor measurements; according to the context, a different confidence will be attributed to the measurements. For instance, all oceanic dynamical models are imperfect, with errors due to the approximate physics (or biology or chemistry) that governs the explicit evolution of the state variables and that parame-

terizes the interaction of the state variables and the discretization of dynamics into a numerical model [13].

Originally, the problem of DA was to determine the initial condition of a dynamical system from observations. Since the same mathematical tools may be used, DA also includes the estimation of model parameters, boundary conditions or the state itself. The development of DA methodology has mainly experienced three stages: objective analysis, statistical interpolation, stochastic methods and variational analysis. Simple analysis methods were mostly used in the 50's, when computers were unavailable or at the beginning stage; these techniques were the earliest bases of DA. In the 60's and 70's, statistical considerations were introduced into the atmospheric DA. Based on these considerations, some forms of optimal interpolation were used to assimilate observations into forecast models. In the same decades the Kalman filter was introduced and efficiently improved (EKF, EnKF, UKF). In the 80's and 90's, atmospheric DA switched to variational methods.

1.1.1 Objective analysis and optimal interpolation

Objective analysis, or interpolation, was introduced, in the context of meteorology, by Panofsky [14] in 1949; the 50's featured the advent of computers and the evolution of numerical analysis. This method interpolates the measurements from the points of observation toward the grid points. Specifically, it is based on a technique of 2-dimensional least squares fitting; it consists in expanding the state variables in a series of polynomials about the observation point, minimizing the square of their difference with the observed values. This procedure was perfected by the idea of Bergthórsson and Döös [15] in 1955, who claimed that it is not possible to get a reasonable estimate only by interpolation of observations; thus, they included a mathematical model in the assimilation process. The method is based on the assumption that some observations are available prior to the assimilation instant (12 hours in advance); then, the estimate

is a weighted mean of the current observations and the state forecast, i.e. the state field obtained by advancing in time from the previous observations via a mathematical (numerical) model. Even though the method is simple to implement, the retrieved fields will not be necessarily consistent from the physical viewpoint. Despite this, these methods were the most commonly used in operational meteorology until the last decade.

Optimal interpolation, also referred to as statistical interpolation in meteorology, can be seen as a simplification of the Kalman Filter (even though it was introduced before it), described in the next section. The assimilated solution is a linear combination of the deterministic solution with the misfit between data and predicted state; as opposed to Kalman approaches, the matrix weighting the misfits is empirically assigned (see [16] for further details).

1.1.2 Kalman filter and its extensions

The Kalman filter[1] (KF) was developed by Kalman in 1960 [17] as a new approach to linear filtering and prediction problems. It is a recursive filter for the estimation of the state of a dynamic system from incomplete and noisy measurements. Because of its limitations in terms of models (designed for linear systems) and memory requirements for the storage of structures involved, several modifications and improvements have been developed, such as the Extended KF (EKF), the Ensemble KF (EnKF) and the Unscented KF (UKF). We report briefly the formulation of the basic KF and we touch on few details of its extensions.

The KF is a scheme designed for linear dynamic systems and it is based on Bayesian estimation; it generates the sequential, unbiased, *minimum error variance* estimate based on a linear combination of all past measurements and dynamics. Following the formulation reported in [12], we summarize the procedure in four simple steps.

[1]Here, with filter we mean a process that removes from a signal some unwanted components, e.g. the noise, as in our case.

Consider a linear model representing the observation process:

$$y_k = H_k u_k + \varepsilon_k; \tag{1.1}$$

here, k is a multiple of the number of time steps between consecutive observations, u_k is the vector of state variables, y_k is the vector of the measures and ε_k is an additive random noise representing the error; this is assumed to be white with zero mean and correlation matrix R_k. For each time step we consider a discretized stochastic dynamic system

$$u_k = M_{k-1} u_{k-1} + \eta_{k-1} \tag{1.2}$$

where M_k describes the model dynamics and η_k is the random error associated with model parameters. We assume that η_k is distributed as ε_k, with correlation matrix Q_k.

$$\begin{aligned} \textit{Algorithm} \quad & \textbf{1}.\ \text{advance in time:} \begin{cases} u_k^f = M_{k-1} u_{k-1}^a \\ P_k^f = M_{k-1} P_{k-1}^a M_{k-1}^{\mathrm{T}} + Q_{k-1} \end{cases} \\ & \textbf{2}.\ \text{compute the Kalman gain: } K_k = P_k^f H_k^{\mathrm{T}} (H_k P_k^f H_k^{\mathrm{T}} + R_k)^{-1} \\ & \textbf{3}.\ \text{state update: } u_k^a = u_k^f + K_k (y_k - H_k u_k^f) \\ & \textbf{4}.\ \text{error correlation matrix update: } P_k^a = (I - K_k H_k) P_k^f \end{aligned} \tag{1.3}$$

Here, $P_k^f = E\{(u_k - u_k^f)(u_k - u_k^f)^{\mathrm{T}}\}$ and $P_k^a = E\{(u_k - u_k^a)(u_k - u_k^a)^{\mathrm{T}}\}$; the superscripts f and a stand for *forecast* and *assimilated* respectively and E refers to the mean value for random variables.

This filter is limited to linear models, but in general many problems in fluid geophysics, including parameter identification, are nonlinear. This limitation explains the introduction of the EKF for nonlinear processes. In this case, equations (1.1) and (1.2) are to be substituted with

$$\begin{aligned} y_k &= h(u_k, \varepsilon_k); \\ u_k &= f(u_{k-1}, \eta_k). \end{aligned} \tag{1.4}$$

The KF, designed for linear problems, cannot be directly applied to equations (1.4). The idea of the EKF is to consider, at each iteration, the linearization of (1.4) around the previous state. In this way, matrices H_k and M_k in algorithm (1.3) are substituted with the Jacobian of h and f respectively, evaluated at u_{k-1}. This estimator is not optimal, might underestimate the covariance matrices and has high memory requirements.

The extension to the EnKF avoids the latter using probability distributions represented by samples, i.e. covariance matrices are replaced by sample covariance matrices.

When the state transition and observation models (f and h) are highly nonlinear the EKF might give poor performance [18]. This is because the covariance is propagated through linearization of the nonlinear model. The UKF represents a derivative-free alternative to the EKF and provides better performance at an equivalent computational complexity. In fact, in the UKF the state distribution is still Gaussian but it is specified using a minimal set of "carefully chosen" sample points or snapshots which completely capture the state mean and covariance. Furthermore, these points, when propagated through the nonlinear system, capture the mean and covariance at the subsequent step to the second order. Such sample points are chosen via *Unscented transform* of the state at the current time step [19].

1.1.3 Nudging method

The nudging, or *dynamic relaxation*, method was introduced in 1977 by Davies and Turner in [20] and it can be classified as a combination of Kalman filtering and a variational approach.

According to [21], we can summarize the procedure in two simple steps. Given some data at time $t = t_0$, **1)** specify an arbitrary but consistent initial condition at time $t = t_0 - T$ (where T is the so called *pre-forecast* period); **2)** solve the governing equations during the pre-forecast, $[t_0 - T, t_0]$, including a forcing term proportional to

the difference between the predicted state at time t_0 and the observation so to *dynamically relax* the solution towards the observations. If we assume to have a mathematical model, discretized in space (using e.g. finite differences, volumes or elements), the time dependent problem reads:

$$\begin{aligned} &\frac{d\mathbf{U}}{dt} = F(\mathbf{U}) \qquad t \in (t_0 - T, t_0]; \\ &\mathbf{U}(t_0 - T) = \mathbf{U}_0. \end{aligned} \tag{1.5}$$

Here, $\mathbf{U}$ is the discretized state variable, and $\mathbf{U}_0$ the initial condition. If $\widetilde{\mathbf{U}}$ is a given measure and $\overline{\mathbf{U}}$ is a projection of the observation onto the discretization space, the assimilation consists in the solution of the following initial value problem.

$$\begin{aligned} &\frac{d\mathbf{U}}{dt} = F(\mathbf{U}) + c\,(\overline{\mathbf{U}} - \mathbf{U}) \quad t \in (t_0 - T, t_0]; \\ &\mathbf{U}(t_0 - T) = \mathbf{U}_0. \end{aligned} \tag{1.6}$$

The relaxation coefficient c has to be chosen so to achieve an optimal compromise between model and observations; its choice might be based on statistical considerations. If c is too large, the non-physical forcing term will dominate and the predicted state would completely fit the noisy measures, amplifying the observational errors and compromising the consistency of the solution. When c is too small, the observation will not significantly affect the estimate. In 1992, Zou, Navon and Le Dimet developed a parameter estimation approach in order to obtain an optimal nudging coefficient [22].

1.1.4 Variational approaches

Control approaches consider the minimization of the misfit between the predicted state and the observations under the constraint of the partial differential equations (PDEs) governing the variables. Such optimization (or control) problem may be solved with a large variety of numerical methods for PDE constrained optimization problems. In the

context of fluid dynamics there is a huge literature for the solution of inverse problems, among many others we mention [23, 24, 25, 26, 27, 28, 29].

In general, the main components in the formulation of a variational problem are a state variable u, a deterministic model, a control variable h, a set of observations and a cost function $\mathcal{J}(u, h; t)$. The model describing the evolution of the variables involved in the process is, in general, a system of nonlinear differential equations

$$\begin{cases} \mathcal{A}(u, h; t) = 0, \\ u(t_0) = u_0. \end{cases} \tag{1.7}$$

Here, $\mathcal{A}$ is a differential operator and u_0 is the initial condition. Most of the time the control variable h is the initial condition (e.g. in meteorology), but it might also consist in model parameters or boundary conditions. In general, we assume that for a fixed value of h the model is well-posed. Additional constraints on the control variable are mandatory in relation to the physical quantities described. The measures, say $\widetilde{\mathbf{U}}$, are considered discrete in space and time and they do not belong to the same space of the state variable. The cost function $\mathcal{J}$ measures the discrepancy between the state variable and the measurements

$$\mathcal{J}(u, h; t) = \int_0^T dist(u;\, \widetilde{\mathbf{U}})\, dt + \mathcal{R}(h; t). \tag{1.8}$$

The function $dist$ will be specified later and it might include information on stochastic properties of the field. The additional term $\mathcal{R}$ is usually introduced with regularization purposes to prevent potential ill-posedness of the formulation and/or to impose smoothness of the control variable; in fact, when the objective functions do not depend explicitly on the control variable, the solution of the problem could lead to unbounded control variables [23]. Optimization methods can be grouped in two main categories: the *optimize then discretize* (OD) and the *discretize then optimize* (DO) approach.

The OD approach We introduce the functional

$$\mathcal{J}(u,h;t) = \int_0^T \|u(h) - \tilde{u}\|\, dt + \mathcal{R}(h;t). \tag{1.9}$$

where $\tilde{u}$ is a projection of $\widetilde{\mathbf{U}}$ into the state functional space $\mathcal{H}$. In order to solve the optimization problem we introduce the *Lagrangian* function $\mathcal{L}$

$$\mathcal{L}(u,h,\lambda) = \mathcal{J}(u,h;t) - \lambda^* \mathcal{A}(u,h;t). \tag{1.10}$$

Here * represents the inner product in $\mathcal{H}$ and λ is the Lagrange multiplier. The optimality is reached when we find u, h and λ such that $\mathcal{L}$ is stationary, i.e. when they solve the system of first order necessary conditions [23]:

$$\begin{cases} \dfrac{\partial \mathcal{L}}{\partial \lambda} = \mathcal{A}(u,h;t) = 0 & \textit{state equation}, \\ \dfrac{\partial \mathcal{L}}{\partial u} = \left(\dfrac{\partial \mathcal{A}}{\partial u}\right)^* \lambda - \left(\dfrac{\partial \mathcal{J}}{\partial u}\right)^* = 0 & \textit{adjoint equation}, \\ \dfrac{\partial \mathcal{L}}{\partial h} = \left(\dfrac{\partial \mathcal{A}}{\partial h}\right)^* \lambda = \left(\dfrac{\partial \mathcal{J}}{\partial h}\right)^* = 0 & \textit{optimality condition}; \end{cases} \tag{1.11}$$

where we make the assumption that each argument is independent from the other. This last system is typically huge and difficult to be numerically solved monolithically (the so called "one-shot" approach); iterative procedures are usually preferred [23, 30]. In this case, given a guess for the control variable, state and adjoint are sequentially solved and used in the optimality equation to update the control variable; this is to be done until some criterion for the convergence is satisfied.

The DO approach In this case we first discretize the functional and the state equations, getting

$$\begin{cases} J(\mathbf{U},\, \mathbf{H}) = \|Q(\mathbf{U}) - \widetilde{\mathbf{U}}\| + R(\mathbf{H}); \\ \\ A(\mathbf{U},\, \mathbf{H}) = 0. \end{cases} \tag{1.12}$$

Here, $\mathbf{U}$ and $\mathbf{H}$ are the discretized state and control variables, Q is the operator that maps the discretized state into the data space, R is a discrete regularizing operator and A is the discretized differential operator. To solve this algebraic optimization problem we introduce the discrete Lagrangian function

$$L(\mathbf{U},\, \mathbf{H},\, \mathbf{\Lambda}) = J(\mathbf{U},\, \mathbf{H}) - \mathbf{\Lambda}^{\mathrm{T}} A(\mathbf{U},\, \mathbf{H}), \tag{1.13}$$

where $\mathbf{\Lambda}$ is the Lagrange multiplier. Optimality is reached when we find $\mathbf{U}$, $\mathbf{H}$ and $\mathbf{\Lambda}$ such that

$$\begin{cases} \dfrac{\partial L}{\partial \mathbf{\Lambda}} = A(\mathbf{U},\, \mathbf{H}) = 0 & \textit{state equation}, \\ \\ \dfrac{\partial L}{\partial \mathbf{U}} = \left(\dfrac{\partial A}{\partial \mathbf{U}}\right)^{\mathrm{T}} \mathbf{\Lambda} - \left(\dfrac{\partial J}{\partial \mathbf{U}}\right)^{\mathrm{T}} = 0 & \textit{adjoint equation}, \\ \\ \dfrac{\partial L}{\partial \mathbf{H}} = \left(\dfrac{\partial A}{\partial \mathbf{H}}\right)^{\mathrm{T}} \mathbf{\Lambda} - \left(\dfrac{\partial J}{\partial \mathbf{H}}\right)^{\mathrm{T}} = 0 & \textit{optimality condition}. \end{cases} \tag{1.14}$$

As for system (1.11), there are plenty of methods for the solution of (1.14), see e.g. [23, 30]. Note that, the DO approach allows to obtain the optimality system in a more straightforward way than working with unknowns belonging to infinite-dimensional functional spaces (for an extensive discussion see [23]). The following example describes how to apply both schemes to a simple PDE.

Application to a simple differential problem We consider the following steady state equation:

$$\begin{cases} -\mu u'' = hf & \text{in } \Omega \\ u = 0 & \text{on } \partial\Omega; \end{cases} \tag{1.15}$$

where μ and f are a given functions defined on $\overline{\Omega}$, and the following objective function:

$$\mathcal{J}(u,h) = \frac{1}{2}\int_{\Omega}(u-\tilde{u})\mathrm{d}\mathbf{x} + \frac{\sigma}{2}h^2. \tag{1.16}$$

Here $\dfrac{\sigma}{2}h^2$ is a penalization term introduced in order to limit the growth of the control variable and $\tilde{u}$ represents observed data assumed to belong to the same space of the state variable u. The OD formulation reads

find u such that $\mathcal{J}$ is minimized subject to (1.15).

The Lagrangian of the problem reads:

$$\mathcal{L}(u,h,\lambda) = \mathcal{J}(u,h) + \int_{\Omega}\lambda\left(\mu u'' - h\,f\right)\mathrm{d}\mathbf{x}. \tag{1.17}$$

In order to obtain the optimality solution, the system of necessary conditions (1.11) is derived and then discretized (by means of any discretization technique).

The first step of the DO method is the discretization of both the objective function, say $J(\mathbf{U},\mathbf{H})$, and of the constraints, say $\mathrm{A}\mathbf{U} = \mathrm{F}\mathbf{H}$. Here, $\mathbf{U}$ and $\mathbf{H}$ are the discretized state and control variable, A and F are the discretized differential and source operators. The second step is the solution of the problem

find $\mathbf{U}$ such that $J(\mathbf{U},\mathbf{H})$ is minimized subject to $\mathrm{A}\mathbf{U} = \mathrm{F}\mathbf{H}$;

This is an algebraic optimization problem which can be solved by finding the stationary points of the Lagrangian function, which reads:

$$L(\mathbf{U}, \mathbf{H}, \mathbf{\Lambda}) = J(\mathbf{U}, \mathbf{H}) - \mathbf{\Lambda}^{\mathrm{T}} \left(\mathrm{A}\mathbf{U} - \mathrm{F}\mathbf{H} \right). \tag{1.18}$$

1.2 Recent advances in DA for the cardiovascular system

The tremendous increase of data gathering and the massive change in computational capabilities in the last few years make the DA problem a very challenging task and stimulate the design of new, efficient and competitive computational tools for the prediction of the state and the evolution of complex systems, such as the cardiovascular one. The enormous amount of information available to us requires the combination of advanced statistical techniques with precise and sophisticated mathematical models, perfected and largely validated in recent years [3, 4, 5, 8, 9]. These new approaches are developments of well-established DA techniques and, furthermore, they feature an overlap between estimation theory, control theory and stochastic approaches. Moreover, they benefit from the continuous improvement of numerical methods for order reduction [31, 32] and advanced discretization techniques [11, 33]. Among the others, we mention and briefly describe the most relevant works.

Least-squares finite elements In 2010 Heys et al. propose a weighted least-squares finite element (WLSFE) method for the inclusion of velocity data in fluid dynamics equations, mainly inspired by hemodynamics applications [11]. They consider particle imaging velocimetry that allows to collect noisy velocity data on 2-dimensional internal layers in a 3-dimensional domain. On the basis of the LSFE method [34, 35, 36], which features flexibility in the enforcement of various boundary conditions, they developed a weighted formulation based on the level of accuracy with which the boundary values are known. Given a system of discretized PDEs $\mathrm{A}\mathbf{U} = \mathbf{F}$ the WLSFE solution is the

minimum of the functional

$$J = \|\mathrm{A}\mathbf{U} - \mathbf{F}\|_{\Omega} + \|\mathbf{U} - \mathbf{H}\|_{\partial\Omega} + \|\mathbf{U} - \widetilde{\mathbf{U}}_1\|_{\Gamma_1} + \|\mathbf{U} - \widetilde{\mathbf{U}}_2\|_{\Gamma_2} + ... \tag{1.19}$$

where A is a discrete differential operator (corresponding generally to the NSE), $\mathbf{F}$ a forcing term, $\mathbf{H}$ the boundary data and $\widetilde{\mathbf{U}}_i$ available noisy data on the layer Γ_i. Using additional terms which penalize the difference between the numerical solution and the experimental data, the assimilation is weakly enforced. Thus DA costs little more than a standard LSFEM calculation. The method can be seen as nudging (for the modification of the model residual), but also as a control approach (for the minimization of a functional). Note that, LSFEM, originally designed for finding the solution of PDEs, has been applied to inverse problems since the 90's [37] for the numerical solution of PDE constrained control problems; main developers have been Bochev and Gunzburger [34, 35, 36]. In the application to the NSE, for recasting the system into a linearized first order differential system, the authors consider a non-primitive variable set. This approach, as opposed to primitive variables formulations, might be less conducive to the straightforward inclusion of available "boundary" conditions.

Bayesian interpretation of the LSFEM In the same year Dwight [33] presents a reinterpretation of the WLSFEM in terms of assimilation of data; in fact, Heys and collaborators do not present their work in an inverse problem framework. Dwight shows that the WLSFE solution can be interpreted as the *maximum a posteriori* (MAP) estimator in a variational Bayesian approach to DA (an extensive description of the Bayesian method is given in Chapter 4).

Reduced-order unscented Kalman filter In 2010, based on the UKF, presented in the previous section, Moireau and Chapelle [31] propose a reduced-order (RO) UKF applied to parameter identification in the context of cardiac biomechanics. Their filter-

ing strategy, usable for any choice of sampling points distribution, provides a tractable filtering algorithm that can be used with large-dimensional systems when the uncertainty space is of reduced size. Such algorithm invokes the original dynamical and observation operators, i.e. it does not require the computation of the tangent operator. Specifically, the covariance matrices are factorized in a form such that the costly computations are performed on a reduced-order matrix of the size of the uncertainty space.

In recent years many works investigated efficient and robust coupling algorithms for fluid-structure interaction (FSI) in large vessels. To impact the clinical practice such techniques have to be patient-specific; for this reason, model parameters have to be adapted to available clinical measurements. Two methods for FSI parameter estimation have been proposed in recent publications using Kalman filtering [32] and control theory [38].

ROUKF applied to fluid-structure interaction problems In a very recent work by Bertoglio et al. [32] the ROUKF is used for the estimation of constitutive parameters in FSI systems. In particular, from wall displacement measurements extracted from medical images, they predict the artery wall stiffness. Using this sequential algorithm, the model prediction is improved at each time step analyzing the difference of the measures and model output.

Control theory approach to the estimation of FSI parameters The same problem has been addressed by Perego et al. in [38]. Here, the estimation of the Young modulus is pursued using an OD technique in control theory. The problem of assimilating vessel displacements from registered medical images is formulated as the minimization of the difference between observation and computed variables tuning the variable representing the stiffness itself.

1.3 Thesis outline

In this work we propose a DA approach for including noisy and sparse measurements of the velocity into the simulation of the NSE, driven by hemodynamics applications. This inverse, potentially ill-posed, problem is addressed using two approaches oriented to finding point and spread estimates for the velocity field. The purpose is **1)** recovering an accurate and noise filtered approximation of the blood flow and **2)** quantifying the reliability of numerical results. The first goal is achieved by solving an optimization problem where we use a DO technique to minimize the misfit between the recovered velocity field and the data, subject to the incompressible NSE. The control variable is the normal stress at the inflow boundary of the domain of interest, the vessel inlet section; the reason for this choice resides in the biomedical application and will be specified in Chapter 3. The DA procedure is a combination of the Newton method for handling the nonlinear term of the NSE and the DA procedure designed and tested for the linearized problem. Then, the uncertainty quantification is addressed using a Bayesian approach to inverse problems recast in a variational formulation. The prediction of probability density functions for velocity and normal stress allows us to estimate how likely are those variables to take values in specific intervals. This approach, that accounts for the nature of the measurement noise, is tested on 2-dimensional and axisymmetric 3-dimensional geometries and compared with deterministic approaches.

In Chapter 2, based on [39], we present preliminary results aimed at finding the most accurate and efficient approach to the solution of the DA problem. Different methods presented in previous sections are considered and compared in terms of accuracy with respect to reference solutions and computational time. The investigation is conducted on the linearization of the NSE, namely the Stokes problem. This preliminary analysis results in the choice of the DO method.

In Chapter 3, based on [40] and [41], we present the core of our methodology.

We design a DA procedure where a DO approach is used to minimize the difference between measures and assimilated solutions for the generalized Stokes problem. The combination of such procedure with the Newton method for the solution of the forward NSE yields an algorithm of assimilation for velocity data. We discuss conditions on the location of measurements that guarantee the existence and uniqueness of an optimal solution for the linearized problem and we give numerical proof of convergence of the algorithm for the nonlinear case. Numerical results, with both noise-free and noisy data, certify the theoretical analysis. Also, we investigate the sensitivity to the noise of non-primitive variables of medical interest.

In Chapter 4 we introduce statistical inverse problems and the Bayesian variational formulation for the discretized variables. This approach yields a probability density function (PDF) for velocity and normal stress which can be used to estimate confidence intervals for such variables. Moreover, statistical parameters of the PDFs are used as point estimators for the control variable (the normal stress on the inflow boundary), specifically the MAP and the *maximum likelihood* (ML) estimators. We also provide details regarding a regularization technique based on the optimality result of Chapter 3 and we discuss how it affects statistical properties of the measurement noise. Then, we show numerical results in 2-dimensional and 3-dimensional geometries for data affected by Gaussian noise.

In Chapter 5 we propose two formulations for the unsteady (linearized and nonlinear) problem. Due to the hemodynamics application we consider time periodic phenomena and we investigate possible techniques for addressing this issue. We show numerical results on 2-dimensional and 3-dimensional geometries where we test the accuracy of the assimilation with respect to reference solutions.

Concluding remarks, future work guidelines and insights are reported in Chapter 6.

2 Preliminary analysis

In Chapter 1 we briefly presented the wide literature on DA for fluid geophysics and the state of the art of emerging techniques for hemodynamics. As we approach the problem of assimilating blood velocity from noisy measures, in this chapter we perform some preliminary tests on candidate methods with the purpose of selecting the most suitable in terms of accuracy and efficiency. Although limiting, for the sake of simplicity, we focus on deterministic approaches and we refer to Chapter 4 for a deeper investigation of stochastic methods.

We present our preliminary analysis, see [39], conducted on the Stokes problem, a simplification of the NSE, where the nonlinearity is removed. At this stage we relax several aspects of the original problem; in fact, the analysis is limited to the 2-dimensional steady case on "toy" problems with synthetic data.

In Section 2.1 we introduce three approaches to the assimilation ranging from interpolation techniques to least squares methods. We present their formulation adapted to hemodynamics equations and we discuss potential advantages and drawbacks we might incur in. In Section 2.2 we give details regarding numerical test cases, we compare the quality of numerical results and we motivate the choice of the assimilation method that we propose in this work. In Section 2.3 we present a more detailed error analysis for the selected method, still on the Stokes problem.

2.1 Candidate methods

In this section we present the assimilation problem for the Stokes model and we describe a typical data configuration for the problem we are interested in. We propose three approaches and we highlight advantages and potential weaknesses.

Let us denote by $\Omega \subset \mathbb{R}^2$ the domain of interest, i.e. the vessel; Γ_{in} and Γ_{out} the inflow and outflow sections; Γ_{wall} the vessel wall. Let $L^2(\Omega)$ be the Hilbert space of square summable functions, $\mathbf{H}^1(\Omega)$ the space of vector functions whose components are in $L^2(\Omega)$ together with their first derivatives and, $\mathbf{H}^1_\Gamma$ the corresponding space of $\mathbf{H}^1$ functions with null trace on the portion Γ of $\partial\Omega$. We denote by $\mathbf{u}(\mathbf{x}) \in \mathbf{H}^1_{\Gamma_{wall}}(\Omega)$ and $p(\mathbf{x}) \in L^2(\Omega)$ velocity and pressure fields respectively. We assume to have N_s velocity measures $\mathbf{d}$ available at some sites $\mathbf{x}_i^m \in \Omega$, for $i = 1, ..., 2N_s$; these measurement points lie on some internal layers, which we denote Γ_d (see Figure 2.1), with $\Gamma_{in} \subset \Gamma_d$. In this preliminary study, we assume sites to correspond to grid nodes, in Chapters 3, 4 and 5 this assumption is relaxed and we consider sites and nodes belonging to different sets. Velocity and pressure are assumed to fulfill the Stokes equations

$$\begin{cases} -\nu\Delta\mathbf{u} + \nabla p = \mathbf{0} & \text{in } \Omega, \\ \nabla \cdot \mathbf{u} = 0 & \text{in } \Omega, \\ \mathbf{u} = \mathbf{0} & \text{on } \Gamma_{wall}, \\ -\nu\nabla\mathbf{u}\,\mathbf{n} + p\,\mathbf{n} = \mathbf{h} & \text{on } \Gamma_{in}, \\ -\nu\nabla\mathbf{u}\,\mathbf{n} + p\,\mathbf{n} = \mathbf{0} & \text{on } \Gamma_{out}. \end{cases} \tag{2.1}$$

Here, $\mathbf{h}(\mathbf{x}) \in \mathbf{H}^{-1/2}(\Gamma_{in})$ is the Neumann data at the inflow boundary, assumed unknown; ν is the kinematic viscosity. We aim at solving the following problem: *find* $\mathbf{u}$ *and* p *so that* $\mathbf{u}$ *fits the available measures* $\mathbf{d}$ *(in some sense) under the constraints (2.1).*

As discussed in the introduction, different methods can be devised for solving this

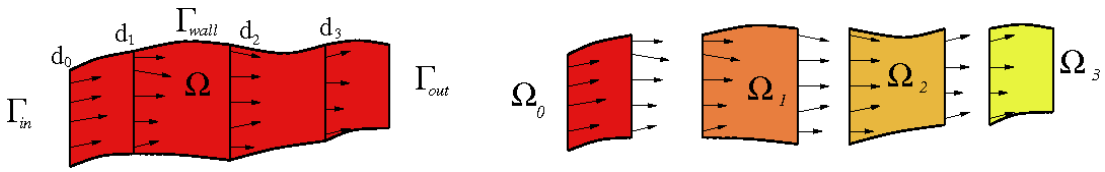

Figure 2.1: Domain splitting - Schematic representation of the domain with velocity measures (left) and its sub domain splitting (right).

problem, with different ways of fitting the data. Here, we address in particular three techniques, which we refer to as *splitting*, *nudging* (or dynamic relaxation) and *control based* techniques. The former is specifically devised for this problem and relies upon the assumption that available measures lie on internal layers of the domain of interest, i.e. points $\mathbf{x}_i^m$ belong to a set of transversal sections of the vascular district at hand, as done in [11] (see Figure 2.1). Although this is a quite restrictive assumption, it reflects the way the measurements are collected and post processed (see Figure 1.1). The key idea of this approach is the interpolation of available data. The second method is based on a more general approach, that relies upon the theory of control for distributed systems. The third one is a nudging technique reinterpreted for our specific problem.

2.1.1 Splitting techniques

We split the domain into sub domains (see Figures 1.1 and 2.1), where Γ_{in}, Γ_{out} and the measurement sections act as domain boundaries. Measures are used as boundary data for solving the global problem by sub domains. More precisely, let us assume to have s sub domains Ω_i ($i = 0, \ldots, s-1$), such that data lie on the interfaces. Let us denote by Γ_i, with $i = 0, \ldots, s$, the layers, so that $\Gamma_0 = \Gamma_{in}$ and $\Gamma_s = \Gamma_{out}$. Let $\mathbf{d}_i$, $i = 0, \ldots, s-1$, be the set of measures on Γ_i, or more precisely an interpolating function (e.g. piecewise linear interpolation) over Γ_i of the data. In principle, we can distinguish two approaches, according to the sequences *split then discretize* or *discretize then split*.

Discretize then split: matrix updating (MU) In this case, using P1bubble-P1 FE spaces for velocity and pressure (inf-sup compatible spaces, see e.g. [42], chap. 9, 10) respectively, we first discretize problem (2.1) to the form $\mathrm{S}\mathbf{V} = \mathbf{F}$, where $\mathbf{V}$ is the vector of the nodal unknowns; S is the Stokes matrix and $\mathbf{F}$ comes from the prescription of boundary conditions. Then, the measurements are regarded as conditions in the form

$$\mathbf{V}(\mathbf{x}_i) = \mathbf{d}_i \tag{2.2}$$

where i ranges over the nodes where measures are available. Conditions (2.2) are forced into the linear system similarly to Dirichlet conditions (see [43], chapter 11), i.e. i-th equations of the linear system corresponding to measurements points are replaced by (2.2). In practice, we set the off-diagonal entries of the i-th rows to 0 and the diagonal entry to 1. The corresponding entries of the right hand side, $\mathbf{F}_i$ are set equal to $\mathbf{d}_i$. Then, $\mathbf{F}_j$, $j \neq i$ are updated accordingly, by setting $\mathbf{F}_j = \mathbf{F}_j - \sum_i [\mathrm{S}]_{ji}\mathbf{d}_i$, see [43].

Clearly, in each sub domain, the incompressibility condition might be violated since data at the inflow and outflow boundary might not fulfill the compatibility condition

$$\int_{\Gamma_i} \mathbf{d}_i \cdot \mathbf{n} \, \mathrm{d}\gamma = \int_{\Gamma_{i-1}} \mathbf{d}_{i-1} \cdot \mathbf{n} \, \mathrm{d}\gamma. \tag{2.3}$$

A possible way to avoid this problem, which has not been investigated in this work, is to "adjust" properly the data so to obtain (2.3), as a pre-processing step. Nevertheless, the updated discretization matrix is not singular (though its conditioning is higher than the original one). This can be explained by the fact that the incompressibility condition is forced in a weak sense in the entire domain, therefore on each sub domain it can be violated.

Split then discretize: domain splitting In this case we first split the differential problem in s sub domains Ω_i, $i = 0, ..., s-1$ and we consider each of them separately. Then, we perform the discretization of each problem; in the first $s-1$ sub domains we have Dirichlet conditions over the entire $\partial\Omega_i$, in Ω_{s-1} we have a homogeneous Neumann condition on $\Gamma_s = \Gamma_{out}$. Note that, while in Ω_{s-1} the pressure is uniquely determined, in Ω_i, $i = 0, ..., s-2$, it is determined up to a constant (since we have a Dirichlet problem). We set such constant prescribing continuity for the pressure in Ω_i with respect to the one in Ω_{i+1} for $i = 0, ..., s-2$.

However, the presence of the noise has three important drawbacks:

- measurements errors affect the solution inside each domain, without filtering;
- the stress is not continuous across the sections;
- the divergence compatibility condition over the whole domain is violated.

Concerning the first point, it is known that perturbations on the boundary affect the solution of a Stokes problem with a decay featuring an exponential dependence on the distance from the boundary (see [44]). Therefore, the presence of noise on the interfaces brings errors inside the domain, yielding inaccurate results. For this reason we do not dwell any longer with this approach. As a matter of fact, preliminary results show that the numerical error with respect to reference solutions is one order of magnitude larger than for other methods, see [39].

2.1.2 Control based methods

In formulating control approaches we introduce the weak form of problem (2.1): for all $\mathbf{v} \in \mathbf{H}^1_{\Gamma_w}(\Omega), q \in L^2(\Omega)$ velocity and pressure satisfy

$$\int_\Omega \nu \nabla \mathbf{u} \cdot \nabla \mathbf{v} \, \mathrm{d}\mathbf{x} - \int_\Omega p \nabla \cdot \mathbf{v} \, \mathrm{d}\mathbf{x} - \int_\Omega q \nabla \cdot \mathbf{u} \, \mathrm{d}\mathbf{x} + \int_{\Gamma_{in}} \mathbf{h}\, \mathbf{v} \, d\gamma = 0. \tag{2.4}$$

We aim at finding the optimal boundary condition $\mathbf{h}$, treated as control variable, such that some distance (to be defined) between velocity and data is minimal. The choice of $\mathbf{h}$ can be motivated by the medical application and will be discussed in Chapter 3. According to the theory presented in Chapter 1, we consider the *optimize then discretize* and the *discretize then optimize* approaches.

Optimize then discretize (OD) We define the distance between solution and data as

$$dist(\mathbf{u},\, \mathbf{d}) = \frac{1}{2}\int_{\Gamma_d} \left(\mathbf{u}-\mathbf{d}\right)^2 \mathbf{v}\, \mathrm{d}\gamma, \tag{2.5}$$

for all $\mathbf{v} \in \mathbf{H}^1_{\Gamma_{wall}}(\Omega)$. Here, with an abuse of notation, $\mathbf{d}$ is an extension (obtained, for instance, by interpolation) of the vector data to a continuous functional space. We solve the problem of minimizing the functional

$$\mathcal{J}(\mathbf{u},\, \mathbf{h}) = dist(\mathbf{u},\, \mathbf{d}); \tag{2.6}$$

under the constraint of (2.1). The Lagrangian of the problem reads

$$\begin{aligned} \mathcal{L}(\mathbf{u}, p, \boldsymbol{\lambda}_\mathbf{u}, \lambda_p, \mathbf{h}) = \quad & \mathcal{J}(\mathbf{u},\, \mathbf{h}) + \textstyle\int_\Omega \nu \nabla \mathbf{u} \cdot \nabla \boldsymbol{\lambda}_\mathbf{u} \mathrm{d}\mathbf{x} + \\ & - \textstyle\int_\Omega p \nabla \cdot \boldsymbol{\lambda}_\mathbf{u} \mathrm{d}\mathbf{x} - \int_{\Gamma_{in}} \mathbf{h}\boldsymbol{\lambda}_\mathbf{u} \mathrm{d}\gamma + \int_\Omega \lambda_p \nabla \cdot \mathbf{u}\, \mathrm{d}\mathbf{x}; \end{aligned} \tag{2.7}$$

where $\boldsymbol{\lambda}_\mathbf{u}$ and λ_p are the Lagrange multipliers associated with velocity and pressure. According to [23], we derive the system of necessary conditions for optimality

$$\begin{cases} \dfrac{\partial \mathcal{L}}{\partial [\boldsymbol{\lambda}_\mathbf{u}, \lambda_p]} = \int_\Omega \nu \nabla \mathbf{u} \cdot \nabla \mathbf{v} \mathrm{d}\mathbf{x} - \int_\Omega p\, \nabla \cdot \mathbf{v} \mathrm{d}\mathbf{x} - \int_{\Gamma_{in}} \mathbf{h}\mathbf{v} \mathrm{d}\gamma + \int \Omega q\, \nabla \cdot \mathbf{u}\, \mathrm{d}\mathbf{x} = 0, \\ \dfrac{\partial \mathcal{L}}{\partial [\mathbf{u}, p]} = \int_{\Gamma_d} (\mathbf{u}-\mathbf{d})\, \mathbf{w} \mathrm{d}\gamma + \int_\Omega \nu \nabla \cdot \boldsymbol{\lambda}_\mathbf{u} \nabla \mathbf{w} \mathrm{d}\mathbf{x} + \int_\Omega \lambda_p \nabla \cdot \mathbf{w} \mathrm{d}\mathbf{x} - \int_\Omega r\, \nabla \cdot \boldsymbol{\lambda}_u \mathrm{d}\mathbf{x} = 0, \\ \dfrac{\partial \mathcal{L}}{\partial \mathbf{h}} = \int_{\Gamma_{in}} \boldsymbol{\lambda}_\mathbf{u} \mathbf{s}\, \mathrm{d}\gamma = 0. \end{cases} \tag{2.8}$$

These conditions are intended in the weak sense for all $\mathbf{v} \in \mathbf{H}^1_{\Gamma_w}$, $q \in L^2$, $\mathbf{w} \in \mathbf{H}^1_{\Gamma_w}$, $r \in L^2$ and $\mathbf{s} \in \mathbf{H}^{1/2}(\Gamma_{in})$ respectively. In the discretization step we rely on the finite element (FE) method. The discretization of (2.8) yields the linear system

$$\begin{bmatrix} \mathrm{S} & \mathrm{O} & \mathrm{N} \\ \mathrm{J} & \mathrm{S} & \mathrm{O} \\ \mathrm{O} & \mathrm{N}^{\mathrm{T}} & \mathrm{O} \end{bmatrix} \begin{bmatrix} \mathbf{V} \\ \mathbf{\Lambda} \\ \mathbf{H} \end{bmatrix} = \mathbf{F} \tag{2.9}$$

where

$$\mathrm{S} = \begin{bmatrix} \mathrm{C} & \mathrm{B}^{\mathrm{T}} \\ \mathrm{B} & \mathrm{O} \end{bmatrix}, \mathbf{V} = \begin{bmatrix} \mathbf{U} \\ \mathbf{P} \end{bmatrix}, \mathbf{\Lambda} = \begin{bmatrix} \mathbf{U}_\lambda \\ \mathbf{P}_\lambda \end{bmatrix}. \tag{2.10}$$

Here, $\mathbf{U} \in \mathbb{R}^{N_u}$ and $\mathbf{P} \in \mathbb{R}^{N_p}$ are the discretization of velocity and pressure belonging to inf-sup compatible FE spaces (see e.g. [42], chap. 9, 10), $\mathbf{H} \in \mathbb{R}^{N_{in}}$ is the discretization of the control variable $\mathbf{h}$, N_u and N_p are the number of degrees of freedom (DOFs) of velocity and pressure and N_{in} is the number of DOFs of the velocity on Γ_{in}. Let $\mathrm{N} = \mathrm{R}^{\mathrm{T}}_{in,u}\mathrm{M}_{in}$, where $\mathrm{R}_{in,u} \in \mathbb{R}^{N_{in},N_u}$ is a *restriction matrix* which selects the DOFs of the velocity on Γ_{in}. The generalization of $\mathrm{R}_{in,u}$ to velocity and pressure DOFs reads

$$\mathrm{R}_{in} = [\mathrm{R}_{in,u} \;\; \mathrm{O}], \quad R_{in} \in \mathbb{R}^{N_{in},N_u+N_p}. \tag{2.11}$$

Let $\mathrm{M}_{in} \in \mathbb{R}^{N_{in},N_{in}}$ be the discretization of the mass operator restricted to inlet boundary nodes, specifically

$$[\mathrm{M}_{in}]_{kl} = \int_{\Gamma_{in}} \boldsymbol{\varphi}_{j_l}|_{\Gamma_{in}} \, \boldsymbol{\varphi}_{i_k}|_{\Gamma_{in}} \, \mathrm{d}\sigma \qquad k, l = 1, ..., N_{in}, \tag{2.12}$$

where $\boldsymbol{\varphi}$ are the Lagrangian basis functions associated with the velocity and $\{i_k\}$ and $\{j_l\}$ are subsets of the velocity indexes, selecting DOFs on Γ_{in}.

Finally, let $\mathrm{C} \in \mathbb{R}^{N_u,N_u}$, and $\mathrm{B} \in \mathbb{R}^{N_p,N_u}$ be the discretization of the diffusion and

divergence operators.

$$\begin{aligned} [\mathrm{C}]_{ij} &= \int_{\Omega} \nu \nabla \boldsymbol{\varphi}_j \nabla \boldsymbol{\varphi}_i \, \mathrm{d}\mathbf{x}, \qquad i,\, j = 1,\, ...,\, N_u, \\ [\mathrm{B}]_{ij} &= \int_{\Omega} \nabla \cdot \boldsymbol{\varphi}_j \, \psi_i \, \mathrm{d}\mathbf{x}, \qquad i = 1,\, ...,\, N_p, \;\; j = 1,\, ...,\, N_u, \end{aligned} \tag{2.13}$$

where ψ are the Lagrangian FE basis functions associated with the pressure.

$\mathbf{U}_\lambda$ and $\mathbf{P}_\lambda$ represent the discrete Lagrangian multipliers; J and $\mathbf{F}$ account for the discretization of the term $\int_{\Gamma_d} (\mathbf{u} - \mathbf{d})\, \mathbf{w} \mathrm{d}\gamma$.

Remark 1 As described in Section 1.1.4, when using control approaches a regularization term may be added to the functional to prevent ill-posedness and improve the convexity of the problem. For reasons discussed in Chapter 3, since the data vector is projected into a continuous functional space, the optimization problem has a unique solution; hence, here we drop the regularization term. For the same reasons we do not consider any regularization also in the discretize then optimize case.

Discretize then optimize (DO) In this case, using the FE method we first discretize the functional and the constraints; the result is an algebraic optimization problem with linear constraints:

$$\begin{aligned} &\min_{\mathbf{H}} J(\mathbf{V},\, \mathbf{H}) = \frac{1}{2} \|\mathrm{D}\mathbf{V} - \mathbf{d}\|_2^2 \\ &\text{s.t. } \; \mathrm{S}\mathbf{V} = \mathrm{N}\mathbf{H}; \end{aligned} \tag{2.14}$$

where the notation is the same of the previous paragraph. We let $\mathrm{Q} \in \mathbb{R}^{2N_s, N_u}$ be a matrix designed such that $[\mathrm{Q}\mathbf{U}]_i$ is the numerical solution evaluated at the data sites and corresponding to $[\mathbf{d}]_i$, for $i = 1,\, ...,\, 2\,N_s$. We extend Q to pressure DOFs introducing the matrix $\mathrm{D} = [\mathrm{Q} \;\; \mathrm{O}]$. For the solution of this minimization problem, we write the Lagrangian

$$L(\mathbf{V}, \mathbf{H}, \boldsymbol{\Lambda}) = \frac{1}{2} \|\mathrm{D}\mathbf{V} - \mathbf{d}\|_2^2 + \boldsymbol{\Lambda}^{\mathrm{T}} (\mathrm{S}\mathbf{V} - \mathrm{N}\mathbf{H}), \tag{2.15}$$

and we derive the induced system of optimality conditions, also known as KKT system [45]

$$\begin{cases} \dfrac{\partial L}{\partial \mathbf{V}} = \mathrm{D}^{\mathrm{T}}(\mathrm{D}\mathbf{V} - \mathbf{d}) + \mathrm{S}^{\mathrm{T}}\boldsymbol{\Lambda} = \mathbf{0} \\ \dfrac{\partial L}{\partial \boldsymbol{\Lambda}} = \mathrm{S}\mathbf{V} - \mathrm{N}\mathbf{H} = \mathbf{0} \\ \dfrac{\partial L}{\partial \mathbf{H}} = -\mathrm{N}^{\mathrm{T}}\boldsymbol{\Lambda} = \mathbf{0}. \end{cases} \tag{2.16}$$

Upon block elimination, we get the reduced system

$$\mathrm{Z}^{\mathrm{T}}\mathrm{Z} = \mathrm{Z}^{\mathrm{T}}\mathbf{d}; \tag{2.17}$$

where $\mathrm{Z} = \mathrm{D}\mathrm{S}^{-1}\mathrm{N}$ is the so called *sensitivity* matrix. It is defined as $\mathrm{Z} = \frac{\mathrm{d}(\mathrm{D}\mathbf{V})}{\mathrm{d}\mathbf{H}}$ and it is a measure of how much perturbations of the control variable may affect the output $\mathrm{D}\mathbf{V}$. For this reason, spectral properties of Z determine the conditioning or well-posedness of the problem. For insights on efficient techniques for the solution of problem (2.16) see [30].

2.1.3 Dynamic relaxation

We propose a reinterpretation of the nudging method, or dynamic relaxation (DR), in a weak sense and we discuss a possible choice of the relaxation parameter. In fluid geophysics the initial condition of the forecast is the final solution of the pre-forecast period (Section 1.1.3). Here, we consider the solution of the steady problem, which we are interested in, as the stationary state of an unsteady problem with artificial terms enforcing data fitting. The initial condition is chosen arbitrarily, but in such a way that it is physically consistent. The formulation of the method in a weak form makes the problem more amenable to a FE discretization.

We solve the problem of finding, for each test function $\mathbf{v}(\mathbf{x}, t)$ and $q(\mathbf{x}, t)$ in the

velocity and pressure spaces, $\mathbf{u}(\mathbf{x},t)$ and $p(\mathbf{x},t)$ such that

$$\begin{cases} \int_\Omega \mathbf{u}_t\ \mathbf{v}d\mathbf{x} + \int_\Omega \nu\nabla\mathbf{u}\nabla\mathbf{v}d\mathbf{x} - \int_\Omega p\ \nabla\mathbf{v}d\mathbf{x} + \int_\Omega q\ \nabla\cdot\mathbf{u}d\mathbf{x} \\ -\int_{\Gamma_{in}} (\nu\,\nabla\mathbf{u}\,\mathbf{n} + p\,\mathbf{n})\,\mathbf{v}d\gamma + c\ \int_{\Gamma_{in}\cup\Gamma_d}(\mathbf{u}-\mathbf{d})\mathbf{v}d\gamma = 0 \\ \\ \mathbf{u}(\mathbf{x},t=0) = \mathbf{u}_0. \end{cases} \tag{2.18}$$

Here, the forcing term is a boundary inner product, between the test function and the difference of data and predicted velocity, evaluated on measurement layers. We note that this term embeds a weak prescription of boundary conditions on Γ_{in}; for this reason the term $\int_{\Gamma_{in}} (\nu\nabla\mathbf{u}\,\mathbf{n} + p\,\mathbf{n})\,\mathbf{v}d\gamma$ is added to the formulation. This fact suggests a way for the selection of the nudging coefficient, which can be thought of as a penalty parameter. We choose c according to the theory of artificial boundary conditions presented in [46]. In the assumption of FE discretization, c is proportional to $\mathcal{D}_{max}$, the largest triangle diameter, $c = k\nu\mathcal{D}_{max}$, where k is a positive parameter and ν the viscosity.

This approach is clearly related to the more sophisticated weighted least squares FE (WLSFE) method for DA, introduced in [11] by Heys et al., already mentioned in Chapter 1. Such method, designed for steady problems, consists in the minimization of a functional given by the sum of the weak formulation of the state equations, weak prescription of boundary conditions and weighted norm of the misfit between data and velocity. The weights are chosen according to a measure of trust in the data. The substantial difference, with respect to nudging, is in setting the method as an optimization problem. This fact allows to account for the noise without altering the nature of the problem since no artificial forcing terms are added to the state equations. Details on the WLSFE can be found in Chapter 1 and in [11].

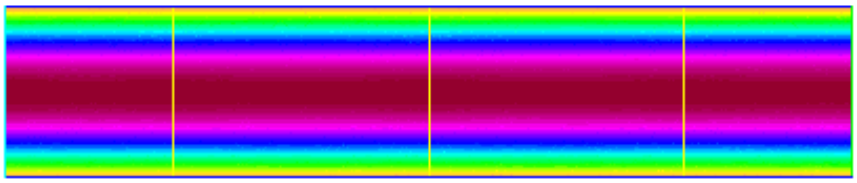

Figure 2.2: Poiseuille flow - Horizontal velocity profile, vertical lines in correspondence of $x \in \{0,\ 1,\ 2.5\ 4\}$ show data location.

2.2 Numerical results

We report numerical results obtained testing the proposed approaches on a toy problem with synthetic data. We consider the Poiseuille flow, a steady flow governed by the Stokes equations in the rectangular domain $\Omega \subset \mathbb{R}^2$, $\Omega = [0, L] \times [-R, R] = [0, 5] \times [-0.5, 0.5]$. The exact solution reads

$$\begin{cases} \mathbf{u}_P(x, y) = \ [1 - 4y^2\ ,\ 0\ ]^{\mathrm{T}}, \\ p_P(x, y) = -8\nu(x - L); \end{cases} \tag{2.19}$$

Figure 2.2 reports the horizontal velocity field computed by the FE solver `FreeFem++`[1] on a fine unstructured grid. According to the problem presented in the introduction, we assume data to be given on three internal layers and on the inflow boundary in correspondence of discretization nodes, i.e. the space discretization step Δ satisfies $\Delta \propto N_s^{-1}$. Precisely, in this configuration $\Gamma_d = \{(x, y) \mid x \in \{0,\ 1,\ 2.5,\ 4\},\ \ y \in [-R, R]\ \}$. Data are generated adding to the exact solution random noise, normally distributed with zero mean and variance determined by the prescription of the signal-to-noise ratio (SNR) defined as the ratio between the peak velocity and the level of noise.

Computational grids are unstructured triangulations generated with `FreeFem++`, see Figure 2.3. We implement the FE method with choice of compatible FE spaces

[1] An open source C++ software for the numerical solution of two dimensional partial differential equations with the FE method. http://www.freefem.org.

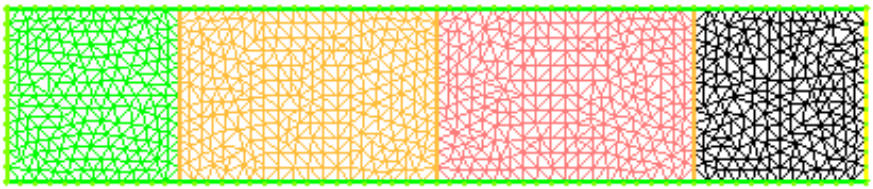

Figure 2.3: Computational grid - Triangulation (80$\times$ 20) generated with `FreeFem++`.

P1bubble-P1 for the velocity and pressure fields respectively (see e.g. [42], chap. 9, 10). At this preliminary stage it is important to answer the question *"is DA worthwhile?"*. In fact, in principle, internal measures could be disregarded and data on Γ_{in}, properly extended to grid nodes, could be used as Dirichlet condition and this would lead to a (cheap) well-posed problem. Mathematically and physically DA is always preferable since it takes into account the mathematical model and produces feasible solutions. On the other hand, at a practical level, the issue is to find a good compromise between accuracy and efficiency. For these reasons we compare the performance of MU, OD, DO and DR with a direct approach, say Dirichlet (D), where the Stokes equations are solved prescribing the noisy velocity data on the inflow as boundary condition. Note that the DR method deserves a separate treatment; in fact, tuning the time interval, the constant k and the discretization time-step different levels of accuracy can be achieved.

We test the methods over a set of noise realizations and we consider the mean relative error as accuracy index

$$\overline{E}_U = \sum_{i=1}^{N_r} \frac{\|\mathbf{U}_i - \mathbf{U}_P\|_2}{\|\mathbf{U}_P\|_2}, \tag{2.20}$$

being $\mathbf{U}_P$ the discretization of $\mathbf{u}_P$ and $\mathbf{U}_i$ the solution computed in correspondence of the i-th noise generation, out of $N_r = 16$ with SNR = 20 and 8; while the first value is chosen for testing the methods, the second is a reasonable SNR for practical

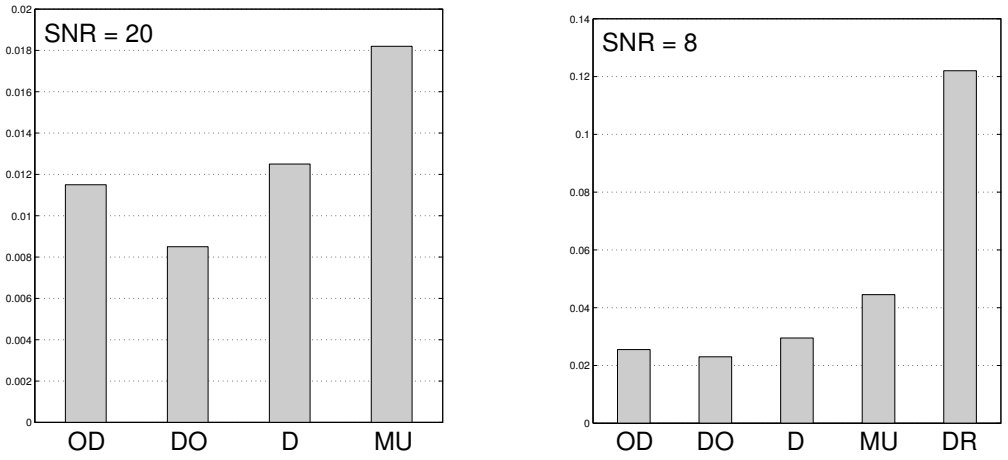

Figure 2.4: Comparison results for the OD, DO, D, MU and DR approaches in terms of relative error $\overline{E}_U$ with SNR = 20 (left) and 8 (right).

applications, e.g. for measures acquired via phase velocity encoded MRIs [10].

For DR simulations we set $c = k\,\nu\,\mathcal{D}_{max}$ with $k = 10^4$, $\nu = 0.035$, a value featured by blood, $\Delta t = 10^{-2}$, $\mathbf{u}_0(\mathbf{x}) = 10^{-5}\mathbf{u}_P(\mathbf{x})$. Here, Δt is the time-step used in the time discretization scheme; in this case we use the Backward-Euler (BE) method [47]. Accuracy results are reported in Figure 2.4; for each method we report the relative error $\overline{E}_U$. The diagram on the right also displays the error associated with the DR method after 150 time steps. Even if much cheaper in terms of computational effort, the MU method is not accurate enough; this is due to the sensitivity to the noise, which makes this approach unreliable. The DR method has a poor accuracy and, furthermore, requires the solution of an unsteady problem, which makes it computationally more expensive. Table 2.1 reports results obtained for SNR = 8 with different number of iterations. In Figure 2.5 we report the horizontal velocity at different iterations of the process: during the transient we notice that we do not have a physical solution due to the prescription of the data at the internal layers. These results show that even with 150 steps the DR approach is much less accurate than other methods. While DR

iter	E_U
50	1.416e-1
100	1.249e-1
150	1.225e-1

Table 2.1: Relative errors in correspondence of SNR = 8 for the DR technique with different number of iterations.

does not require an adjoint operator computation, the high number of iterations and the poor accuracy make this method not competitive. We note that the choice of c has not been investigated in this work; we do not exclude that an optimal choice of this parameter might yield more accurate results.

Selection of the DA method The four candidate methods, MU, OD, DO and DR, present significant differences in terms of accuracy and time saving.

The MU method is computationally cheap, costs a forward solve, but its accuracy is poor. In fact, the reference method, Dirichlet approach, can achieve more accurate results. This is somehow expected since data are incorporated without taking care of the presence of the noise and no filtering mechanism is active. With the same purpose of using measures as boundary data, a valid alternative would be a weighted weak prescription of boundary conditions where weights depend on how much we trust the measures. This approach results in a modified weak formulation, with additional terms of the form

$$\int_{\Gamma_d} \mathbf{w}\,(\mathbf{u}-\mathbf{d})\,\mathbf{v}\,\mathrm{d}\gamma \tag{2.21}$$

where $\mathbf{w}$ is the weight function. Methods of this sort can be considered a combination of splitting and nudging techniques. A sophisticated formulation of this approach is the WLSFE approach [11], already mentioned in Section 2.1.3. Here, boundary penalty terms as in (2.21) are added to the weak formulation; the minimizer of the resulting functional is the assimilated solution. Modification, improvement, and comparison of

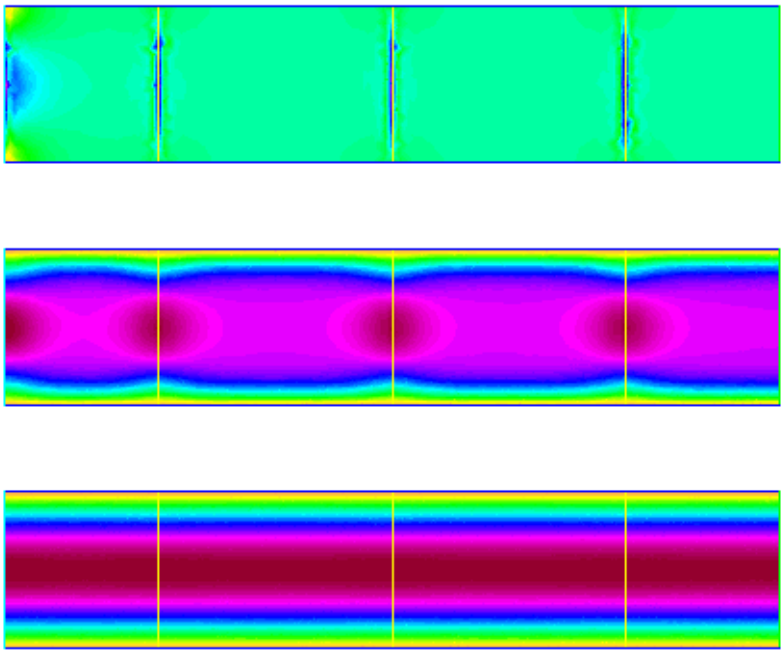

Figure 2.5: Numerical solutions for the horizontal velocity field obtained at different iterations, specifically, 0, 20 and 150 of the DR process.

splitting techniques is part of future work. Nevertheless, it is important to recall that these approaches have a limiting feature; in fact, they are suitable only for problems where data are located on internal slices and do not allow for generalization to sparse data.

On the other hand, DR is not reliable in terms of accuracy and requires the solution of a time-dependent problem, which makes the method computationally expensive. Nevertheless, these facts qualify DR to be considered as a candidate method for approaching the assimilation problem for time dependent data.

Control approaches are the most accurate; however they require higher computational effort. In average, the computational time required by OD is 1.4 times larger than DO's. With the purpose of improving computational aspects we consider the DO approach as the most promising; in fact, we believe that accuracy has a primary im-

portance in biomedical applications. Besides that, current techniques for optimization problems allow fast and efficient solution of inverse problems [30]; improving the computational efficiency of the DO approach is part of the current work and it is fundamental in treating real data.

2.3 Further analysis of the DO method

We conduct a deeper investigation of the DO approach applied to the Stokes equations. In particular, we analyze the behavior of the error with respect to the analytic solution (still the Poiseuille flow) versus the discretization error, the number of data and the SNR. We discuss implementation issues and we report numerical results which highlight the promising filtering properties of our approach. At this stage we utilize `lifeV`[1], an efficient and flexible open source C++ FE library.

2.3.1 The software

The FE library `lifeV` is a software for scientific computing, whose development started in 1999 as a joint work project involving Ecole Polytechnique Fédérale de Lausanne (CMCS) in Switzerland, Politecnico di Milano (MOX) in Italy, INRIA (REO) in France. Since 2008 Emory University (Department of Mathematics and Computer Science) in Georgia, US, has become part of the developers community. `lifeV` is a free software, subject to the LGPL license, and it is compilable on Unix-like systems. This software implements in C++ language algorithms and data structures to approximate numerically systems of PDEs, that arise from mathematical modeling applied to fluid-dynamics, fluid-structure interaction, flow in porous media and electrocardiology. `lifeV` has been employed in joint collaborations with medical and industrial partners (for instance Emory University, School of Medicine (GA - USA); Policlinico di Milano (Italy).

[1] `www.lifev.org`.

The library is composed of a core part which provides an abstract framework for the implementation of Galerkin FE methods, and of a set of solvers for specific applications. Although the library was originated as a serial software, recently the developers community implemented a parallel version of the library (in this work we use the serial version). Moreover, the software interfaces with external libraries like Boost for containers, basic algorithms and smart pointers, BLAS and LAPACK for standard linear algebra tools, Aztec or Trilinos for matrix manipulation and linear systems solution. Results obtained by the solvers can be post processed using `lifefilters` methods which take care of writing results on files, in a format compatible with common visualization software like Paraview[1], Ensight[2] or Medit[3].

2.3.2 Implementation issues

The core of the data assimilation solver is the solution of the reduced system (2.17). The bottleneck of the computations is the Stokes system, corresponding to either S^{-1} or $\mathrm{S}^{-\mathrm{T}}$; for its solution we do not consider a monolithic solver, instead, we perform an exact algebraic factorization and we split the original matrix into two block-triangular matrices. We rewrite the matrix S as

$$\mathrm{S} = \begin{bmatrix} \mathrm{C} & \mathrm{B}^{\mathrm{T}} \\ \mathrm{B} & \mathrm{O} \end{bmatrix} = \begin{bmatrix} \mathrm{C} & \mathrm{O} \\ \mathrm{B} & -\mathrm{B}\mathrm{C}^{-1}\mathrm{B}^{\mathrm{T}} \end{bmatrix} \begin{bmatrix} \mathrm{I} & \mathrm{C}^{-1}\mathrm{B}^{\mathrm{T}} \\ \mathrm{O} & \mathrm{I} \end{bmatrix}. \tag{2.22}$$

[1] http://www.paraview.org
[2] http://www.ensight.com/
[3] http://www.ann.jussieu.fr/ËIJfrey/publications/RT-0253.pdf

In this way we can solve separately the two following block triangular systems:

$$\begin{cases} \mathrm{C}\widetilde{\mathbf{U}} = \mathbf{b}_1 \\ \mathrm{B}\widetilde{\mathbf{U}} - \mathrm{B}\mathrm{C}^{-1}\mathrm{B}^{\mathrm{T}}\widetilde{\mathbf{P}} = \mathbf{b}_2; \end{cases} \tag{2.23}$$

$$\begin{cases} \mathrm{C}\mathbf{U} = \mathbf{b}_1 - \mathrm{B}^{\mathrm{T}}\mathbf{P} \\ \mathbf{P} = \widetilde{\mathbf{P}}; \end{cases} \tag{2.24}$$

where $\widetilde{\mathbf{P}}$ and $\widetilde{\mathbf{U}}$ are two auxiliary variables; these systems are solved with iterative approaches, namely GMRES-type solvers.

2.3.3 Numerical results

Using `FreeFem++` we generate unstructured triangulations of dimension n (number of edges on the longest side of Ω), we set n = 40, 60, 80, 120, 160. We do not add any regularization term to the formulation; also in this case, we assume to have measures on each grid node on Γ_{in}, this assumption ensures the existence and uniqueness of a minimizer for the problem as we will see Chapter 3.

In Figure 2.6 we report, for $\Delta = 1/40$, the assimilated pressure and velocity fields with noise-free data; in correspondence of the internal layers the velocity matches the data (the exact solution). Figure 2.7 reports computed velocity and noisy data with SNR = 10. The noise mainly affects the vertical components of the field (zero in the analytic solution); in the assimilated velocity such vertical the noise is filtered; see the zoomed area on the right.

We consider the behavior of the discretization error versus the discretization step Δ using noise-free data. This is a consistency check; numerical results, displayed in Figures 2.8 (left) are consistent with the FE theory (for the specific choice of FE spaces), i.e. $E_U = \frac{\|\mathbf{U}-\mathbf{U}_P\|_2}{\|\mathbf{U}_P\|_2} = \mathcal{O}(\Delta^2)$ and $E_P = \frac{\|\mathbf{P}-\mathbf{P}_P\|_2}{\|\mathbf{P}_P\|_2} = \mathcal{O}(\Delta)$.

In Figure 2.9 we report in logarithmic scale E_U versus Δ for SNR =20 (left) and

SNR	$n = 40$	$n = 60$	$n = 80$	$n = 120$	$n = 160$
∞	1.1874e-02	5.1610e-03	3.0476e-03	1.3949e-03	8.1229e-04
20	3.5414e-02	2.9724e-02	2.4532e-02	2.0646e-02	1.7957e-02
8	7.4238e-02	6.7801e-02	5.8876e-02	4.6559e-02	4.1652e-02

Table 2.2: Velocity relative errors in correspondence of different values of the discretization step for different choices of SNR.

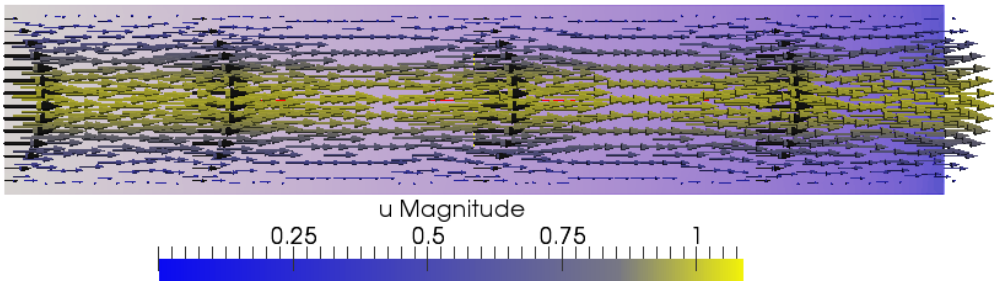

Figure 2.6: Computed pressure on the background, computed velocity and the noise-free data (black vector field).

8 (right). We observe a behavior proportional to $\Delta^{0.5}$ (see Table 2.2 for the complete report of the test case). To understand this result we note that, at this initial stage, the number of data on Γ_{in} is mesh dependent, more precisely $N_s \propto \Delta^{-1}$; hence, $E_U \propto N_s^{-1}$. This is coherent with statistical theory: the standard deviation of the sample mean of N random variables is proportional to $N^{-0.5}$. In Chapter 3 further results confirm this interpretation.

Figure 2.8 (right) reports in a logarithmic scale E_U versus SNR^{-1}; here, the error increases linearly with the amount of noise, which is reasonable in the case of linear problems.

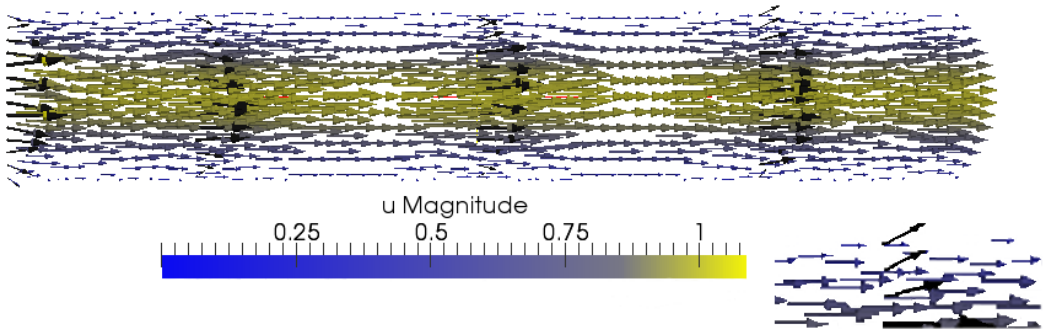

Figure 2.7: Computed pressure on the background, computed velocity and the noisy data with SNR = 10 (black vector field).

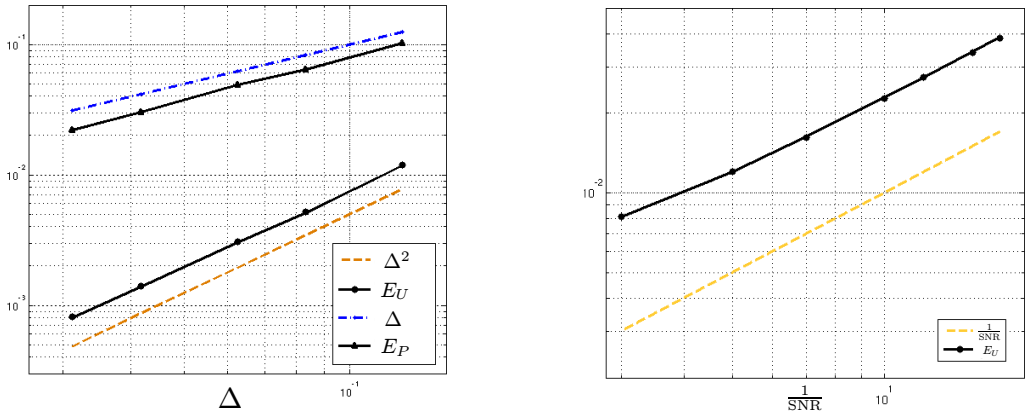

Figure 2.8: Left: relative errors for velocity and pressure versus Δ with noise-free data. Right: mean relative errors, over 20 realizations, versus $\text{SNR}^{-1} = 0.03, 0.05, 0.07, 0.10, 0.12, 0.15, 0.17$, $n = 60$.

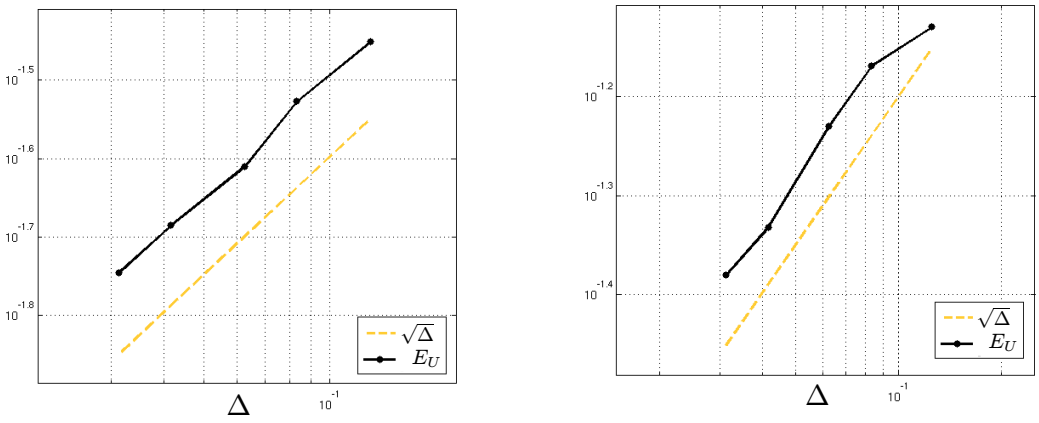

Figure 2.9: Mean relative errors, over 20 realizations, for the velocity field versus $\Delta = 1/8, 1/12, 1/16, 1/24, 1/32$, with SNR = 20 (left) and SNR =8 (right).

3 A deterministic approach to DA

Preliminary results on the Stokes problem reported in Chapter 2 provide the ground for the design of a robust, noise filtering method for the estimation of blood flow from noisy velocity measures and numerical simulations. The discretize then optimize (DO) technique is the basis for the development of a flexible and reliable assimilation tool.

Objectives are challenging: we want to construct an accurate estimator which works in case of highly noisy data and complex geometries regardless (as much as possible) of the dynamics, turbulent or laminar, of the flow. We want to provide conditions that guarantee good mathematical properties to the estimator, including existence and uniqueness and its stability with respect to data perturbation.

In this chapter, mainly based on [40] and [41], we present the core of the assimilation procedure. We show how our estimator is able to accomplish such goals, fundamental in the design of a prediction tool for the medical practice. We introduce a robust and noise filtering DO method for the linearized Navier-Stokes equations (NSE) and we provide a possible alternative to common Tikhonov-like regularization methods. The latter are in general mandatory in the treatment of ill-posed inverse problems, and, however, might be computationally demanding. Our regularization approach is based on an optimality result for the control problem; we find conditions on the number and location of the data which ensure the existence of a unique estimator. The extension of the method to the NSE is an iterative algorithm that still features the desired properties, also in presence of advection dominated phenomena, i.e. high Reynolds number. The application to non-trivial domains approximating cardiovascular geometries gives

promising results in both the prediction of the flow and of flow related variables of high medical interest, namely the wall shear stress.

In Section 3.1 we present the continuous formulation of the DA problem for the NSE; in Section 3.2 we describe in detail the discrete formulation applied to the linearization of the NSE, we prove the existence and uniqueness of the assimilated solution under a condition on the location of the measurements. Moreover, we discuss the sharpness of this condition and introduce the associated regularization technique. Numerical results for noise-free data are consistent with the theory. With noisy data results point out the noise-filtering action of the assimilation procedure. In Section 3.3 we generalize the technique to the steady NSE; numerical results show the robustness of the proposed iterative algorithm. In Section 3.4 we use the DA estimator on more complex test cases; simulations on 2-dimensional non-trivial domains and axisymmetric geometries show the flexibility, accuracy and reliability of the method in the prediction of velocity and velocity related variables.

3.1 Mathematical formulation of the DA problem

Following the results obtained in Chapter 2 we formulate the assimilation technique as a control problem where the misfit between the predicted velocity and the data is minimized.

Let us denote by Ω a domain in $\mathbb{R}^d$ ($d = 2,\ 3$; in real applications $d = 3$). We assume (see Figure 1.1 and 3.1) that the domain of interest Ω features an inflow boundary Γ_{in}, an outflow boundary Γ_{out} and the physical wall of the vessel Γ_{wall}. Γ_{in} and Γ_{out} can possibly consist of several sections. Variables of interest are velocity $\mathbf{u}(\mathbf{x}) \in \mathbf{H}^1_{\Gamma_{wall}}(\Omega)$ and pressure $p(\mathbf{x}) \in L^2(\Omega)$ which are assumed to obey the NSE in Ω. Also, we assume to have N_s velocity measures $\mathbf{d}$ available at some sites[1] $\mathbf{x}_i^m \in \Omega$, for $i = 1,\ ...,\ dN_s$. We

[1]Notice that we use the word "sites" for the location of measurements, as opposed to the word "nodes" for points where velocities are computed. In general sites and nodes are different, but we do not exclude

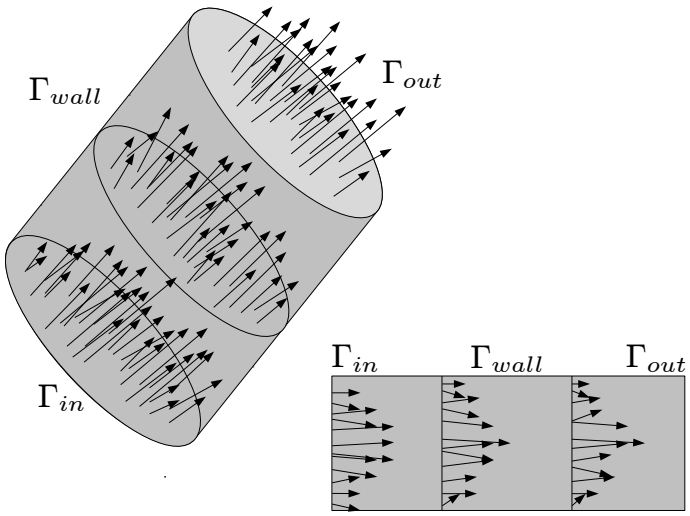

Figure 3.1: Possible 2-dimensional and 3-dimensional domains with associated measured sparse data.

formulate the DA problem as an inverse problem of the form

$$\min_{\mathbf{h}} \mathcal{J}(\mathbf{u},\, \mathbf{h}) = dist(f(\mathbf{u}),\, \mathbf{d}) + \mathcal{R}(\mathbf{h})$$

$$\text{s.t.} \begin{cases} -\nu\, \nabla \cdot (\nabla \mathbf{u} + \nabla \mathbf{u}^{\mathrm{T}}) + (\mathbf{u} \cdot \nabla)\mathbf{u} + \nabla p = \mathbf{s} & \text{in } \Omega, \\ \nabla \cdot \mathbf{u} = 0 & \text{in } \Omega, \\ \mathbf{u} = \mathbf{0} & \text{on } \Gamma_{wall}, \\ -\nu\, (\nabla \mathbf{u} + \nabla \mathbf{u}^{\mathrm{T}})\mathbf{n} + p\, \mathbf{n} = \mathbf{h} & \text{on } \Gamma_{in}, \\ -\nu\, (\nabla \mathbf{u} + \nabla \mathbf{u}^{\mathrm{T}})\mathbf{n} + p\, \mathbf{n} = \mathbf{g} & \text{on } \Gamma_{out}. \end{cases} \tag{3.1}$$

Here, $dist(\cdot,\, \cdot)$ is a distance which will be specified later on; f is an observation operator for the velocity field; $\mathbf{s} \in \mathbf{H}^{-1}(\Omega)$ is the source term; $\mathbf{g} \in \mathbf{H}^{-1/2}(\Gamma_{out})$ is the Neumann boundary condition on the outflow section; $\mathcal{R}$ is a regularization term added to improve properties of the functional to be minimized (as we will see later). A New-

that the intersection of sites set and nodes set in non-empty.

tonian rheology is supposed to hold, since it is a common assumption in large and medium blood vessels [3]; ν is the kinematic viscosity. The choice of homogeneous Dirichlet boundary conditions on Γ_{wall} is due to the fact that we consider fixed geometries. We use the inflow normal stress data $\mathbf{h} \in \mathbf{H}^{-1/2}(\Gamma_{out})$ as control variable; this choice is arbitrary but can be justified by the fact that an accurate knowledge of inflow-outflow boundary conditions is quite problematic in real applications, since these are "artificial" boundaries (see [48, 49]). We present the method for the linearized equations at first; here, the nonlinear convection term $(\mathbf{u} \cdot \nabla)\mathbf{u}$ is replaced with $(\boldsymbol{\beta} \cdot \nabla)\mathbf{u}$, where $\boldsymbol{\beta}$ is a known advection field. Then, we proceed by treating the nonlinear case in Section 3.3.

3.2 Discretize then optimize method for the linear problem

For the numerical solution of the optimization problem we focus on the linearized problem introduced in the previous section. The choice of the optimization scheme relies upon the comparison analysis presented in Chapter 2 and in [39] where the DO technique proved to be the most efficient method. In this procedure we first discretize the continuous formulation by means of the finite element (FE) method; this yields the following algebraic optimization problem (for $\alpha \geq 0$)

$$\begin{aligned} &\min_{\mathbf{H}} J(\mathbf{V}, \mathbf{H}) = \frac{1}{2}\|\mathrm{D}\mathbf{V} - \mathbf{d}\|_2^2 + \frac{\alpha}{2}\|\mathrm{L}\mathbf{H}\|_2^2 \\ &\text{s.t. } \mathrm{S}\mathbf{V} = \mathrm{R}_{in}^{\mathrm{T}}\mathrm{M}_{in}\mathbf{H} + \mathbf{F}. \end{aligned} \tag{3.2}$$

For $\alpha > 0$, the term $\frac{\alpha}{2}\|\mathrm{L}\mathbf{H}\|_2^2$ has a regularization purpose (Tikhonov regularization, see [50]) and it is intended to improve the convexity of the functional to be minimized. More in general, it improves the conditioning of the problem, that can be affected by the presence of noise. L is selected such that $\mathrm{L}^{\mathrm{T}}\mathrm{L}$ is positive definite. Different techniques can be used for an optimal choice of the regularization parameter α; among the others,

we mention the discrepancy principle (DP) and the generalized cross validation (GCV) [50]. $\mathbf{V} = [\mathbf{U}\ \mathbf{P}] \in \mathbb{R}^{N_u+N_p}$ is the vector of discretized velocity $\mathbf{U} \in \mathbb{R}^{N_u}$ and pressure $\mathbf{P} \in \mathbb{R}^{N_p}$ belonging to inf-sup compatible FE spaces (see e.g. [42], chap. 9, 10). $\mathbf{H} \in \mathbb{R}^{N_{in}}$ is the discretization of the control variable $\mathbf{h}$; N_{in} is the number of degrees of freedom (DOFs) of the velocity on Γ_{in}. We introduce the matrix S, a modification of the matrix introduced in Chapter 2.

$$\mathrm{S} = \begin{bmatrix} \mathrm{C}+\mathrm{A} & \mathrm{B}^{\mathrm{T}} \\ \mathrm{B} & \mathrm{O} \end{bmatrix}. \tag{3.3}$$

Here, we let $\mathrm{C},\ \mathrm{A} \in \mathbb{R}^{N_u,N_u}$ and $\mathrm{B} \in \mathbb{R}^{N_p,N_u}$ be the discretization of the diffusion, advection and divergence operators.

$$\begin{aligned} [\mathrm{C}]_{ij} &= \int_\Omega \nu(\nabla\boldsymbol{\varphi}_j + \nabla\boldsymbol{\varphi}_j^{\mathrm{T}}) \cdot \nabla\boldsymbol{\varphi}_i \,\mathrm{d}\mathbf{x}, && i,\, j = 1,\, ...,\, N_u, \\ [\mathrm{A}]_{ij} &= \int_\Omega \boldsymbol{\beta} \cdot \nabla\boldsymbol{\varphi}_j \boldsymbol{\varphi}_i \,\mathrm{d}\mathbf{x} && i,\, j = 1,\, ...,\, N_u, \\ [\mathrm{B}]_{ij} &= \int_\Omega \nabla \cdot \boldsymbol{\varphi}_j \,\psi_i \,\mathrm{d}\mathbf{x}, && i = 1,\, ...,\, N_p,\ \ j = 1,\, ...,\, N_u, \end{aligned} \tag{3.4}$$

where $\boldsymbol{\varphi}$ and ψ are the Lagrangian FE basis functions associated with velocity and pressure respectively.

Let us recall some notations introduced in the previous chapter. We let $\mathrm{Q} \in \mathbb{R}^{dN_s,N_u}$ be a matrix such that $[\mathrm{Q}\mathbf{U}]_i$ is the numerical solution evaluated at the data sites and corresponding to $[\mathbf{d}]_i$, for $i = 1,\, ...,\, dN_s$. When measurement sites coincide with DOFs $[\mathrm{Q}\mathbf{U}]_i$ is simply the corresponding entry of $\mathbf{U}$; when measurement sites do not correspond to DOFs points, $[\mathrm{Q}\mathbf{U}]_i$ is the value of the FE numerical solution evaluated at $\mathbf{x}_i^m$ obtained by a weighted sum of the FE Lagrangian basis functions. As an example, let us consider the grid of Figure 3.2, with a P1bubble-P1 discretization for the velocity and pressure. Two possible sites location on Γ_{in} are illustrated. The row of the matrix Q (relative to the first velocity component, denoted by Q_x) in correspondence of the site

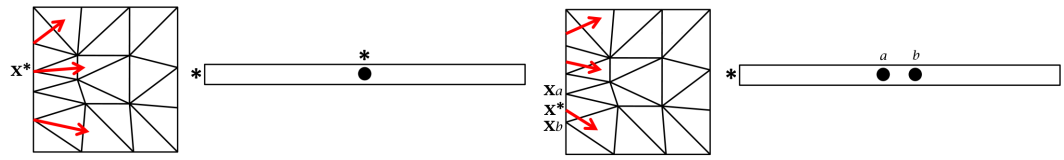

Figure 3.2: Possible choices of sites location and corresponding rows for the matrix Q (only Q_x is reported) in correspondence of site $\mathbf{x}^*$. Left: sites coincident with grid nodes. Right: sites non-coincident with grid nodes.

$\mathbf{x}^*$, is also reported for each case. While in the first case at row $*$ we have one non-zero entry, in the second case, we have two non-zero entries corresponding the grid nodes of the edge $\mathbf{x}^*$ belongs to. We extend the selection matrix to pressure DOFs, introducing the matrix $\mathrm{D} = [\mathrm{Q} \;\; \mathrm{O}]$.

We let $\mathrm{R}_{in,u} \in \mathbb{R}^{N_{in},N_u}$ be a *restriction matrix* which selects the DOFs of the velocity on Γ_{in}. The generalization of $\mathrm{R}_{in,u}$ to velocity and pressure DOFs reads

$$\mathrm{R}_{in} = [\mathrm{R}_{in,u} \;\; \mathrm{O}], \quad \mathrm{R}_{in} \in \mathbb{R}^{N_{in},N_u+N_p}. \tag{3.5}$$

We let $\mathrm{M}_{in} \in \mathbb{R}^{N_{in},N_{in}}$ be the discretization of the mass operator restricted to inlet boundary nodes, specifically

$$[\mathrm{M}_{in}]_{kl} \;\; = \;\; \int_{\Gamma_{in}} \boldsymbol{\varphi}_{j_l}\big|_{\Gamma_{in}} \, \boldsymbol{\varphi}_{i_k}\big|_{\Gamma_{in}} \, \mathrm{d}\sigma \qquad k,\, l = 1,\, ...,\, N_{in}, \tag{3.6}$$

where $\boldsymbol{\varphi}$ are the Lagrangian basis functions associated with the velocity and $\{i_k\}$ and $\{j_l\}$ are subsets of the velocity indexes, selecting DOFs on Γ_{in}. For the solution of problem (3.2), we use the reduced Hessian method to solve the system necessary conditions for optimality induced by the Lagrangian

$$L(\mathbf{V}, \mathbf{H}, \boldsymbol{\Lambda}) = \frac{1}{2}\|\mathrm{D}\mathbf{V} - \mathbf{d}\|_2^2 + \frac{\alpha}{2} \, \|\mathrm{L}\mathbf{H}\|_2^2 + \boldsymbol{\Lambda}^{\mathrm{T}}(\mathrm{S}\mathbf{V} - \mathrm{R}_{in}^{\mathrm{T}}\mathrm{M}_{in}\mathbf{H} - \mathbf{F}), \tag{3.7}$$

where $\boldsymbol{\Lambda} \in \mathbb{R}^{N_u+N_p}$ is the discrete Lagrange multiplier. The set of necessary conditions

for optimality is given by the KKT system (see e.g. [45]).

$$\begin{cases} \dfrac{\partial L}{\partial \mathbf{V}} = \mathrm{D}^{\mathrm{T}}(\mathrm{D}\mathbf{V} - \mathbf{d}) + \mathrm{S}^{\mathrm{T}}\boldsymbol{\Lambda} = \mathbf{0} \\ \dfrac{\partial L}{\partial \mathbf{H}} = \alpha \mathrm{L}^{\mathrm{T}}\mathrm{L}\mathbf{H} - \mathrm{M}_{in}^{\mathrm{T}}\mathrm{R}_{in}\boldsymbol{\Lambda} = \mathbf{0} \\ \dfrac{\partial L}{\partial \boldsymbol{\Lambda}} = \mathbf{S}\mathbf{V} - \mathrm{R}_{in}^{\mathrm{T}}\mathrm{M}_{in}\mathbf{H} - \mathbf{F} = \mathbf{0}. \end{cases} \tag{3.8}$$

By defining $\mathrm{Z} = \mathrm{D}\mathrm{S}^{-1}\mathrm{R}_{in}^{\mathrm{T}}\mathrm{M}_{in}$ and $\mathrm{W} = \mathrm{Z}^{\mathrm{T}}\mathrm{Z} + a\,\mathrm{L}^{\mathrm{T}}\mathrm{L}$ the reduced system reads

$$\mathrm{W}\mathbf{H} = \mathrm{Z}^{\mathrm{T}}(\mathbf{d} - \mathrm{D}\mathrm{S}^{-1}\mathbf{F}), \tag{3.9}$$

where W is the reduced Hessian associated with L and $\mathrm{Z} = \frac{\mathrm{d}(\mathrm{D}\mathbf{V})}{\mathrm{d}\mathbf{H}}$ is the so-called *sensitivity* matrix [45]. Spectral properties of Z determine the conditioning and well-posedness of the problem.

3.2.1 Non-singularity of the reduced Hessian

Sufficient and necessary conditions for the existence of a unique minimizer of problem (3.2) are based on optimization theory.

Sufficient and necessary conditions

We analyze the existence of a unique minimizer for the optimization problem (3.2) under suitable assumptions on number and location of the data. It is worth mentioning that the results we present are strictly related to the specific choice of the control variable; a different choice (e.g. the pressure drop, the inflow/outflow velocity, the outflow Neumann boundary condition, etc...) would imply different optimality conditions.

According to the formulation presented in Section 3.2 the DO technique yields an algebraic optimization problem; necessary (sufficient) conditions for optimality are satisfied when the reduced Hessian matrix W is positive semi-definite (definite). In our

case, it is enough to show that W is non-singular, i.e. system (3.8) has a unique solution.

Let $\mathbf{v} \in \mathbb{R}^{N_u+N_p}$ be the vector such that

$$\mathbf{v} = \mathrm{S}^{-1}\mathrm{R}_{in}^{\mathrm{T}}\mathrm{M}_{in}\mathbf{x}, \tag{3.10}$$

where $\mathbf{x} \in \mathbb{R}^{N_{in}}$ is a generic non-null vector. Then, we can write

$$\mathbf{x}^{\mathrm{T}}\mathrm{W}\mathbf{x} = \mathbf{v}^{\mathrm{T}}\mathrm{D}^{\mathrm{T}}\mathrm{D}\mathbf{v} + \alpha\,\mathbf{x}^{\mathrm{T}}\mathrm{L}^{\mathrm{T}}\mathrm{L}\mathbf{x}. \tag{3.11}$$

Since $\mathbf{x} \neq \mathbf{0}$, $\mathrm{D}^{\mathrm{T}}\mathrm{D} \geq 0$ and $\mathrm{L}^{\mathrm{T}}\mathrm{L} > 0$, we conclude that using a regularization term, i.e. $\alpha > 0$, *always* yields the well-posedness of the problem, no matter how the measures are located in the domain. Since regularization might be computationally expensive in searching the optimal regularization parameter, we prove a non-singularity result also for $\alpha = 0$.

From now on, we assume $\alpha = 0$ and we focus on the first term in (3.11).

Proposition 3.2.1 For $\alpha = 0$, W is non-singular $\Leftrightarrow$

$$Null(\mathrm{D}) \cap Range(\mathrm{S}^{-1}\mathrm{R}_{in}^{\mathrm{T}}\mathrm{M}_{in}) = \{\mathbf{0}\}. \tag{3.12}$$

Proof $\Leftarrow$ Take $\mathbf{x} \neq \mathbf{0}$; then, $\mathbf{v} = \mathrm{S}^{-1}\mathrm{R}_{in}^{\mathrm{T}}\mathrm{M}_{in}\mathbf{x} \neq \mathbf{0}$ since M_{in} and S are non-singular and R_{in} is full rank. Under the condition (3.12) $\mathrm{D}\mathbf{v} \neq \mathbf{0}$; hence, $\mathbf{x}^{\mathrm{T}}\mathrm{W}\mathbf{x} > 0$ for all $\mathbf{x} \neq \mathbf{0}$. $\Rightarrow$ By contradiction, assume (3.12) does not hold. Then, there exists $\mathbf{v} \neq \mathbf{0}$, defined as in (3.10), such that $\mathrm{D}\mathbf{v} = \mathbf{0}$, which implies that $\exists\,\mathbf{x} \neq \mathbf{0}$ such that $\mathbf{x}^{\mathrm{T}}\mathrm{W}\mathbf{x} = \mathbf{0}$, so W has a non-trivial kernel.

We need to analyze how the fulfillment of (3.12) is subordinated to the reciprocal location (and number) of sites and nodes. In view of Proposition 3.2.3, we prove the following Lemma.

Lemma 3.2.2 For $\mathbf{v}$ defined as in (3.10), $\mathrm{R}_{in}\mathbf{v} \neq \mathbf{0} \ \ \forall\, \mathbf{x} \in \mathbb{R}^{N_{in}}$ such that $\mathbf{x} \neq \mathbf{0}$.

Proof Let $\mathbf{w} = \mathrm{R}_{in}^{\mathrm{T}}\mathrm{M}_{in}\mathbf{x}$; then, definition (3.10) implies $\mathrm{S}\mathbf{v} = \mathbf{w}$. Without loss of generality, assume that inflow DOFs are numbered in the first N_{in} entries such that

$$\mathbf{w} = \begin{bmatrix} \mathrm{M}_{in}\mathbf{x} \\ \mathbf{0} \end{bmatrix}. \tag{3.13}$$

We rewrite matrix S and vector $\mathbf{v}$ accordingly as

$$\mathrm{S} = \begin{bmatrix} \mathrm{A}_{11} & \mathrm{A}_{12} \\ \mathrm{A}_{21} & \mathrm{A}_{22} \end{bmatrix}, \qquad \mathbf{v} = \begin{bmatrix} \mathbf{v}_1 \\ \mathbf{v}_2 \end{bmatrix}, \tag{3.14}$$

where $\mathrm{A}_{11} \in \mathbb{R}^{N_{in},N_{in}}$ and $\mathbf{v}_1 \in N_{in}$. Note that A_{22} is the matrix of a generalized Stokes problem with homogeneous Dirichlet boundary conditions on $\Gamma_{in} \cup \Gamma_{wall}$ and Neumann conditions on Γ_{out}, so it is non-singular [42]. Assume by contradiction that $\mathrm{R}_{in}\mathbf{v} = \mathbf{0}$. This implies that $\mathbf{v}_1 = \mathbf{0}$. System $\mathrm{S}\mathbf{v} = \mathbf{w}$ reads:

$$\begin{bmatrix} \mathrm{A}_{11} & \mathrm{A}_{12} \\ \mathrm{A}_{21} & \mathrm{A}_{22} \end{bmatrix} \begin{bmatrix} \mathbf{0} \\ \mathbf{v}_2 \end{bmatrix} = \begin{bmatrix} \mathrm{M}_{in}\mathbf{x} \\ \mathbf{0} \end{bmatrix}. \tag{3.15}$$

We get $\mathrm{A}_{22}\mathbf{v}_2 = \mathbf{0}$ so that $\mathbf{v}_2 = \mathbf{0}$, which implies that $\mathrm{M}_{in}\mathbf{x} = \mathbf{0}$. This is a contradiction since M_{in} is non-singular and $\mathbf{x} \neq \mathbf{0}$.

Remark 2 Note that Lemma 3.2.2 is not strictly specific for the Stokes problem; in fact, it typically holds also for FE discretization of several differential problems, e.g. elliptic PDEs. As a matter of fact, we only require that the discretization matrix corresponding to the homogeneous Dirichlet problem on Γ_{in} is non-singular. Despite this, numerical experiments in Section 3.2.3 show that the sufficient condition, in the subsequent

Proposition 3.2.3, is sharp.

Proposition 3.2.3 A sufficient condition for the existence of a unique minimizer for problem (3.2) is that there exists a subset of sites such that the restriction Q_r of Q to such sites fulfills

$$\mathrm{Q}_r(I - \mathrm{R}_{in,u}^{\mathrm{T}}\mathrm{R}_{in,u}) = \mathrm{O} \qquad \text{and} \qquad rank(\mathrm{Q}_r) = N_{in}. \tag{3.16}$$

Proof Notice that (3.16) implies that $\mathrm{Q}_r\mathrm{R}_{in,u}^{\mathrm{T}}$, where $\mathrm{R}_{in,u} \in \mathbb{R}^{N_{in},N_u}$, has full rank; in fact

$$\begin{aligned} N_{in} = rank(\mathrm{Q}_r) = rank(\mathrm{Q}_r\mathrm{R}_{in,u}^{\mathrm{T}}\mathrm{R}_{in,u}) \leq \min\{rank(\mathrm{Q}_r\mathrm{R}_{in,u}^{\mathrm{T}}), rank(\mathrm{R}_{in,u})\} \\ = \min\{rank(\mathrm{Q}_r\mathrm{R}_{in,u}^{\mathrm{T}}),\ N_{in}\}, \end{aligned} \tag{3.17}$$

hence $rank(\mathrm{Q}_r\mathrm{R}_{in,u}^{\mathrm{T}})$ cannot be less than N_{in}. Let us denote by D_r the sub-matrix of D corresponding to Q_r, so that $\mathrm{D}_r = [\mathrm{Q}_r \ \ \mathrm{O}]$.

We prove that, under condition (3.16), for $\mathbf{v} = \mathrm{S}^{-1}\mathrm{R}_{in}^{\mathrm{T}}\mathrm{M}_{in}\mathbf{x}$ and $\mathbf{x} \neq \mathbf{0}$, $\mathrm{D}_r\mathbf{v} \neq \mathbf{0}$.

As a consequence of Lemma 3.2.2, we have that $\mathrm{R}_{in}\mathbf{v} \neq \mathbf{0}$, this implies $\mathrm{R}_{in,u}\mathbf{v}_u \neq \mathbf{0}$, where $\mathbf{v}_u$ is the restriction of vector $\mathbf{v}$ to velocity DOFs. Consequently,

$$\mathrm{D}_r\mathbf{v} = \mathrm{Q}_r\mathbf{v}_u = \mathrm{Q}_r(I - \mathrm{R}_{in,u}^{\mathrm{T}}\mathrm{R}_{in,u} + \mathrm{R}_{in,u}^{\mathrm{T}}\mathrm{R}_{in,u})\mathbf{v}_u = \mathrm{Q}_r\mathrm{R}_{in,u}^{\mathrm{T}}\,\mathrm{R}_{in,u}\mathbf{v}_u. \tag{3.18}$$

Since $\mathrm{Q}_r\mathrm{R}_{in,u}^{\mathrm{T}}$ has rank N_{in}, $\mathrm{D}_r\mathbf{v} \neq \mathbf{0}$ and the thesis follows.

Proposition 3.2.3 corresponds to design the selection matrix D such that its restriction to sites on Γ_{in} has N_{in} independent rows. As an example, in Figure 3.3, we report two possible configurations of sites selection using P1bubble FE for the velocity. Note that, with this choice of FE spaces, sufficient conditions are satisfied when we have sites on each DOF on Γ_{in}. This fact opens the question of mesh refinement. For $\Delta \to 0$ we

gain accuracy but, in the limit, we loose well-posedness (since $\Delta = 0$ corresponds to having an infinite number of sites on Γ_{in}). However, the presence of the noise makes the refinement, after a certain level, unnecessary since the accuracy is determined by the amount of noise only. More in general, this suggests that the selection of the parameter α for the regularizing term should depend on Δ.

Remark 3 Conditions for the existence and uniqueness of the optimal solution might be unexpected. However, we notice that in the limit case of data given on DOFs of Γ_{in} only (i.e. $\mathrm{D} = \mathrm{R}_{in}$) the problem is equivalent to the solution of the linearized NSE where Dirichlet boundary conditions on the inflow section are prescribed in a weak sense.

Remark 4 Proposition 3.2.3 states that it is mandatory to have velocity measures at the inflow section; in our application this is not prohibitive. In fact, it is always possible to collect velocity data on internal layers transversal to the blood flow. Nevertheless, we cannot expect data to satisfy sufficient conditions for optimality (i.e. to be located on velocity DOFs); in the next section we present a technique to overcome this problem.

Remark 5 Lemma 3.2.2 shows that, given a non-homogeneous Neumann boundary condition on Γ_{in}, the corresponding computed velocity restricted to inflow DOFs, $\mathbf{v}_{in}$, has at least one non-zero entry. In order to relax conditions (3.16) (i.e. $Rank(\mathrm{Q}_r) = \overline{N}$, $\overline{N} < N_{in}$), an upper bound to the number of zero entries of $\mathbf{v}_{in}$ would be needed. However, this is not possible since we can always find a Neumann condition on Γ_{in} such that the corresponding $\mathbf{v}_{in}$ has only one non-zero entry (consider the Dirichlet-to-Neumann map with $\mathbf{v}|_{\Gamma_{in}} = \mathbf{v}_{in}$).

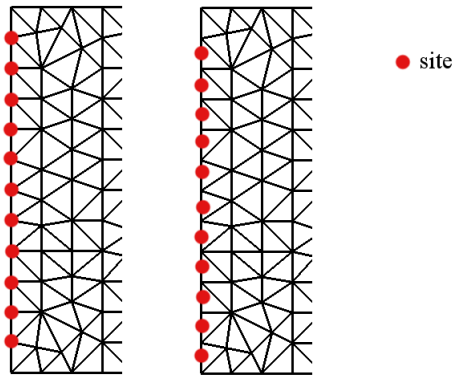

Figure 3.3: Example of sites location sufficient for theoptimality on grid nodes (left) and not on grid nodes (right) using P1bubble FE for the velocity.

3.2.2 Forcing optimality via interpolation

The existence of a unique minimizer with a regularization term $\alpha > 0$ does not suffer from any constraint on sites and nodes. Despite this, there can be some drawbacks, among which we mention the fact that it alters the solution of the problem (especially when $\alpha \gg 1$). Also, Tikhonov regularization requires the choice of the optimal parameter α, which might be computationally expensive, e.g. the DP, see next section, requires the iterative solution of linear systems of the form $\mathrm{W}\mathbf{H} = \mathrm{Z}^{\mathrm{T}}(\mathbf{d} - \mathrm{D}\mathrm{S}^{-1}\mathbf{F})$ [50]. There is however another possible way for forcing the optimality, exploiting the result of Proposition 3.2.3.

Let us assume that some data are available at the inflow, not necessarily fulfilling sufficient conditions. We can extend the given data to the entire set of DOFs on the inflow boundary by interpolation (e.g. piece-wise linear) of available data and Dirichlet boundary conditions on Γ_{wall}. In this way, inflow data are virtually extended to inflow DOFs and condition (3.16) is automatically fulfilled. More specifically, if we assume data $\widetilde{\mathbf{d}}$ to be given, then, after interpolation, we can write $\mathbf{d} = \Pi\widetilde{\mathbf{d}}$, where $\Pi \in \mathbb{R}^{N_s+N_{in},N_s}$ is the interpolation matrix associated with piece-wise linear Lagrangian polynomials.

Example Assume Γ_{in} to be parallel to the y axis in the reference plane $(x,\, y)$, then, Π is defined as follows.

$$
\begin{aligned}
&[\Pi]_{i,j} = -\frac{y_{j+1}^m - y_i^{DOF}}{\Delta_j}; \qquad [\Pi]_{i,j+1} = \frac{y_j^m - y_i^{DOF}}{\Delta_j} \\
&\qquad \text{for } \; y_i^{DOF} \in [y_j^m,\, y_{j+1}^m] \quad i = 1,\, ...,\, N_{in},\; j = 1,\, ...,\, N_{s,in}; \\
&[\Pi]_{i+N_{in},i} = 1 \qquad\qquad\qquad\qquad i = 1,\, ...,\, N_s.
\end{aligned}
\tag{3.19}
$$

Here, y_i^m is such that $\mathbf{x}_i^m = (x_i^m,\, y_i^m)$ lies on Γ_{in}; $N_{s,in}$ is the number of sites on Γ_{in} and $\Delta_j = y_{j+1}^m - y_j^m$. Also, y_i^{DOF} such that $\mathbf{x}_i^{DOF} = (x_i^{DOF},\, y_i^{DOF})$ corresponds to a DOF on Γ_{in}.

The interpolated data are clearly affected by the interpolation error. More precisely, if we assume that

$$\widetilde{\mathbf{d}} = \mathbf{d}^{sparse} = \mathbf{u}_{exact} + \boldsymbol{\varepsilon}, \tag{3.20}$$

where $\boldsymbol{\varepsilon}$ is the random noise; then, on boundary DOFs the interpolated data can be written as

$$\mathbf{d}^{interp} = \mathbf{u}_{exact} + \boldsymbol{\eta}_{\boldsymbol{\varepsilon}}, \tag{3.21}$$

where $\boldsymbol{\eta}_{\boldsymbol{\varepsilon}}$ is a linear combination of noise and exact velocity on the original sites. More precisely, the statistical features of $\boldsymbol{\eta}_{\boldsymbol{\varepsilon}}$ are affected by the interpolation error and the additional error that occurs when interpolating noisy data [51].

In this way, the functional to minimize reads

$$\frac{1}{2}\|\mathrm{D}^{sparse}\mathbf{V} - \mathbf{d}^{sparse}\|_2^2 + \frac{1}{2}\|\mathrm{D}^{interp}\mathbf{V} - \mathbf{d}^{interp}\|_2^2, \tag{3.22}$$

where D^{sparse} and D^{interp} select respectively components of the velocity field on sparse sites and DOFs on Γ_{in}. Representation (3.22) highlights the role of interpolation as

a regularizing technique. In Section 3.2.3 we investigate this strategy and compare it with the classical Tikhonov regularization. A careful investigation of the effect of the interpolation error in statistical terms will be carried out in Chapter 4.

3.2.3 Numerical results

In this section we test our technique on 2-dimensional cases. We consider both noise-free and noisy data, the former for a consistency analysis, the latter for a discussion on the reliability of the DA process. At this preliminary stage data are synthetic, i.e. they do not come from measures, but from a given analytical solution suitably perturbed with additional noise. We present results for a validation of Proposition 3.2.3.

Implementation details We implement the FE method with choice of compatible FE spaces P1bubble-P1 for velocity and pressure respectively. The mesh is generated with the software `FreeFem++`. For Tikhonov regularization we use $\mathrm{L} = \nabla_d$, the discretized gradient, and we generate the optimal parameter α by means of DP [50]. Here, the optimal $\bar{\alpha}$ is such that $\|\mathrm{D}\mathbf{V}_{\bar{\alpha}} - \mathbf{d}\|_2^2 - \tau^2$ is minimized, being $\mathbf{V}_{\bar{\alpha}}$ the optimal solution computed with $\bar{\alpha}$ and $\tau^2 = \|\boldsymbol{\varepsilon}\|_2^2$, the norm of the noise. In practical applications, the DP method is not commonly used for the search of the optimal parameter since the norm of the noise, τ^2, is usually unknown. Since we have an estimate of the noise variance σ^2 (for each component of the noise vector), we use $\tau^2 \cong dN_s\sigma^2$.

For the solution of the reduced system (3.9) and of the state and adjoint systems we use inexact Krylov subspace iterations; more specifically, we solve the reduced Hessian matrix W with the GMRESR method [52, 53], which allows to change the preconditioner at each iteration, and the matrices S and S^{T} with the GMRES method (inner iterations). For such nested iterations it is possible to bound the inner tolerance so that the global residual norm falls below a prescribed tolerance. This issue has been investigated in [54] and [55] for several applications in scientific computing. In the numerical

simulations presented in this work outer and inner tolerances are chosen empirically; in view of applications to real data we plan to take into account an adaptive choice of the inner tolerance.

The bottleneck is the solution of linear systems associated with S and S^{T} where an efficient preconditioner is required; we solve these systems monolithically with the pressure-convection-diffusion (PCD) preconditioner proposed by Kay in [56] and by Silvester et al. in [57]. Table 3.1 reports stopping criteria used for each linear system involved. $\mathrm{P}(\mathrm{S})$ stands for the preconditioned system, $\mathbf{r}_k$ is the residual at iteration k and $\mathbf{rhs}$ is the right hand side of the current system. Note that these parameters refer to the solution of problems featuring non-trivial geometries or low viscosity values; in fact, such problems require an accurate solution of inner systems.

The PCD preconditioner exploits an approximation of the Schur complement based on considerations on the continuous operators involved. We report its formulation, details regarding motivation and performance can be found in [58]. We define the preconditioner P as follows:

$$\mathrm{P} = \mathrm{L}_p \mathrm{F}_p^{-1} \mathrm{M}_p. \tag{3.23}$$

Here, L_p is the FE discretization of the pressure Laplacian

$$[\mathrm{L}_p]_{i,j} = \int_\Omega \nabla\psi_j \cdot \nabla\psi_i; \tag{3.24}$$

being ψ the pressure basis functions. F_p is the discretization of the momentum equation for the pressure variable

$$[\mathrm{F}_p]_{i,j} = \mu \int_\Omega \nabla\psi_j \cdot \nabla\psi_i + \int_\Omega (\boldsymbol{\beta} \cdot \nabla\psi_j)\, \psi_i. \tag{3.25}$$

M_p is the pressure mass matrix and $\boldsymbol{\beta}$ is the advection field. Note that, using an iterative solver, we only specify the matrix-vector product for $\mathrm{P}^{-1}\mathbf{v}$; hence, we only require

linear system	solver	tol	stopping criteria
$\mathrm{C}+\mathrm{A}$	GMRES	1.e-9	$\|\mathbf{r}_k\|/\|\mathbf{r}_0\|$
$\mathrm{P(S)}$	GMRES	1.e-9	$\|\mathbf{r}_k\|/\|\mathbf{rhs}\|$
W	GMRESR	1.e-6	$\|\mathbf{r}_k\|/\|\mathbf{rhs}\|$

Table 3.1: Parameters setting for the iterative solvers (implemented in the `AZTEC` library).

solvers for the pressure Laplacian and the mass matrix. As reported in [58] we can assemble these matrices prescribing natural boundary conditions on all boundaries but the inflow section, where a Dirichlet boundary condition is required. When solving the adjoint operator S^{T}, we prescribe Dirichlet boundary conditions on the outflow section.

Numerical results are obtained with the C++ FE library `lifeV` and post-processed with `ParaView`, see Section 2.3.1.

Analytic test case Simulations presented in this section are based on the 2-dimensional Navier-Stokes flow in the domain $\Omega = [-0.5,\, 1.5] \times [0,\, 2]$ whose analytic solution, $\mathbf{u}_{anl}$, reads

$$\begin{cases} [\mathbf{u}]_1(x,y) = 1 - e^{\lambda x}\cos(2\pi y), \\ [\mathbf{u}]_2(x,y) = \dfrac{\lambda}{2\pi} e^{\lambda x}\sin(2\pi y), \\ p(x,y) = \dfrac{1}{2}e^{2\lambda x} - \dfrac{1}{4\lambda}e^{2\lambda}. \end{cases} \tag{3.26}$$

Here, the kinematic viscosity of the fluid is $\nu = 0.035$, a value featured by blood (lower parameters induce advection-dominated problems, see Figure 3.4, right). The adimensional parameter λ is such that $\lambda = \frac{1}{2}(\nu^{-1} - \sqrt{\nu^{-2} + 16\pi^2})$. In Figure 3.4 we report the analytical velocity computed on a fine grid in correspondence of $\nu = 0.035$ (left) and 0.005 (right). In these test cases the index of accuracy is the relative error with respect to the analytic solution, $E_U = \frac{\|\mathbf{U}-\mathbf{U}_{anl}\|_2}{\|\mathbf{U}_{anl}\|_2}$, where $\mathbf{U}_{anl}$ is the discretization of $\mathbf{u}_{anl}$.

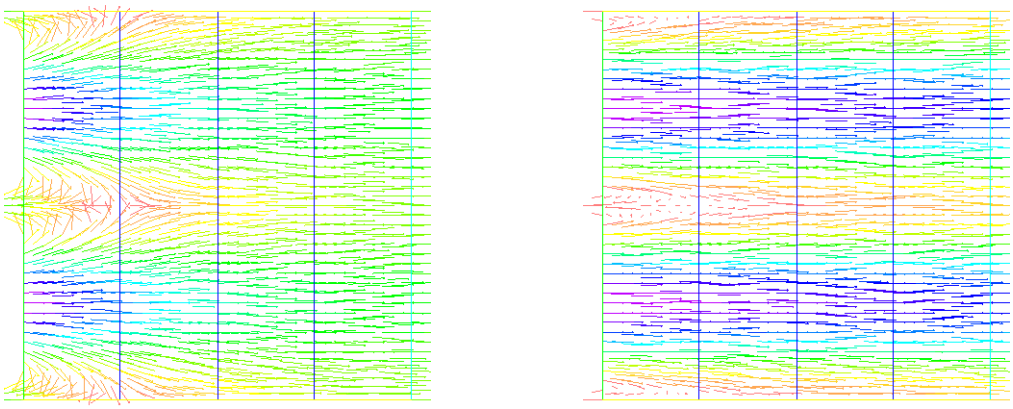

Figure 3.4: Exact velocity field in correspondence of $\nu = 0.035$ (left) and $\nu = 0.005$ (right).

Data Generation We assume data to be given on the inflow boundary and on some internal points in the computational domain, not necessarily in correspondence of grid points. In the case of noise-free measures the data vector coincides with the exact solution, for the noisy case data are generated by adding Gaussian noise to the exact solution.

Noise-free data We consider the linearized problem with $\boldsymbol{\beta} = \mathbf{u}_{anl}$ and we analyze the error with respect to the exact solution. In this test case we set $\alpha = 0$ and we consider data on DOFs on Γ_{in} and on three internal layers (in correspondence of grid nodes at $x = 0, 0.5, 1$). In Figure 3.5 we report the relative error E_U in logarithmic scale versus the discretization step Δ. Here, $\mathbf{U}_{anl}$ is the discretization of the analytic solution. Consistently with the Céa Lemma [42] we observe the expected convergence rate (for the chosen FE spaces), $E_U = \mathcal{O}(\Delta^2)$.

Verification of the optimality condition With the purpose of validating and testing the sharpness of Proposition 3.2.3, we focus on the conditioning of the problem and we inspect singular values of W. We choose $\Delta = 0.076$ and SNR $= 20$. This value corresponds to adding a low amount of noise and it is chosen for testing the method.

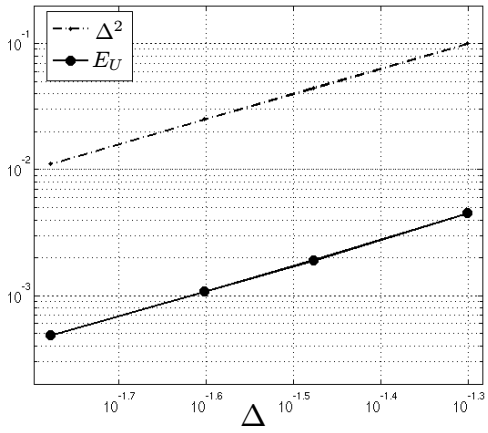

Figure 3.5: Relative error versus Δ for noise-free data, a reference curve, Δ^2, is reported.

BS	IS	K_1	E_U	it	K_1(reg)	E_U(reg)	it(reg)
27	0	3.1e+05	0.0500	19	1.1e+04	0.0492	16
13	0	1.3e+20	0.0756	13	9.7e+03	0.0567	13
9	0	7.9e+19	0.1957	15	9.8e+03	0.1050	17
27	100	1.3e+06	0.0367	15	3.0e+04	0.0354	12
13	114	1.1e+11	0.0443	11	4.6e+04	0.0379	11
9	118	1.5e+11	0.0478	13	6.1e+04	0.0348	12

Table 3.2: Condition number, relative error and number of iterations for different choices of sites with SNR = 20.

Later on in the chapter realistic values, such as SNR = 8, are also considered. In this set of simulations $N_{in} = 27$. In Table 3.2 we report the condition number K_1 of W, for $\alpha = 0$ and $\alpha =$ 1e-2, for different values of N_s; on the inflow boundary sites (BS) correspond to grid nodes, while inside the domain they do not necessarily. The value of the regularization parameter is fixed a priori on an empirical basis. In Figures 3.6 and 3.7 we report in a semilogarithmic scale the singular values of the reduced Hessian W, properly rescaled, with and without regularization. Let us focus on the case of data *not* satisfying optimality conditions. When the number of internal sites (IS) = 0 and $\alpha = 0$ the distribution of the singular values features a gap and we can classify the problem as *rank-deficient* (see [50]). In these cases it is not worth using

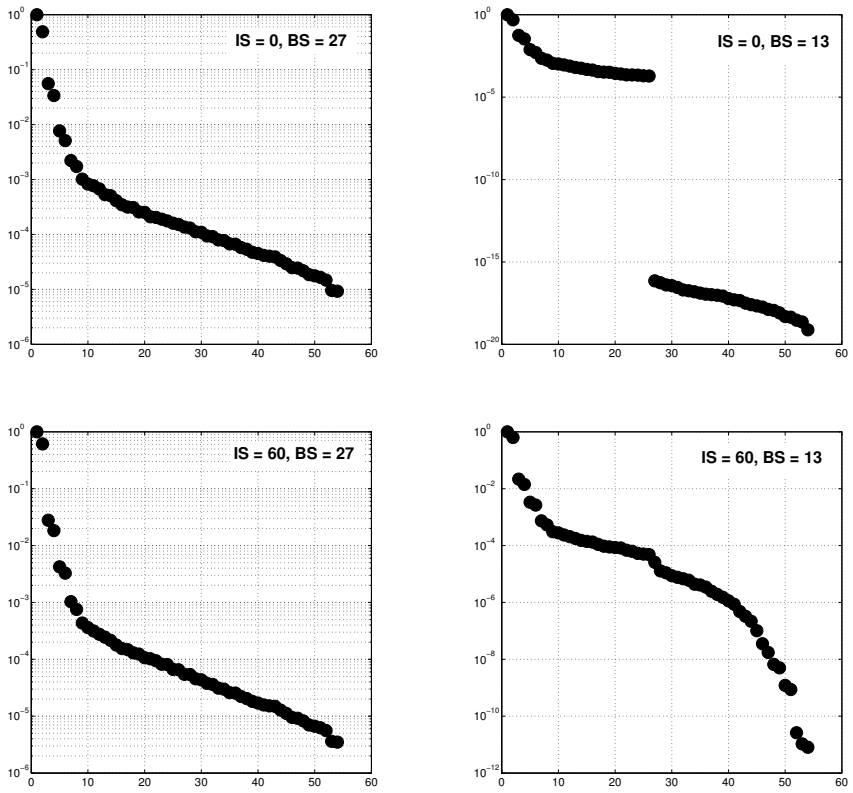

Figure 3.6: Singular values of W with $\alpha = 0$ for IS =0 and 60 and BS = 27 and 13.

Tikhonov regularization; in fact, in a certain sense, regularization induces a shift of the eigenvalues (see Figure 3.7, top right). It is rather effective to identify such gap using methods such as truncated singular value decomposition (TSVD) or modified TSVD, see [50]. In our case the system is solved by means of the GMRES method setting empirically a tolerance so to stop iterations before the gap. When conditions are not satisfied, IS $\neq 0$ and $\alpha = 0$ there is no gap in the singular values distribution and the problem can be classified as *discrete ill-posed* [50]. Also, the addition of internal data does not improve significantly the condition number and the relative error.

We also investigate the behavior of the procedure for different values of the kinematic viscosity ν, i.e. for different Reynolds number. The choice of $\nu_1 = 0.1$ and

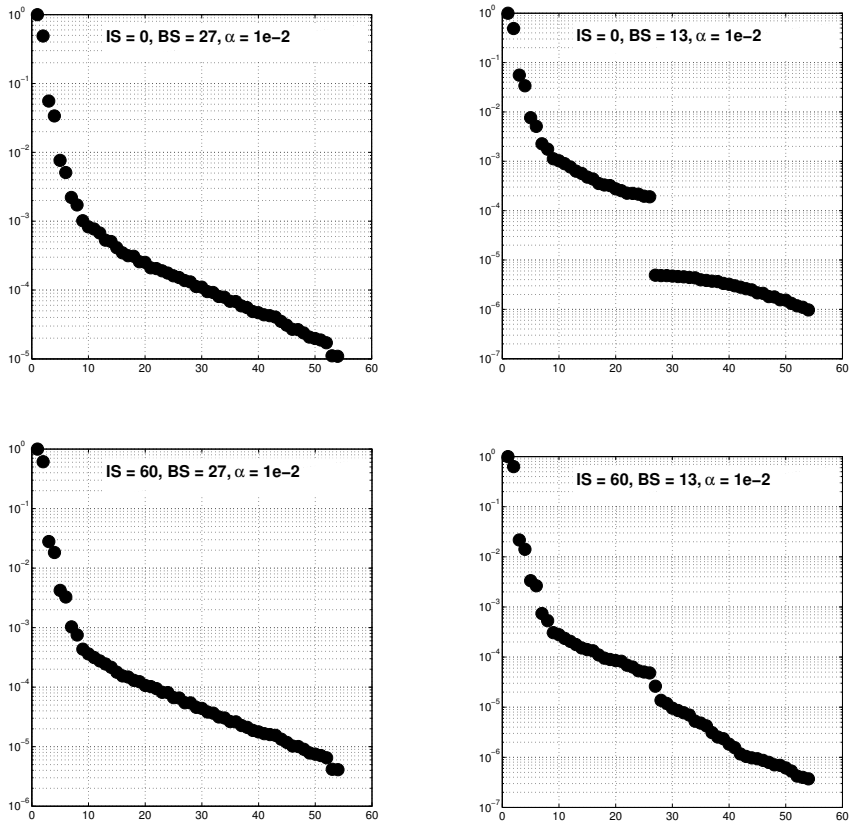

Figure 3.7: Singular values of W with α = 1e-2 for IS = 0 and 60 and BS = 27 and 13.

$\nu_2 = 0.01$ is driven by the fact that ν_2 induces ill-conditioning of the forward problem associated with the matrix S.

From results reported in Table 3.3 we can infer two considerations. With high Reynolds number the accuracy of the recovered solution is worse, this is due to numerical instability which arises with problems dominated by advection phenomena. Despite this, the condition number of the control problem is lower than in the stable case. This is consistent with the theory presented by Lions in [59] and by Gunzburger in [23], Chapter 1. In these works the key idea is that the more a system is unstable (and more sensitive to perturbations), the simplest, or the cheapest, it is to achieve exact or

BS	IS	K_1	E_U	it
27	0	1.3e+06	0.0380	17
13	0	2.0e+21	0.0802	12
9	0	5.7e+21	0.2566	15
27	27_{in}	2.5e+06	0.0303	15
27	27_{out}	1.6e+06	0.0348	14
27	27_{mid}	1.9e+06	0.0331	14

BS	IS	K_1	E_U	it
27	0	1.8e+05	0.0616	21
13	0	4.0e+19	0.0877	17
9	0	7.1e+19	0.1372	14
27	27_{in}	3.7e+05	0.0574	19
27	27_{out}	3.7e+05	0.0498	19
27	27_{mid}	3.7e+05	0.0461	18

Table 3.3: Condition number, relative error and number of iterations with SNR = 20 for different choices of sites and viscosity: $\nu = 0.1$ (left) and $\nu = 0.01$ (right). Subscripts in, out and mid refer respectively to IS close to the inflow, outflow and middle of the domain.

approximate controllability. Also, results of Table 3.3 are consistent with the result reported in [60] which states that the noise affecting the data decays exponentially with respect to the distance from the inflow boundary. With a low Reynolds number the introduction of sites located close to Γ_{in} improves the accuracy; for high Reynold number the solution of the forward problem has a slower decay as we move far form Γ_{in}; this fact implies that internal sites significantly determine the accuracy of the solution.

Remark 6 When the value of the kinematic viscosity induces advection-dominated phenomena we can stabilize the formulation adding artificial terms to the weak form of the problem, see [42] chap. 6. These terms modify the matrix and in some cases they might also circumvent the inf-sup condition so to allow the choice of incompatible FE spaces. Using a simple and straightforward method we stabilize the problem and check possible effects on the DA process. We consider the *Streamline Diffusion* method; we add artificial viscosity in the predominant direction of the advection field. Formally we add the term

$$s(\mathbf{u}, \mathbf{v}) = \xi(\Delta, \boldsymbol{\beta}) \int_{\Omega} (\boldsymbol{\beta} \cdot \nabla \mathbf{u}) (\boldsymbol{\beta} \cdot \nabla \mathbf{v}) \ \mathrm{d}\mathbf{x}; \tag{3.27}$$

where the stabilization coefficient ξ is defined as $\xi(\Delta, \boldsymbol{\beta}) = \frac{\Delta}{2\|\boldsymbol{\beta}\|_2}$. According to the Strang Lemma for generalized Galerkin methods (see [42]), the expected convergence rate for the velocity discretization error is only linear. Figure 3.8 displays results ob-

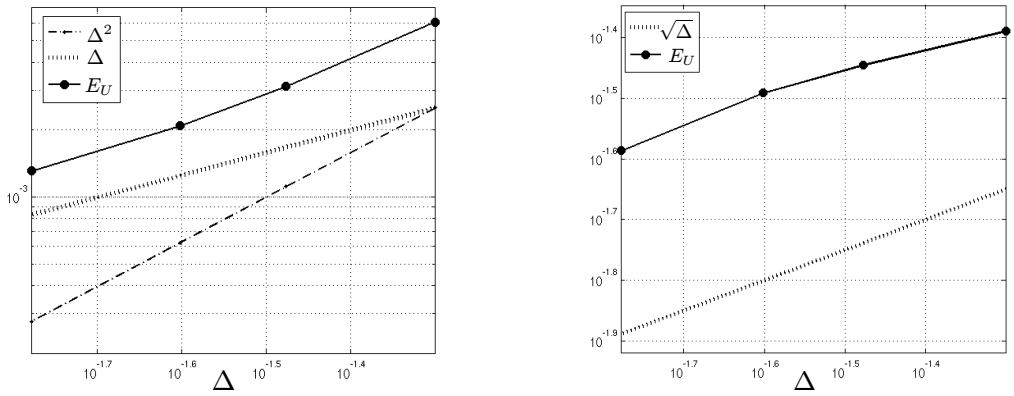

Figure 3.8: Relative errors versus Δ for noise-free (left) and noisy data (right) problem. Reference curves, Δ^2 and Δ (left) and $\sqrt{\Delta}$ (right), are reported for a comparison.

tained with $\nu = 0.005$, SNR $= \infty$ (left) and SNR $= 8$ (right) and data on Γ_{in} satisfying well-posedness conditions. In case of noise-free data, the discretization error E_U versus Δ, as expected, has linear convergence rate. In the noisy case, convergence rate is of the order of $\mathcal{O}(\sqrt{\Delta}) \sim \mathcal{O}(\sqrt{N_s^{-1}})$, as observed for the Stokes problem in Chapter 2. Again, we note that, for a given set of N independent identically distributed random variables, the standard deviation is proportional to $N^{-0.5}$; this explains our results. We conclude that including artificial stabilizing term does not compromise the assimilation process, indeed it improves the conditioning of the forward problem.

The interpolation strategy We report numerical results on the interpolation technique addressed in Section 3.2.2; our main aim is to investigate its reliability and competitiveness with respect to the usual Tikhonov regularization. Also, we point out some facts related to the dependence of the conditioning of the problem on sites location as a further confirmation of results presented in Section 3.2.1.

In Table 3.4 in correspondence of different choices of location and number of sites we report the relative error and the number of GMRES iterations for two different grids. Here, in the first column, “grid” stands for “points located on grid nodes”, i.e. on DOFs;

note that $N_{in} = 12$ (right) and 27 (left). The case where neither Tikhonov regularization or interpolation are performed is reported as a reference test. α_{DP} is the optimal regularization parameter obtained using DP. The activation of the interpolation process is determined by the flag `i`: when 0 no interpolation is performed and $\mathbf{d}$ corresponds to given data; when 1, $\mathbf{d}$ corresponds to both the original data and the interpolated values on grid nodes. From these results, we can infer the following considerations.

The interpolation process has the effect of yielding the well-posedness of the problem, moreover, interpolation can improve both the conditioning and the accuracy of the computed solution. We note that interpolation is a competitive technique with respect to common regularization methods in terms of accuracy. Tikhonov regularization is not a consistent technique, even in absence of noise; in fact, it modifies the nature of the problem adding an artificial term to the formulation. As opposed to this, using interpolation with noise free data, the assimilated solution is as accurate as a FE solution of the forward problem with exact boundary conditions. Furthermore, it requires much less computational time. In fact, we recall that the DP requires the iterative solution of reduced systems for retrieving the optimal parameter α_{DP}.

In order to get the picture of what has been implemented, in Figure 3.9 we report the sparse and interpolated data (left) and the corresponding assimilated solution (right).

3.3 Iterative procedure for the nonlinear problem

We consider the nonlinear advection term $(\mathbf{u} \cdot \nabla)\mathbf{u}$ and we solve a nonlinear PDE constrained optimization problem. In literature several methods are available for the solution of the discretized problem; among those we mention the Newton method [45] and its variants (common optimization methods will be addressed in future works with comparison purposes). Here, we address this issue by combining the DA procedure for

BS	i	α_{DP}	E_U	it
11 (grid)	0	-	0.108	14
5 (grid)	0	-	0.831	9
6	0	-	0.182	10
6	0	0.047	0.150	11
6	1	-	0.167	14
3 (grid)	0	-	0.888	6
4	0	-	0.312	8
4	0	0.056	0.214	14
4	1	-	0.262	13

BS	i	α_{DP}	E_U	it
27 (grid)	0	-	0.050	19
13 (grid)	0	-	0.076	13
14	0	-	0.068	14
14	0	0.021	0.061	15
14	1	-	0.059	18
9 (grid)	0	-	0.196	15
8	0	-	0.199	11
8	0	0.038	0.137	18
8	1	-	0.139	17

Table 3.4: Relative error and number of GMRES iterations (GMRES tolerance tol=1.e-6) in correspondence of $\Delta = 1/6$ (left) and $1/14$ (right). IS = 0 and SNR = 20.

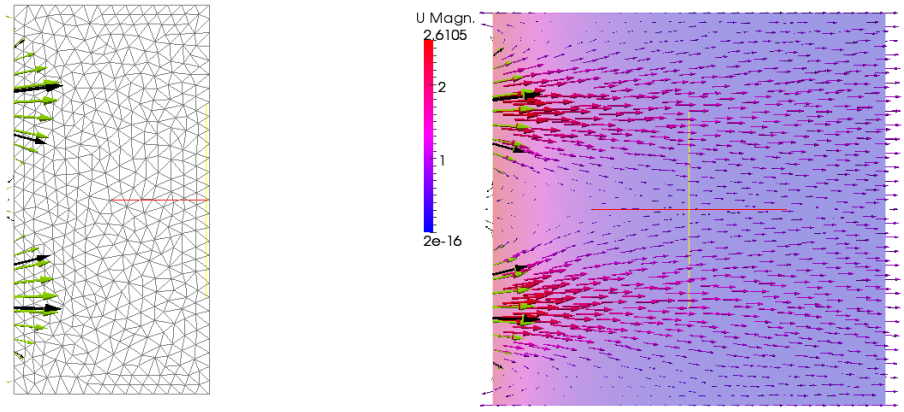

Figure 3.9: On the left, actual data used in the DA process (original and interpolated). On the right, pressure and velocity regularized solution and data.

the linear case presented in the previous section with classical fixed point linearization schemes. In particular, we refer to Picard and Newton methods [42]. The DA assimilation problem is solved iteratively as follows. Let $\mathbf{U}_k$ be a given guess for the velocity field at iteration $k+1$. The discrete iterative procedure reads

$$\begin{aligned} &\min_{\mathbf{H}_k} \frac{1}{2}\|\mathrm{D}\mathbf{V}_{k+1} - \mathbf{d}\|_2^2 + \frac{\alpha}{2}\|\mathrm{L}\mathbf{H}_{k+1}\|_2^2 \\ &\text{s.t.} \quad \mathrm{S}_k\mathbf{V}_{k+1} = \mathrm{R}_{in}^{\mathrm{T}}\mathrm{M}_{in}\mathbf{H}_{k+1} + \mathbf{F}_k \end{aligned} \tag{3.28}$$

up to fulfillment of a convergence criterion (typically $\|\mathbf{V}_k - \mathbf{V}_{k+1}\| \leq \delta$, being δ a user defined tolerance chosen empirically in our case). We use the following notation

$$\mathrm{S}_k = \begin{bmatrix} \mathrm{C} + \mathrm{A}_k & \mathrm{B}^{\mathrm{T}} \\ \mathrm{B} & \mathrm{O} \end{bmatrix}, \qquad \text{and} \qquad \mathbf{F}_k = \mathbf{F} + w\mathbf{Y}_k. \tag{3.29}$$

Here, A_k comes from the discretization of $(\overline{\mathbf{u}}_k \cdot \nabla)\mathbf{u}_{k+1} + w(\mathbf{u}_{k+1} \cdot \nabla)\overline{\mathbf{u}}_k$ ($w = 0$ for Picard method, 1 for Newton); $\mathbf{Y}_k$ is the discretization of $(\overline{\mathbf{u}}_k \cdot \nabla)\overline{\mathbf{u}}_k$. Here $\overline{\mathbf{u}}_k$ is defined as $\vartheta\mathbf{u}_{k-1} + (1-\vartheta)\mathbf{u}_k$, being $\vartheta \in [0,\, 1]$, w is a relaxation parameter, also chosen empirically. A necessary condition for the convergence of algorithm (3.28) is the existence of a unique solution, at each iteration of the optimization problem, which has been proved in Section 3.2.1. In Figure 3.10 (left) we show numerical evidence of the convergence: in a logarithmic scale we report, at each iteration of algorithm (3.28) with w = 0.8, the relative error, with respect to a reference solution, defined as $E_U = \frac{\|\mathbf{U}_k - \mathbf{U}_{anl}\|_2}{\|\mathbf{U}_{anl}\|_2}$, $\mathbf{U}_{anl}$ being as in (3.26). For increasing number of iterations the graph shows a convergence to a limit value in correspondence of different values of SNR. Also, numerical tests show that the number of iterations is almost Δ-independent, where Δ is the discretization step used for the FE approximation. Figure 3.10 (right) reports relative errors E_U and number of iterations `it` for different values of Δ. In the table SNR and N_s are fixed.

Due to the local convergence of the Newton method for the forward problem, a common procedure is to perform a few Picard iterations and use the resulting velocity as initial guess (we refer to this method as Picard-Newton). The activation of the Newton method is driven by the parameter $w \in [0,\, 1]$.

3.3.1 Numerical results

In this Section we test the DA procedure for the NSE on 2-dimensional and axisymmetric cases. With noise-free and noisy data, we conduct a consistency analysis, and we discuss the filtering properties of the method on an analytic test case. Synthetic

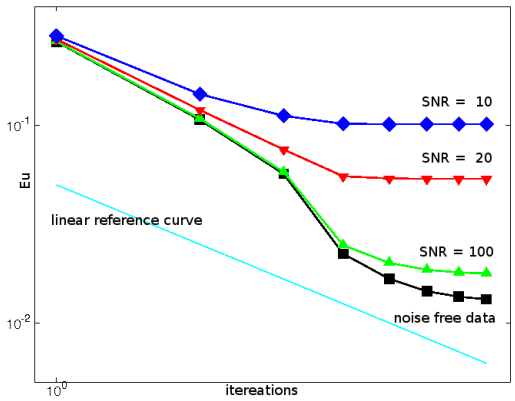

Δ	E_U	it
1.7e-1	0.0534	9
7.1e-2	0.0288	9
5.0e-2	0.0241	9

Figure 3.10: Left: relative error $E_{\mathbf{U}}$ versus number of iterations in correspondence of different values of SNR. Right: Relative error $E_{\mathbf{U}}$ and number of iterations of algorithm (3.28) for SNR $= 20$ and $N_s = 160$.

data are generated either from a given analytical solution or a numerical solution of the forward problem. We also show results obtained on 2-dimensional non-rectangular domains, retrieving from the assimilated velocities a flow-related variable of medical relevance, namely the wall shear stress (WSS). Finally, we present results obtained with an axisymmetric formulation of the problem in a cylindrical domain.

Noise-free data We analyze the error with respect to the analytic solution. We set $\alpha = 0$ and consider data on DOFs on Γ_{in} and on three internal layers ($x = 0,\ 0.5,\ 1$).

In Table 3.5 (left) we report for the Picard-Newton method the error E_U and the number of Picard-Newton iterations (the number of Newton iterations to get convergence is reported in brackets) in correspondence of different mesh sizes Δ. Same results are reported in Figure 3.11 (left) in a logarithmic scale with a reference quadratic curve, the expected FE convergence rate is recovered. Moreover, we observe that the number of iterations needed for the convergence is almost mesh independent.

Noisy data We investigate the dependence of the relative error E_U on the number of available measures and on the amount of noise. Regularization parameter and data

Δ	E_U	it
0.160	4.97e-2	5 (3)
0.072	9.49e-3	4 (2)
0.050	4.73e-3	4 (2)

N_s	E_U	it
22 (11+11)	9.01e-2	7 (3)
44 (22+22)	6.01e-2	9 (5)
88 (44+44)	4.52e-2	7 (3)

Table 3.5: On the left results for noise-free simulations; on the right results for SNR =20 and $\Delta = 0.160$, in the first column N_s = (BS + IS). In the third column, in brackets, the number of Newton iterations.

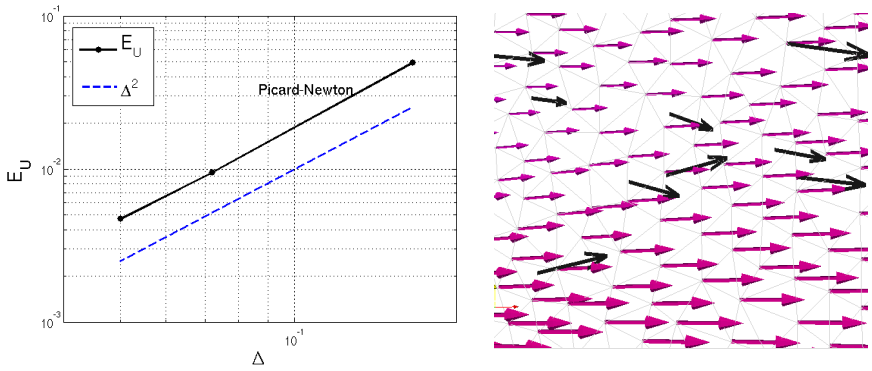

Figure 3.11: Left: relative errors versus Δ, Picard-Newton iterations with noise free data. Right: assimilated velocity with noisy data (black) for SNR =20 in a region with horizontal analytical solution.

are set as in the previous paragraph. In Table 3.5 (right) we report the discretization error and the number of iterations for the Picard-Newton method in correspondence of SNR = 20 and $\Delta = 0.160$ for different number of sites N_s = BS + IS, where BS and IS are the number of boundary and internal sites. In this case $w = 0.8$. In Figure 3.12 (left) we report the average discretization error over 100 noise realizations, E_{100}, and a reference curve $\mathcal{O}(N_s^{-0.5})$. Same statistical considerations reported in Section 2.3.3 and 3.2.3 may be inferred. In Figure 3.12 (right) we report in a logarithmic scale the average error versus the inverse of SNR for SNR = 33.3, 20, 10, 8.3 and $\Delta = 0.072$. We can notice a linear behavior by a comparison with the dashed reference curve. In Figure 3.13 we report the relative error E_U of the sample mean of the velocity over N_r noise realizations: $\overline{\mathbf{U}} = \frac{1}{N_r}\sum_{i=1}^{N_r}\mathbf{U}_i$, where $\mathbf{U}_i$ is the velocity corresponding to the i-th

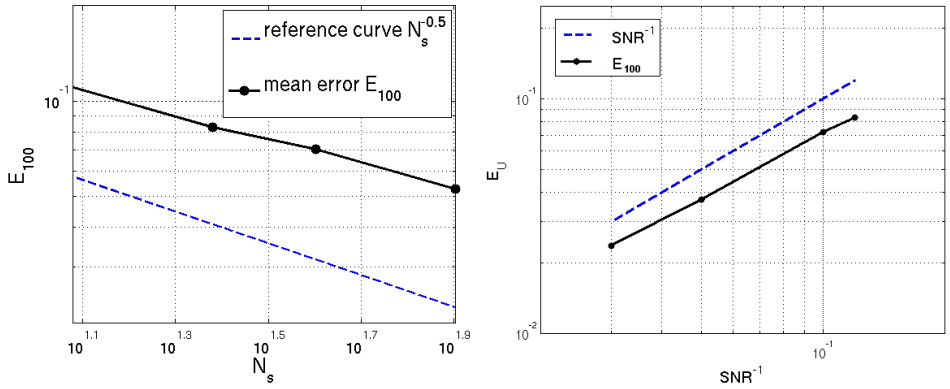

Figure 3.12: Relative errors E_U versus Δ with noisy data (left); relative errors E_U versus SNR^{-1} (right) for Picard-Newton iterations.

noise realization. As expected, the error converges with rate -0.5 to the discretization error for noise-free data.

In Figure 3.11 (right) we report a zoom of the computed field and the noisy data in a region with horizontal analytical solution; the presence of the noise is evident in the vertical components and in low magnitude velocities; this happens since the amount of noise does not depend on the local magnitude of the velocity vector field. In correspondence of these low magnitude values the recovered assimilated field differs significantly from the data and it is closer to the exact solution. This pinpoints the role of the assimilation procedure as a sophisticated way for filtering noise from the data, based on the mathematical model of the process at hand.

3.4 Towards real geometries

In this section we consider more complex geometries, which are intended to resemble vessels of medical interest. In Test case I and II we reproduce in 2-dimensional curved computational domains a section of the carotid and of the aorta respectively. In test case III we consider a 3-dimensional cylindrical domain treated with an axisymmetric formulation.

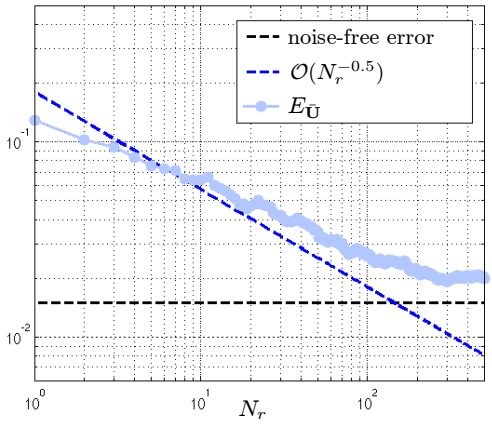

Figure 3.13: Relative error of $\overline{\mathbf{U}}$ versus number of noise realizations N_r.

Test case I We assume that some measurements of the blood velocity are available on Γ_{in} and on sparse internal sites, see Figure 3.14 (left) for domain and data. In real applications the SNR is strongly determined by the biomedical tools used to observe the data; when using data processed from a scan of the aorta, it can be as low as 10 for flow measures (personal communication of Dr. M. Brummer, Emory CHOA). In Figure 3.14 (left) a comparison between reference velocity and noisy data is reported. Data on Γ_{in} do not satisfy conditions for the well-posedness, consequently interpolation is performed. In this test case, since we are not provided with real data and an analytic solution is not available, we consider synthetic data generated from a reference solution, $\mathbf{U}_{\mathrm{FE}}$. This is a FE solution computed on very fine grid (300% of nodes used for the test case) where the discretization error is considered fairly small. For the computation of $\mathbf{U}_{\mathrm{FE}}$ we prescribe the following boundary conditions:

$$\mathbf{u} = \mathbf{0} \ \text{ on}\,\Gamma_{wall}, \ -\nu\,(\nabla\mathbf{u} + \nabla\mathbf{u}^{\mathrm{T}})\mathbf{n} + p\,\mathbf{n} = \mathbf{0} \ \text{ on}\,\Gamma_{out}, \ \mathbf{u} = [0 \ \ g(x)]^{\mathrm{T}} \ \text{ on}\,\Gamma_{in}, \quad (3.30)$$

where $g(x) = k\,x\,(2r - x)$, $\nu = 3.5\,\frac{mm^2}{s}$, $2r = 7\,mm$ (Γ_{in} length) and $k = 12\,ms^{-1}$.

In the generation process, we introduce a projection matrix, P from the fine to the coarse grid. Data are generated adding random noise to $\mathrm{P}\mathbf{U}_{\mathrm{FE}}$ on selected sites. The reference solution is affected both by the FE approximation error and the projection one; however, this fact does not penalize the reliability of results since approximation and projection errors can be regarded as part of the noise. As index of accuracy we consider the ratio $E_{\mathbf{U}} = \frac{\|\mathbf{U}-\mathrm{P}\mathbf{U}_{\mathrm{FE}}\|_2}{\|\mathrm{P}\mathbf{U}_{\mathrm{FE}}\|_2}$.

In Figure 3.14 (center) we report the magnitude of velocity field assimilated from noisy data with SNR = 20. In this case, with Tikhonov regularization (α = 0.1), $E_{\mathbf{U}}$ = 8.074e-2 after 60 Picard-Newton iterations. We note that the noise mainly affects the components of the velocity which are transversal to the flow; despite this, the recovered field is close to the reference solution. This fact confirms the noise-filtering property of the proposed method. It is interesting to observe the streamlines in the bulb area (see Figure 3.14, right) where we expect to have recirculation and vortex formation.

To test the competitiveness of the DA procedure we compare the relative error of the assimilated velocity with the one of the velocity obtained from a forward simulation (here, Dirichlet boundary conditions are prescribed using the interpolated data retrieved from sparse sites on Γ_{in}) in this case $E_{\mathbf{U}}$ = 15.957e-2. This comparison confirms the reliability of the DA procedure and the gain, in accuracy, that we obtain with respect to solving a forward problem, even if computationally expensive.

The wall shear stress We consider the computation of the WSS $\boldsymbol{\tau}$ which is a quantity of medical interest. An accurate approximation of the WSS is fundamental in the investigation of cardiovascular pathologies since it is an index of the possibility of rupture of the vessel wall and formation of stenosis [3]. It is defined as the tangential component of the stress exerted by the fluid (blood in this case) on the wall, formally

$$\boldsymbol{\tau} = \nu(\nabla\mathbf{u} + \nabla\mathbf{u}^{\mathrm{T}})\mathbf{n} - \nu\left(\left((\nabla\mathbf{u} + \nabla\mathbf{u}^{\mathrm{T}})\mathbf{n}\right)\cdot\mathbf{n}\right)\mathbf{n}, \tag{3.31}$$

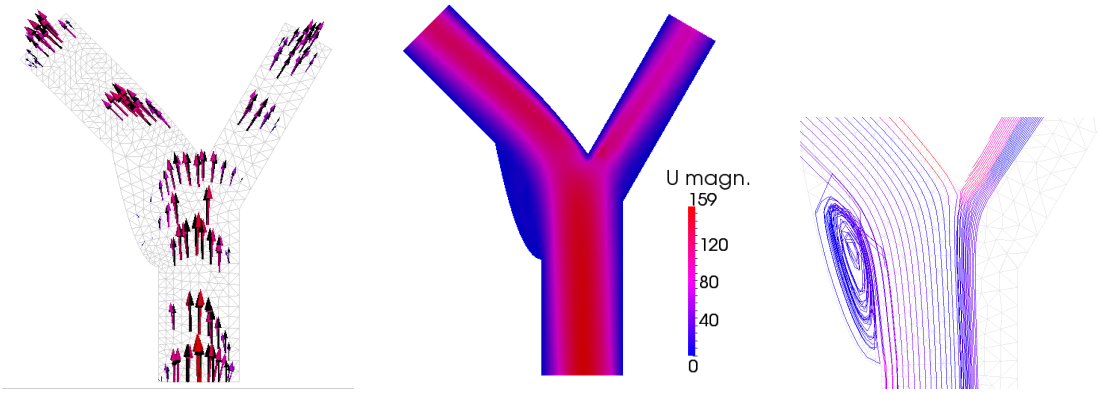

Figure 3.14: Left: actual data used in the DA process (original, in black, and interpolated). Center: magnitude of the velocity vector field. Right: detail of the stream lines.

where $\mathbf{n}$ is the normal vector in correspondence of the wall. Approximations of the WSS retrieved from indirect measurements are in general unreliable because of the post-processing numerical errors and the noise affecting the measures. Including measurements in simulations is a way for improving the reliability of computed solutions. In fact, the introduction of the numerical blood flow model results in noise filtering: thanks to the assimilation process, the recovered WSS catches accurately the behavior of the reference one. These preliminary results pinpoint again the role of DA as a way for filtering and eventually computing hemodynamics indexes with good accuracy. In order to have a quantitative comparison with the reference solution we introduce an index of accuracy of the magnitude of the WSS vector field on Γ_{wall}, $E_{\mathrm{WSS}} = \frac{\|\mathrm{WSS}-\mathrm{WSS}_{\mathrm{FE}}\|_2}{\|\mathrm{WSS}_{\mathrm{FE}}\|_2}$; where $\mathrm{WSS}_{\mathrm{FE}}$ is the value retrieved from the reference solution $\mathrm{P}\mathbf{U}_{\mathrm{FE}}$.

Table 3.6 (left) reports, in correspondence of decreasing SNR, errors obtained with the assimilated velocity field, $E_{\mathrm{WSS,DA}}$, compared with those obtained from a forward simulation on the same grid with Dirichlet boundary conditions (interpolating function retrieved from sparse data) on Γ_{in}, $E_{\mathrm{WSS,FW}}$. With high SNR the gain obtained with DA process is not significant, as we decrease SNR we can obtain up to the 50% of gain

SNR	$E_{\mathrm{WSS,DA}}$	$E_{\mathrm{WSS,FW}}$
100	0.2536	0.2667
20	0.2591	0.3030
10	0.2738	0.3861
5	0.3149	0.6114

slices	S	E_U
none	0	0.01600
s_1	5	0.00985
s_1, s_2	5	0.00576
s_1, s_2, s_3	5	0.00992
s_1	10	0.00554
s_1, s_2	10	0.00535
s_1, s_2, s_3	10	0.00647
s_4, s_5	10	0.00724

Table 3.6: Left: comparison of relative errors for the WSS computed with DA and forward solution for test case I. Right: relative errors for different s and S for test case II.

with respect to the forward simulation. The accuracy in the computation of the WSS can be improved; nevertheless, the comparison with results from a forward simulation highlights the strength of the assimilation procedure and the relevance of internal data. Also, numerical tests proved that, as we increase the number of internal data, we obtain more accurate solutions.

Test case II We consider a 2-dimensional computational domain approximating a section of the aortic arc. We assume to have velocity measurements on Γ_{in} and on three internal layers Γ_d, as shown in Figure 3.15 (left), with the purpose of mimicking Figure 1.1. Data are synthetic and, as in test case I, they are generated from a reference solution, $\mathbf{U}_{\mathrm{FE}}$, computed on a very fine grid (300% of nodes used for the test case). For its computation we prescribe the following boundary conditions

$$\mathbf{u} = \mathbf{0} \text{ on } \Gamma_{wall}; \quad -\nu(\nabla\mathbf{u}+\nabla\mathbf{u}^{\mathrm{T}})\mathbf{n}+p\,\mathbf{n} = 0 \text{ on } \Gamma_{out}; \quad \mathbf{u} = [\,0 \;\; (x-r_1)(r_2-x)\,]^T \text{ on } \Gamma_{in}, \tag{3.32}$$

where $r1 = 2$ and $r_2 = 6$. In Figure 3.15 (right) we report the computed pressure, the velocity vector field and noisy data (SNR = 10). The noise mainly affects the components of the velocity which are transversal to the flow; in the recovered field such components are filtered. Here, $E^*_{\mathbf{U}} = 5.12\text{e-}2$ after 40 Picard-Newton iterations.

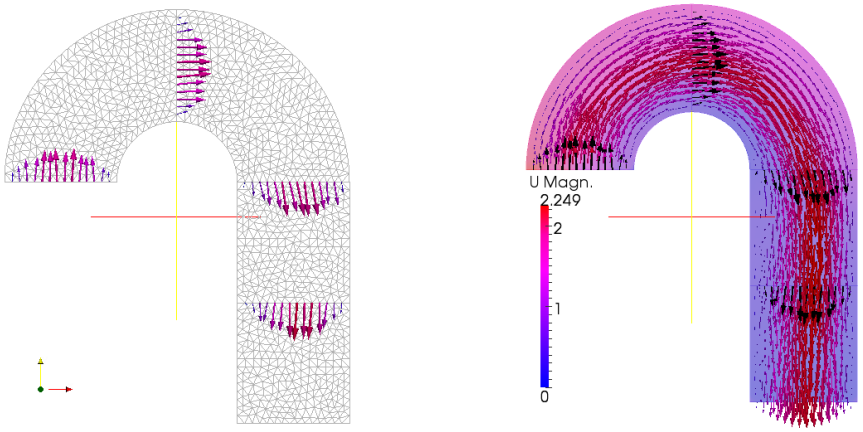

Figure 3.15: On the left, computational mesh reproducing the aortic arc and noise free data. On the right, pressure and velocity fields recovered from noise free data.

In Figure 3.16 we report a comparison between the WSS computed using the reference solution $\mathbf{PU}_{\mathrm{FE}}$ and the one computed upon assimilated velocities; the assimilated WSS approximate the reference WSS with $E_{\mathrm{WSS,DA}} = 0.2401$.

Test case III We consider a 3-dimensional cylindrical domain with radius r and height h. Exploiting symmetry, we formulate the problem in an axisymmetric formulation and we solve it problem in a rectangular domain, the shaded area in Figure 3.17 (left). We assume to have data on the inflow boundary not satisfying optimality conditions and we perform interpolation. We also assume that additional internal data are available. More precisely, we consider s internal slices (sections) with S data per slice, with the purpose of reproducing the setting of Figure 1.1. Data are generated adding to the Poiseuille flow random noise with SNR = 20. In Figure 3.17 (right) we report, for r = 1.5 cm, h = 6 cm, s = 5 and S = 10, the data and the recovered vector field. The relative error with respect to the Poiseuille reference solution is E_U = 0.007793. In Figure 3.18 we report, for s = 5 and S = 17, a 3-dimensional visualization the data and the assimilated velocity: the magnitude of the velocity is displayed in three sections in the lower part of the cylinder, the vector field in the upper ones.

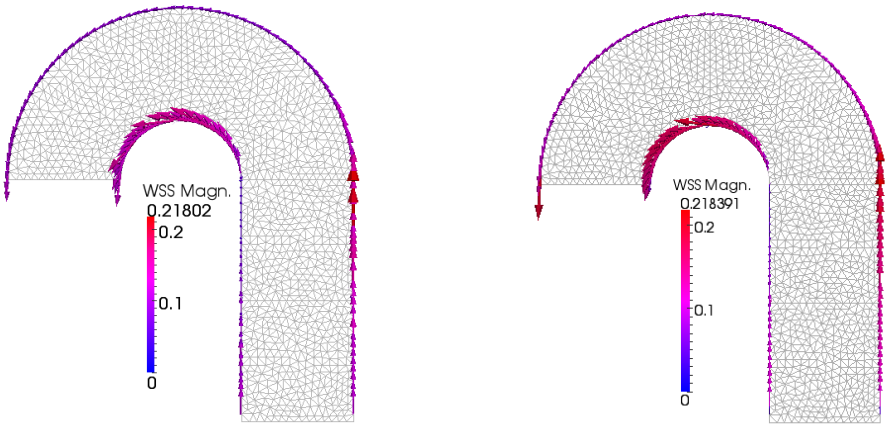

Figure 3.16: Comparison between the map of the stress exerted by the blood in the arterial wall recovered from the reference solution, on the left, and from noisy velocity data of Figure 3.15 (left), on the right.

We investigate the accuracy of the assimilated solution using fixed SNR and Δ, results are reported in Table 3.6 (right). In this test case we consider s slices such that each slice $s_k,\ k = 1, ..., s$ is placed at distance $k\,cm$ from Γ_{in}. The non-monotonic behavior of the error as a function of s might be surprising. The explanation resides in the presence of the noise, which has two different effects on the accuracy of the solution. On one hand additional data help the well-conditioning and accuracy (in absence of noise) of the problem, no matter their location. On the other hand, coherently with the result in [60], the incidence of noise in distal sections is supposed to be more relevant than in proximal sections. As a confirmation of this fact, we observe that using s_1 and s_2 gives a more accurate solution than s_4 and s_5.

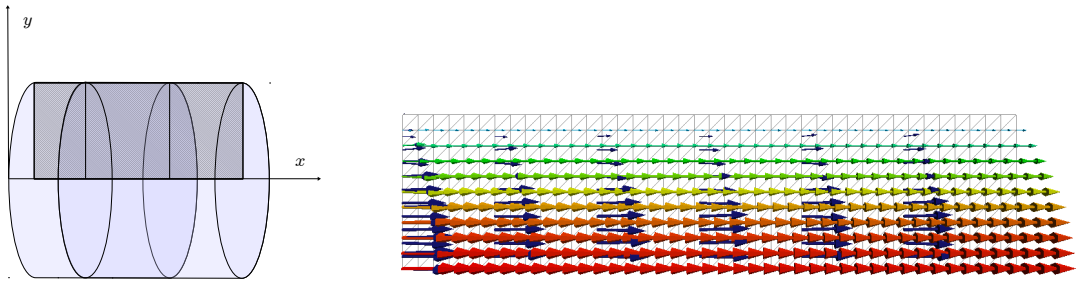

Figure 3.17: Left: in the axisymmetric formulation a rectangle is selected to be the computational domain. Right: data and assimilated vector field for $s = 5$ and $S = 10$.

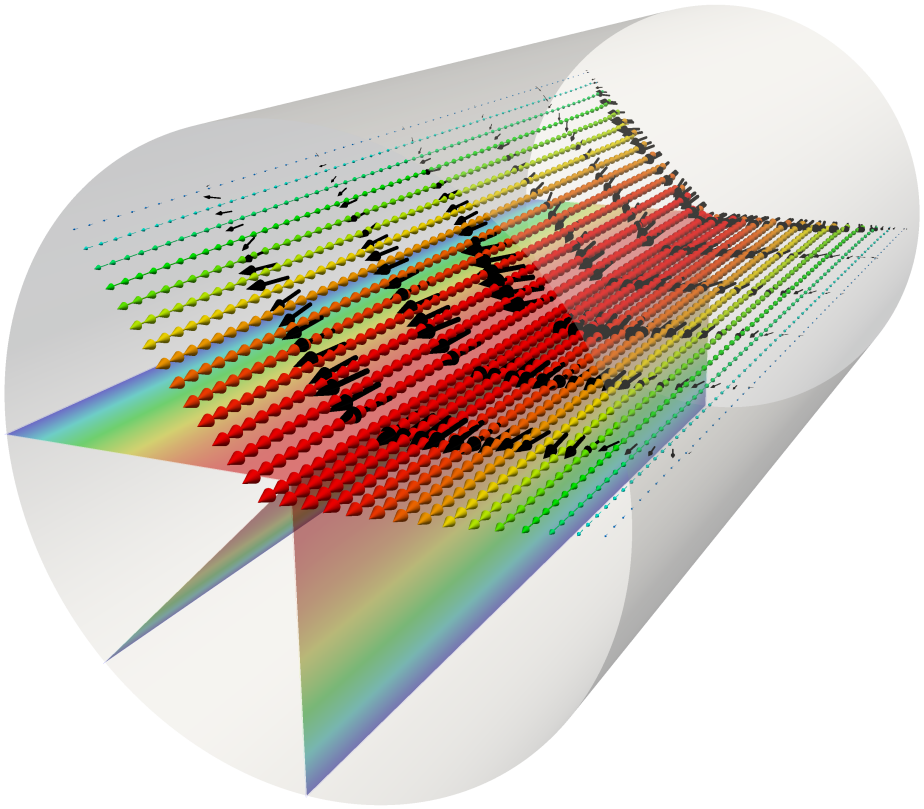

Figure 3.18: 3-dimensional visualization the data and the assimilated velocity.

4 A statistical approach to DA

The deterministic approach to DA presented in Chapter 3 provides an accurate and noise filtering estimator of the velocity of the fluid retrieved from noisy measures. A weak point of such approach is that, relying on a specific realization of noise it produces a single estimate of the state which might not be representative of the whole state distribution. Moreover, in the deterministic approach measures are considered as if they were independent. In the context of hemodynamics, which is characterized by complex phenomena, this is a limiting feature since additional a priori information regarding the noise is not taken into account.

In medical applications an evaluation of reliability of simulations and numerical results is mandatory; for our method to be a valid tool supporting medical practice it is important to quantify the credibility of predictions in statistical terms. These include computing the most likely value for the velocity or a set of values which the state is most likely to belong to. These goals are achieved when we determine the statistical distribution of the velocity and related variables; this task requires prior information about the variables involved and of the noise affecting the observations.

In this chapter, based on [61] (in preparation), we present a Bayesian approach to DA; the purpose is to find a probability distribution for the state variable, treated as random. Parameters of the probability density function (PDF), such as mean value and variance, and induced confidence regions allow to quantify the uncertainty of numerical simulations.

In Section 4.1 we introduce basic statistical notation and properties of normal ran-

dom vectors which are useful in dealing with our application. In Section 4.2 we introduce the mathematical formulation of the Bayesian method applied to the linearized NSE and we extend the formulation to the nonlinear case using the algorithm for the nonlinear equations introduced in Chapter 3. Then, we present point estimators, namely the maximum a posteriori (MAP) and the maximum likelihood (ML) estimators, and spread estimators (confidence regions) based on the PDF of the normal stress on the inflow boundary. In Section 4.3 we recall the regularization technique based on interpolation developed in Chapter 3 and we show how it affects the statistical formulation. In Section 4.4 we present numerical results in correspondence of the same test cases used to test the deterministic formulation in Chapter 3. We compare statistical and deterministic point estimators and we compute confidence regions for the velocity ans the wall shear stress WSS.

4.1 The multivariate normal distribution

In this section we report basic concepts regarding the normal distribution for random vectors and we introduce properties and results specifically related to our application. In particular, we focus on statistical properties of affine transformations of normal random vectors which are used in Section 4.2.3 to derive the velocity PDF.

4.1.1 The multivariate normal PDF

The multivariate normal distribution is a generalization to dimensions $d \geq 2$ of the univariate normal distribution. For the univariate case, a Gaussian random variable X with mean μ and variance σ^2 has PDF

$$f(x) = \frac{1}{\sqrt{2\pi\sigma^2}} exp\left\{-\frac{(x-\mu)^2}{2\sigma^2}\right\} \quad \forall\, x \in (-\infty, \infty), \tag{4.1}$$

and it is denoted $X \sim \mathcal{N}(\mu, \sigma^2)$.

In the multivariate case the formula is generalized to a d-dimensional vector; in particular, the exponent has the form

$$(\mathbf{x}-\boldsymbol{\mu})^{\mathrm{T}}\Sigma^{-1}(\mathbf{x}-\boldsymbol{\mu}) \tag{4.2}$$

where $\boldsymbol{\mu} \in \mathbb{R}^d$ represents the expected value of the multivariate random variable $\mathbf{X}$ and Σ is the symmetric positive definite covariance matrix of $\mathbf{X}$, i.e. $\Sigma_{i,i} = var(\mathbf{X}_i)$ and $\Sigma_{i,j} = \Sigma_{j,i} = cov(\mathbf{X}_i, \mathbf{X}_j)$ for $i, j = 1, ..., d$. The normalizing constant $1/\sqrt{2\pi\sigma^2}$ has to be generalized to a constant such that the volume under the density surface is unitary. It can be shown, see [62] that such constant is

$$\frac{1}{\sqrt{(2\pi)^d det(\Sigma)}}. \tag{4.3}$$

Thus, the multivariate normal PDF has the form

$$f(\mathbf{x}) = \frac{1}{\sqrt{(2\pi)^d det(\Sigma)}} exp\left\{-(\mathbf{x}-\boldsymbol{\mu})^{\mathrm{T}}\Sigma^{-1}(\mathbf{x}-\boldsymbol{\mu})\right\} \quad \forall\, x_i \in (-\infty, \infty),\ i = 1, ..., d \tag{4.4}$$

and we say $\mathbf{X} \sim \mathcal{N}(\boldsymbol{\mu}, \Sigma)$. It is easy to show that $\boldsymbol{\mu}$ is the point of maximum density, mode and expected value [62].

Contour lines Contours of constant density c play a central role in determining confidence regions for multivariate normal variables. For the d-dimensional distribution these are ellipsoids generated by the equation

$$(\mathbf{x}-\boldsymbol{\mu})^{\mathrm{T}}\Sigma^{-1}(\mathbf{x}-\boldsymbol{\mu}) = c^2; \tag{4.5}$$

these ellipsoids are centered in $\boldsymbol{\mu}$ and have axes $\pm c\sqrt{\lambda_j}\mathbf{e}_j$, where λ_j are the eigenvalues of Σ and $\mathbf{e}_j$ the associated eigenvectors for $j = 1, ..., d$.

4.1.2 Properties of the multivariate normal distribution

In this section we report a few properties which are relevant for results discussed in this chapter and we introduce the chi-squared, χ^2, distribution.

For a d-dimensional normal random vector $\mathbf{X} \sim \mathcal{N}(\boldsymbol{\mu}, \Sigma)$ we have the following properties:

P1 Affine transformations of $\mathbf{X}$ are normally distributed. In particular, given $\mathrm{A} \in \mathbb{R}^{q \times d}$ and $\mathbf{b} \in \mathbb{R}^q$, then $\mathbf{Y} = \mathrm{A}\mathbf{X} + \mathbf{b} \sim \mathcal{N}_q(\mathrm{A}\boldsymbol{\mu} + \mathbf{b}, \mathrm{A}\Sigma\mathrm{A}^{\mathrm{T}})$.

P2 All subsets of the components of $\mathbf{X}$ have normal distribution. If we rearrange the vector as

$$\mathbf{X} = \begin{bmatrix} \mathbf{X}_1 \\ \mathbf{X}_2 \end{bmatrix}, \quad \boldsymbol{\mu} = \begin{bmatrix} \boldsymbol{\mu}_1 \\ \boldsymbol{\mu}_2 \end{bmatrix}, \quad \Sigma = \begin{bmatrix} \Sigma_{1,1} & \Sigma_{1,2} \\ \Sigma_{2,1} & \Sigma_{2,2} \end{bmatrix}, \tag{4.6}$$

where $\mathbf{X}_1 \in \mathbb{R}^q$ and $\mathbf{X}_2 \in \mathbb{R}^{d-q}$; then, $\mathbf{X}_1 \sim \mathcal{N}_q(\boldsymbol{\mu}_1, \Sigma_{1,1})$ and $\mathbf{X}_2 \sim \mathcal{N}_{d-q}(\boldsymbol{\mu}_2, \Sigma_{2,2})$.

P3 We first introduce the chi-squared distribution.

The chi-squared distribution The chi-squared distribution with d degrees of freedom is the distribution of a sum of the squares of d independent standard normal random variables. If $X_1, ..., X_d$ are independent, standard, normal random variables, then the sum of their squares,

$$Z = \sum_{i=1}^{d} X_i^2, \tag{4.7}$$

is distributed according to the chi-squared distribution with d degrees of freedom. This is usually denoted as

$$Z \sim \chi_d^2. \tag{4.8}$$

The PDF of Z is given by

$$f(z;\, d) = \begin{cases} \dfrac{1}{2^{d/2}\Gamma(d/2)}\, z^{d/2-1} e^{-z/2}, & z \geq 0; \\ 0, & \text{otherwise} \end{cases} \tag{4.9}$$

where Γ denotes the Gamma function defined as $\Gamma(n) = (n-1)!$, for an integer n, and as $\Gamma(\frac{n}{2}) = \pi \frac{(n-2)!!}{2^{(n-1)/2}}$ for a half-interger $\frac{n}{2}$.

The third property relates normal vectors and the chi-squared random variable and allows us to draw confidence regions for Gaussian vectors.

- $(\mathbf{X} - \boldsymbol{\mu})^{\mathrm{T}} \Sigma^{-1} (\mathbf{X} - \boldsymbol{\mu})$ is distributed as χ^2_d, where χ^2_d denotes the chi-squared distribution [62] with d DOFs.
- The $\mathcal{N}(\boldsymbol{\mu},\, \Sigma)$ distribution assigns probability $(1-\alpha)$ to the ellipsoid $\{\mathbf{x} : (\mathbf{x} - \boldsymbol{\mu})^{\mathrm{T}} \Sigma^{-1} (\mathbf{x} - \boldsymbol{\mu}) \leq \chi^2_d(\alpha)\}$ where $\chi^2_d(\alpha)$ denotes the upper $(100\,\alpha)$-th percentile of the χ^2_d distribution.

4.2 Mathematical formulation

In this section we formulate the assimilation problem as a statistical inverse problem using the Bayesian approach; an extensive introduction to statistical inverse problems can be found in the book by Kaipio and Somersalo [63]. As done in Chapter 3 we present the formulation for the linearized NSE and then we extend it to the nonlinear formulation. Then, we derive statistical estimators for the velocity $\mathbf{U}$ in Ω.

The purpose of statistical inversion is the prediction of stochastic features of the variables of interest in order to quantify the credibility of numerical methods and simulations. The prediction of the uncertainty affecting the variables is based on the knowledge of (i) the measurement process; (ii) deterministic models of the unknowns [63].

In formulating the inverse problem we assume to deal with discretized variables, all treated as random. The randomness is in the degree of information of their realizations and such degree resides in the probability distributions. The entities involved are PDFs; in this respect, statistical approaches are different from deterministic ones which produce a single estimate of the unknown. Here the method delivers a distribution. In the following sections the bold variables denote random vectors while the capital plain variables a specific realization. With an abuse of notation we introduce the random variable $\mathbf{H}$ which describes the normal stress of the fluid at the inflow section; $\mathbf{M}$ is the random variable that describes the measures and ε the noise perturbing the measurements. We let $\pi_{pr}(H)$ be the PDF of $\mathbf{H}$, usually called *prior*, and $\pi_{noise}(\varepsilon)$ the one of ε; these distributions are assumed to be known. The *likelihood* function $\pi(M|H)$ denotes the PDF of the measurement conditioned on a realization of $\mathbf{H}$. The distribution of $\mathbf{H}$ conditioned on a realization of $\mathbf{M}$, $\pi(H|M) = \pi_{post}(H)$, is usually called *posterior*. The purpose of the Bayesian procedure is to estimate the posterior exploiting the Bayes formula (see e.g. [63])

$$\pi(H|M) = \pi_{post}(H) = \frac{\pi(M|H)\pi_{pr}(H)}{\pi(M)}; \tag{4.10}$$

where $\pi(M)$ is the PDF of the measures. Since we are interested in finding the variable $\mathbf{H}$, that maximizes the posterior distribution, the denominator does not affect the optimization process and we can simply consider the relation

$$\pi(H|M) = \pi_{post}(H) \propto \pi(M|H)\pi_{pr}(H). \tag{4.11}$$

Also, let us consider the linearized model that relates $\mathbf{H}$ and $\mathbf{M}$,

$$\mathrm{Z}\mathbf{H} + \varepsilon = \mathbf{M}. \tag{4.12}$$

Here, $\mathrm{Z} = \mathrm{D}\mathrm{S}^{-1}\mathrm{R}_{in}\mathrm{M}_{in}$ is the matrix introduced in Section 3.2, which relates the random variable representing the velocity measures to the variable $\mathbf{H}$ according to the deterministic model introduced in the previous section. This relation holds in the linearized case and takes into account the presence of the noise. The random variable ε accounts for the discrepancy between $\mathrm{Z}\mathbf{H}$ and $\mathbf{M}$. Models in the form (4.12) are referred to as *additive noise* and they are used with the assumption of mutual independence of $\mathbf{H}$ and ε. This assumption implies that the PDF of ε is independent of any realization of $\mathbf{H}$, say $\overline{H}$. Hence, the likelihood function can be expressed as

$$\pi(M|\overline{H}) = \pi_{noise}(M - \mathrm{Z}\overline{H}). \tag{4.13}$$

If we consider $M = \mathbf{d}$, a specific realization of $\mathbf{M}$, we rewrite (4.11) as

$$\pi_{post}(H) \propto \pi_{noise}(\mathbf{d} - \mathrm{Z}H)\pi_{pr}(H). \tag{4.14}$$

When we consider Gaussian random variables we can derive an explicit form for $\pi_{post}(H)$. We introduce the PDFs of $\mathbf{H}$ and ε, according to the notation reported in Section 4.1:

$$\begin{aligned} \pi_{pr}(H) &\propto exp\left\{-\frac{1}{2}(H - H_0)^{\mathrm{T}}\Sigma_{pr}^{-1}(H - H_0)\right\}, \\ \pi_{noise}(\varepsilon) &\propto exp\left\{-\frac{1}{2}(\varepsilon - \varepsilon_0)^{\mathrm{T}}\Sigma_{noise}^{-1}(\varepsilon - \varepsilon_0)\right\}; \end{aligned} \tag{4.15}$$

where H_0 and ε_0 are the expectation values and Σ_{pr} and Σ_{noise} are the correlation matrices for $\mathbf{H}$ and ε respectively. In the Gaussian assumption, using Theorem 3.7, Chapter 3 of [63], we can write (4.14) as

$$\pi_{post}(H) \propto exp\left\{-\frac{1}{2}(H - H_{post})^{\mathrm{T}}\Sigma_{post}^{-1}(H - H_{post})\right\}; \tag{4.16}$$

where the correlation matrix and the expectation value read

$$\begin{aligned} &\Sigma_{post} = (\Sigma_{pr}^{-1} + \mathrm{Z}^{\mathrm{T}}\Sigma_{noise}^{-1}\mathrm{Z})^{-1}, \\ &H_{post} = \Sigma_{post}(\mathrm{Z}^{\mathrm{T}}\Sigma_{noise}^{-1}(\mathbf{d} - \varepsilon_0) + \Sigma_{pr}^{-1}H_0) \Rightarrow \\ &(\Sigma_{pr}^{-1} + \mathrm{Z}^{\mathrm{T}}\Sigma_{noise}^{-1}\mathrm{Z})H_{post} = \mathrm{Z}^{\mathrm{T}}\Sigma_{noise}^{-1}(\mathbf{d} - \varepsilon_0) + \Sigma_{pr}^{-1}H_0. \end{aligned} \tag{4.17}$$

Using this result one can calculate point and spread estimates. As an example, we can answer questions like “how likely is the unknown inside a set of values?”.

4.2.1 The formulation for the nonlinear NSE

In treating the nonlinearity we do not replace (4.12) with a nonlinear model; instead, we consider an iterative approach inspired by the deterministic one. Also in this case, we rely on the Newton method for the NSE; the algorithm reads as follows. Given a guess for the velocity at iteration $k+1$, we find $H_{post,k+1}$ solving

$$H_{post,k+1} = (\Sigma_{pr}^{-1} + \mathrm{Z}_k^{\mathrm{T}}\Sigma_{noise}^{-1}\mathrm{Z}_k)^{-1}(\mathrm{Z}^{\mathrm{T}}\Sigma_{noise}^{-1}(\mathbf{d} - \varepsilon_0) + \Sigma_{pr}^{-1}h_0). \tag{4.18}$$

Here, Z_k is defined as in 3.3, i.e. $\mathrm{Z}_k = \mathrm{D}\mathrm{S}_k^{-1}\mathrm{R}_{in}^{\mathrm{T}}\mathrm{M}_{in}$ where

$$\mathrm{S}_k = \begin{bmatrix} \mathrm{C} + \mathrm{A}_k & \mathrm{B}^{\mathrm{T}} \\ \mathrm{B} & \mathrm{O} \end{bmatrix}. \tag{4.19}$$

A_k is the discretization of the advection operator with advection field U_k, the velocity vector associated with the normal stress $H_{post,k}$. We perform iterations (4.18) until a convergence criterion is satisfied. Since in our application the variable of interest is the velocity, we check the convergence using $\|U_k - U_{k+1}\| \leq \delta$, a user defined tolerance. Note that with this formulation $\mathbf{H}$ and $\mathbf{U}$, at each iteration, are related by a linear model and, for this reason, $\mathbf{U}$ can still be considered normally distributed.

4.2.2 Statistical point estimators

One of the most common point estimators is the maximum a posteriori (MAP) estimator. We let H_{MAP} be the MAP estimator for $\mathbf{H}$. It is defined as the most likely value of $\mathbf{H}$ given $\mathbf{d}$, formally

$$H_{MAP} = \arg\max_{H} \ \pi_{post}(H). \tag{4.20}$$

In the Gaussian assumption H_{MAP} corresponds to H_{post}, the expected value of the posterior distribution and can be found by solving

$$(\Sigma_{pr}^{-1} + \mathrm{Z}^{\mathrm{T}}\Sigma_{noise}^{-1}\mathrm{Z})H_{post} = \mathrm{Z}^{\mathrm{T}}\Sigma_{noise}^{-1}(\mathbf{d} - \varepsilon_0) + \Sigma_{pr}^{-1}H_0. \tag{4.21}$$

This leads to a computational problem similar to classical deterministic regularization methods; nevertheless, the estimate comes from different motivation and relies on different information.

Another common estimator is the maximum likelihood (ML) estimator; this is the value of $\mathbf{H}$ which is most likely to produce the data $\mathbf{d}$. It is defined as

$$H_{ML} = \arg\max_{H} \ \pi(M|H). \tag{4.22}$$

For the Gaussian distribution, combining (4.13) and (4.15), this corresponds to solving

$$\arg\max_{H} \ exp\left\{-\frac{1}{2}(\mathbf{d} - \mathrm{Z}\,H - \varepsilon_0)^{\mathrm{T}}\Sigma_{noise}^{-1}(\mathbf{d} - \mathrm{Z}\,H - \varepsilon_0)\right\} \tag{4.23}$$

or, equivalently

$$\arg\min_{H} \ -\frac{1}{2}(\mathbf{d} - \mathrm{Z}\,H - \varepsilon_0)^{\mathrm{T}}\Sigma_{noise}^{-1}(\mathbf{d} - \mathrm{Z}\,H - \varepsilon_0). \tag{4.24}$$

This leads to the solution of the following linear system

$$(\mathrm{Z}^{\mathrm{T}}\Sigma_{noise}^{-1}\mathrm{Z})H_{ML} = \mathrm{Z}^{\mathrm{T}}\Sigma_{noise}^{-1}(\mathbf{d} - \varepsilon_0). \tag{4.25}$$

It is important to note that this is not a Bayesian estimator since it does not rely on the Bayes formula; it only requires the knowledge of stochastic features of the measurement process, i.e. the likelihood function. Note that, when the matrix of system (4.25) is singular the estimator is not well-defined. This happens when either Σ_{noise} is singular or Z is rank-deficient. In the latter case, as proved in Chapter 3, Proposition 3.2.3, singularity is due to data location. When sites on Γ_{in} do not satisfy optimality sufficient conditions we can prevent singularity of $\mathrm{Z}^{\mathrm{T}}\mathrm{Z}$ using interpolation, see Section 3.2.2. This process alters the noise; in Section 4.3 we provide details on how statistical properties of the noise are affected by data interpolation.

MAP and ML estimators are strictly related and the choice between the two depends on the level of prior knowledge on the variable of interest; H_{ML} corresponds to rejecting (or not trusting) our prior belief on $\mathbf{H}$, while the MAP estimation pulls the estimate towards the prior.

In a certain sense the H_{ML} can be considered as the limit case of H_{MAP} [64]. Consider the following iterative algorithm. Let π_{j-1} be an estimate of the PDF of $\mathbf{H}$ at iteration $j-1$; then,

1. set $\pi_{pr} = \pi_{j-1}$;
2. compute π_{post} and H_{post} using (4.17);
3. set $\pi_j = \pi_{post}$, $H_{MAP,j} = H_{post}$, $j = j+1$;

It is possible to show that, regardless of how we choose π_0 and H_0, iterating the procedure we have $\lim_{j\to\infty} H_{MAP,j} = H_{ML}$ [64].

In using the MAP estimator some knowledge on the distribution of $\mathbf{H}$ must be assumed. For this reason, we introduce the "Gaussian smoothness" priors [63]; they correspond to prior models with structural information on $\mathbf{H}$. When (4.12) comes form the discretization of PDEs, as in our case, it is a common assumption to consider $\mathbf{H}$ having smoothness properties (e.g. second order differentiability). In this work we choose $\Sigma_{pr}^{-1} = \frac{1}{\sigma^2}\mathrm{L}^{\mathrm{T}}\mathrm{L}$, where L corresponds to the discretization of a differential operator. As an example, when L is the identity operator and $\sigma^2 = 1$, we are assuming $\mathbf{H}$ to be corrupted by white noise.

4.2.3 Statistical spread estimators

Beyond point estimates, much broader information is carried by the posterior distribution. In this section we define credibility regions for the velocity vector, i.e. set of values the variable belongs to with a certain probability.

Using properties of affine transformations of random variables and the theory of confidence regions for the multivariate normal distribution, see Section 4.1.2, we introduce the PDF of $\mathbf{U}$ (the random variable associated with the discretized velocity) and credibility regions for components of the velocity vector in each DOF.

For the linearized NSE, an affine transformation relates the normal stress $\mathbf{H}$ and the velocity field $\mathbf{U}$, i.e. the discretization of the state equation: $\mathrm{S}\mathbf{V} = \mathrm{R}_{in}^{\mathrm{T}}\mathrm{M}_{in}\mathbf{H} + \mathbf{F}$. Solving for $\mathbf{V}$, where $\mathbf{V} = [\mathbf{U}\ \mathbf{P}]$, we have

$$\mathbf{V} = \mathrm{S}^{-1}\mathrm{R}_{in}^{\mathrm{T}}\mathrm{M}_{in}\mathbf{H} + \mathrm{S}^{-1}\mathbf{F}. \tag{4.26}$$

This is equivalent to

$$\mathbf{U} = \mathrm{E}(\mathrm{S}^{-1}\mathrm{R}_{in}^{\mathrm{T}}\mathrm{M}_{in}\mathbf{H} + \mathrm{S}^{-1}\mathbf{F}); \tag{4.27}$$

where E is the matrix that extracts the velocity, i.e. such that $\mathrm{E}\mathbf{V} = \mathbf{U}$. From now on we set $\mathrm{T} = \mathrm{E}\mathrm{S}^{-1}\mathrm{R}_{in}^{\mathrm{T}}\mathrm{M}_{in}$. This affine transformation maps the Gaussian variable $\mathbf{H} \sim$

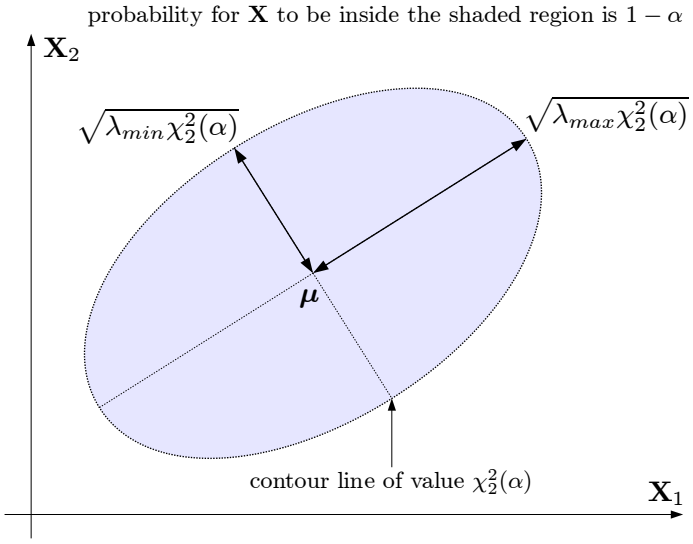

Figure 4.1: Confidence region associated with $\chi^2_2(\alpha)$.

$\mathcal{N}(H_{post},\, \Sigma_{post})$ into the Gaussian variable $\mathbf{U} \sim \mathcal{N}(U,\, \Sigma_U)$ where $U = \mathrm{T}\, H_{post} + \mathrm{ES}^{-1}\mathbf{F}$ and $\Sigma_U = \mathrm{T}\Sigma_{post}\mathrm{T}^{\mathrm{T}}$, since we do not consider $\mathbf{F}$ affected by uncertainties. Our goal is to have a measure of how likely the velocity, or one of its components, falls within a set of values, or, conversely, how large is the set of values corresponding to probability α for the velocity to belong to such set. To this end, we introduce confidence regions for the velocity field; more specifically, we focus on credibility regions for the horizontal and vertical velocity in each DOF of the computational grid, i.e. $[\mathbf{U}_i \;\; \mathbf{U}_{i+N_u/2}]^{\mathrm{T}} \in \mathbb{R}^2$, for $i = 1,\, ...,\, N_u/2$. Note that we assume horizontal velocities to be stored in the first half of the vector. This 2-dimensional vector has a bivariate normal distribution;

$$\begin{bmatrix} \mathbf{U}_i \\ \mathbf{U}_{i+N_u/2} \end{bmatrix} \sim \mathcal{N}\left(\begin{bmatrix} U_i \\ U_{i+N_u/2} \end{bmatrix}, \begin{bmatrix} \Sigma_{U;\,i,i} & \Sigma_{U;\,i,i+N_u/2} \\ \Sigma_{U;\,i+N_u/2,i} & \Sigma_{U;\,i+N_u/2,i+N_u/2} \end{bmatrix} \right) \tag{4.28}$$

For the sake of notation, we use the same notation of Section 4.1 and we rewrite (4.28) as $\mathbf{X} \sim \mathcal{N}(\boldsymbol{\mu},\, \Sigma)$. Confidence intervals for $\mathbf{U}$ can be found using property **P3**

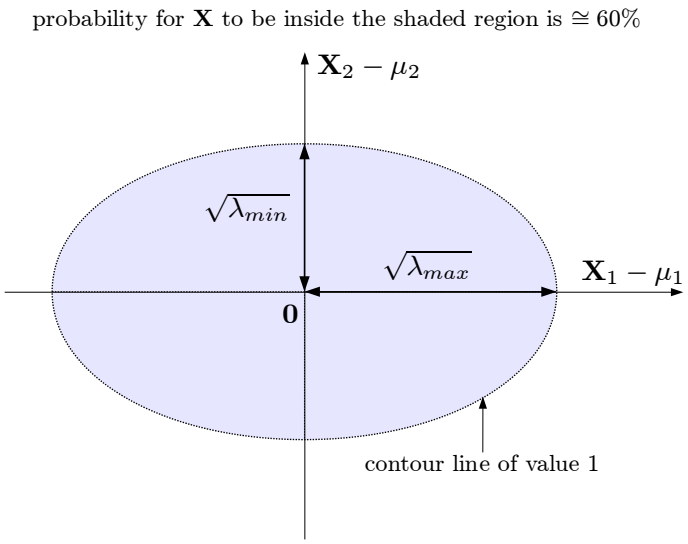

Figure 4.2: Confidence region for the standardized variable corresponding to percentile 1.

(see section 4.1.2) for the 2-dimensional case. Since $(\mathbf{X} - \boldsymbol{\mu})^{\mathrm{T}}\Sigma^{-1}(\mathbf{X} - \boldsymbol{\mu})$ has a chi-squared distribution with 2 degrees of freedom, probability of $1 - \alpha$ can be assigned to the ellipsis $\{\mathbf{x} : \ (\mathbf{x}-\boldsymbol{\mu})^{\mathrm{T}}\Sigma^{-1}(\mathbf{x}-\boldsymbol{\mu}) \leq \chi^2_2(\alpha)\}$ in the $(x,\, y)$ plane, where $\chi^2_2(\alpha)$ denotes the upper (100α)-th percentile of the distribution. Using this result, for a fixed value of α, we can draw regions in the 2-dimensional plane as shown in Figure 4.1. Spectral properties of the correlation matrix Σ play a fundamental role; the eigenvectors of Σ are the directions of the main axes and the eigenvalues are a relative measure of the variability of the velocity components. On the other hand the ellipsis in Figure 4.2 is a rotation and translation of the previous one and corresponds to the equation

$$\frac{x^2}{\lambda_{max}} + \frac{y^2}{\lambda_{min}} = 1, \qquad \text{or} \ \ \mathbf{x}^{\mathrm{T}}\Lambda^{-1}\mathbf{x} = 1, \tag{4.29}$$

where, Λ is the diagonal matrix of the eigenvalues of the correlation matrix. Note that $\mathbf{x}^{\mathrm{T}}\Lambda^{-1}\mathbf{x}$ still has a chi-squared distribution with two DOFs; moreover $1 \cong \chi^2_2(40\%)$. Thus, λ_{max} represents the maximum deviation from the mean for the components of $\mathbf{X}$

in a 60% confidence region. In our investigation we consider a map, over the computational grid, of the max eigenvalue of the correlation matrix for the bivariate distribution and, for selected DOFs, an 80% confidence region.

Remark 7 When using the posterior distribution to infer statistical properties of the variable it is important to understand the meaning of confidence regions. In fact, the result of Bayesian inversion is not the real distribution of the state (or related variables); it is rather an estimate of such PDF based on two assumptions: the knowledge of the noise distribution and of the prior. For this reason, finding a confidence region based on the posterior does *not* correspond to finding the set of values the "true" unknown belongs to, but just an estimate of that [63]. In fact, it can happen that a significant part of "true" values lies outside a 90% confidence region (see [63] Section 3.5 for a formal explanation).

4.3 Interpolation of data

In Chapter 3 on the basis of Proposition 3.2.3, we introduced a form of regularization alternative to Tikhonov techniques. Such result states that, in order to have the warranty of a unique minimizer without using Tikhonov regularization, the selection matrix, restricted to inflow boundary site, should have rank N_{in}. Using available data on Γ_{in} not satisfying sufficient conditions, we build an interpolating function to be evaluated on DOFs on Γ_{in}, now considered part of the sites set. More specifically, if we assume data $\widetilde{\mathbf{d}}$ to be given, then, after interpolation, we can write $\mathbf{d} = \Pi\widetilde{\mathbf{d}}$, where $\Pi \in \mathbb{R}^{N_s+N_{in},N_s}$ is the interpolation matrix associated with piece-wise linear Lagrangian polynomials (see Section 3.2.2 for a 2-dimensional example).

It is important to note that the interpolation process alters the noise distribution (specifically Σ_{noise}) introducing additional correlation among the data. Let us assume to know the correlation matrix of $\boldsymbol{\varepsilon}$, say Σ_{ε}, this is associated with data $\widetilde{\mathbf{d}}$ on available

sites. After interpolation we write (4.12) as $\mathrm{Z}\mathbf{H} + \boldsymbol{\eta} = \mathbf{M}$. Here, the random vector $\boldsymbol{\eta} = \Pi\boldsymbol{\varepsilon}$ is associated with a new set of sites: the given ones and the DOFs on Γ_{in}. In the Gaussian assumption, $\boldsymbol{\eta}$ is still normally distributed with mean $\Pi\varepsilon_0$ and correlation matrix $\Sigma_\eta = \Pi\Sigma_\varepsilon\Pi^{\mathrm{T}}$, see Section 4.1.2. Note that Σ_η is singular by construction; this fact makes H_{ML}, in equation 4.25, not well-defined and, as anticipates above, Gaussian smoothness priors or modified interpolation matrices should be considered; more details are given in the following section.

4.4 Numerical results

In this section we present numerical results obtained testing the Bayesian formulation on 2-dimensional and axisymmetric 3-dimensional geometries for both the linearized and nonlinear NSE. In order to test the effectiveness of this approach we compare the MAP and ML estimators with deterministic estimates obtained using the formulation of Chapter 3. In particular, we compare accuracy and number of iterations in the solution of linear systems. The index of accuracy is related to the velocity fields retrieved from H_{MAP}, H_{ML} and H_{det} (the deterministic estimate); it is defined as $E_U = \frac{\|\mathbf{U}-\mathbf{U}_{anl}\|_2}{\|\mathbf{U}_{anl}\|_2}$, where $\mathbf{U}_{anl}$ is the discretized analytic solution, see equation (3.26), assumed known. We also define an average error over a set of noise realizations, $\overline{E}_U = \frac{1}{n}\sum_{i=1}^{n}\overline{E}_{U,i}$ where $E_{U,i}$ is associated with the i-th realization. In addition, we consider a measure of the gain, γ, in using statistical estimators as opposed to deterministic ones: $\gamma = 1 - \frac{\overline{E}_{U,stat}}{\overline{E}_{U,det}}$ where $stat$ stands for either MAP or ML.

Statistical spread estimators for the velocity and for the WSS are derived and possible interpretations are discussed.

We test two possible sites configurations on Γ_{in} and we discuss numerical results in terms of accuracy and statistical interpretation. We consider the solution of the linearized problem first; then, we treat the nonlinear case.

Implementation details We implement the FE method with choice of compatible FE spaces P1bubble-P1 for velocity and pressure respectively. Numerical results are obtained with the C++ FE library `lifeV` and post-processed with `ParaView`. For the solution of the linear system (4.17) we refer to the GMRESR method [52, 53]; for the matrix S we consider the PCD preconditioner proposed by Kay in [56] and by Silvester et al. in [57].

As smoothness prior we use $\Sigma_{pr}^{-1} = \alpha \mathrm{L}^{\mathrm{T}}\mathrm{L}$, $\alpha \geq 0$, where L is the discrete gradient. This is a common choice for PDE constrained problems and it is not based on any physical consideration. Nevertheless, we note that in hemodynamics applications some prior knowledge of the velocity and pressure distribution can be derived from the anatomy of the human body; this might be used to infer statistical properties of the control variable $\mathbf{H}$ using the relation between flow and boundary stress.

Data generation We assume to have sites on Γ_{in} and in Ω either on selected layers (featuring the configuration of Figure 3.1) or uniformly distributed in the domain. At this preliminary stage data are synthetic, i.e. generated adding random noise to a known analytic solution (see equation (3.26)). Moreover, we set the available data (the specific realization of $\mathbf{M}$) $\mathbf{d} = \mathrm{Q}\mathbf{U}_{anl} + \boldsymbol{\varepsilon}$, Q being the selection matrix introduced in Chapter 3. Here, the Gaussian random vector $\boldsymbol{\varepsilon}$ is generated coloring white noise: $\boldsymbol{\varepsilon} = \mathrm{G}\mathbf{w}$, where $\mathbf{w} \sim \mathcal{N}(0, \mathrm{I})$ and G is such that $\mathrm{G}\mathrm{G}^{\mathrm{T}} = \Sigma_{\varepsilon}$, the correlation matrix for the noise on sites, assumed known. We compute G as the Cholesky factor of Σ_{ε}.

The likelihood function In the choice of the noise expected value it is reasonable to consider $\varepsilon_0 = \mathbf{0}$ (personal communication of Dr. Brummer, Emory CHOA). We assume that the noise correlation depends on the mutual distance between sites. In particular, we assume that close data highly affect each other, and that data significantly far from each other are almost independent. For this reasons, we consider an exponential decay

	H_{det}		H_{ML}			H_{MAP}		
IS	$\overline{E}_U$	α	$\overline{E}_U$	α	γ	$\overline{E}_U$	α	γ
0	0.08077	0.1	0.06290	0	22%	0.06296	0.001	22%
100	0.03080	0	0.03033	0	2%	0.04170	0.15	-35%
200	0.06868	0.15	0.03751	0	41%	0.04853	0.15	29%
300	0.08837	0.15	0.02049	0	77%	0.02662	0.2	70%

Table 4.1: Accuracy results for statistical and deterministic solutions.

with respect to the mutual distance. Formally,

$$[\Sigma_{noise}]_{ij} = [\Sigma_{\varepsilon}]_{ij} = exp\left\{-\frac{1}{l^2}\|\mathbf{x}_i^m - \mathbf{x}_j^m\|_2^2\right\}; \tag{4.30}$$

l being a reference distance for the domain of interest. In this way Σ_{noise} is a symmetric positive definite matrix. As mentioned in the previous section, when we perform interpolation the correlation matrix is of the form $\Sigma_{noise} = \Sigma_{\eta} = \Pi\Sigma_{\varepsilon}\Pi^{\mathrm{T}}$ and, in general, it is singular.

4.4.1 Point estimators

Test case I In the square domain $\Omega = [-0.5,\ 1.5] \times [0,\ 2]$ we consider the analytic solution (3.26). Data on the inflow boundary satisfy the conditions for optimality (specifically, one measurement per grid node, which ensures well-posedness using the FE pair P1bubble-P1), IS internal data are sparse in Ω and the reference distance is l = 1.

Table 4.1 reports E_U and α, fixed a priori, for H_{det}, H_{ML} and H_{MAP}; with SNR set to 20. Note that the most accurate solution corresponds to the ML estimator. In fact, system (4.25) is non-singular and we do not make any assumptions on the prior probability. In this case, we can observe that the gain increases as we increase the number of internal data; the more noisy information we have, the better we can get from the statistical solution. Furthermore, the number of iterations required by the

GMRESR for convergence is approximately 8 for both the approaches.

4.4.2 Test case II

In this case, using the same analytical solution and reference distance $l = 1$, we consider data on the inflow boundary not satisfying sufficient conditions for optimality and additional internal data located on internal slices parallel to Γ_{in} (with the purpose of imitating Figure 3.1). We want to compare statistical and deterministic estimators and to investigate the role of interpolation.

We first focus on the regularized case *without* interpolation and we compare H_{MAP} and H_{det}. The regularization parameter α is strongly data dependent; since we want to test the estimators over a set of noise realizations, finding the optimal α would be highly time consuming. For this reason, we compare deterministic and statistical approaches in correspondence of three fixed values of α.

In Table 4.2 (top) we report relative errors $\overline{E}_U$, for H_{det} and H_{MAP} in correspondence of α = 0.5, 0.05, 0.005. In this case we consider 300 internal data distributed on 10 slices (30 sites per slice, not in correspondence of grid nodes); also, SNR = 20 and 10, the number of noise realizations is n = 20, Δ = 0.076, and the number of sites on Γ_{in} is $N_{s,in}$ = 14.

From these results we infer the following facts. Compared to the deterministic estimator, H_{MAP} is always more accurate since it takes into account additional information brought by statistical properties of the data. We stress that, since synthetic data are generated using the matrix G, the noise correlation matrix is exact.

In average the number of GMRES iterations is higher for H_{MAP} (1.3 times bigger than the one required by H_{det}); this is due to the presence of Σ_{noise}^{-1} in the formulation.

As mentioned above, since using regularization is computationally expensive, we also want to compare H_{ML} and H_{det} without the additional regularizing term (i.e. α = 0 for both of them) and using interpolation. We recall that when interpolating the

SNR	α	$\overline{E}_{U,det}$	$\overline{E}_{U,MAP}$	γ
20	0.5	0.0665	0.0530	24%
20	0.05	0.0666	0.0550	17%
20	0.005	0.0706	0.0579	18%
10	0.5	0.1272	0.0946	26%
10	0.05	0.1514	0.1032	32%
10	0.005	0.1256	0.1059	28%

SNR	$\overline{E}_{U,det}$	$\overline{E}_{U,ML},\ (mod)$	γ
20	0.0709	0.0552	22%
10	0.1518	0.1256	17%

Table 4.2: Accuracy results for statistical and deterministic solutions for the linearized NSE.

induced correlation matrix Σ_η is singular by construction making the problem potentially ill-posed. In our numerical results we consider two options: the first consists in solving the correlation matrix Σ_η in a least-squares sense, i.e. $\Sigma_\eta^{\mathrm{T}}\Sigma_\eta\mathbf{x} = \Sigma_\eta^{\mathrm{T}}\mathbf{y}$ where $\mathbf{x}$ is the unknown and $\mathbf{y}$ is a right hand side. The second option consists in using a modified correlation matrix constructed with the assumption of independent and identically distributed interpolated data. This is equivalent to setting the diagonal block of Σ_η corresponding to DOFs on Γ_{in} equal to $\sigma^2\mathrm{I}$, where I is the identity matrix of dimension N_{in}, which avoids singularity. Since the statistical information associated with interpolated data is redundant, the modification to the correlation matrix does not compromise the accuracy of the statistical estimator; in fact, the statistical surplus value is brought only by statistical properties of measurements. In Table 4.2 (bottom) we report results obtained in correspondence of the same 20 noise realizations used in the regularized case. Using the modified matrix Σ_η, system (4.25) is well-posed and the additional knowledge brought by the noise correlation matrix makes the statistical estimator more accurate than H_{det}. On the other hand, the number of iterations in solving for H_{ML} is 1.5 times bigger than the one required by H_{det}. As mentioned above, the higher number of iterations is expected and it is due to the presence of

SNR	$\overline{E}_{U,det}$	$\overline{E}_{U,MAP}$	γ
20	0.0822	0.07371	10%
10	0.1394	0.1041	25%

SNR	$\overline{E}_{U,det}$	$\overline{E}_{U,ML}$	γ
20	0.0855	0.0579	6%
10	0.1675	0.1363	18%

Table 4.3: Accuracy results for statistical and deterministic solutions for the NSE.

Σ_{noise}^{-1}; nevertheless, we believe that the gain in accuracy makes the computational effort worthwhile.

4.4.3 Test case III

We present numerical results obtained solving the NSE using the same analytic solution and reference distance of test case I and II. We consider data on Γ_{in} not satisfying sufficient conditions for optimality and internal data located on 10 internal slices (with 30 data/slice). The numerical problem is solved using algorithm (3.28). In Table 4.3 we report results obtained in correspondence of $\Delta = 0.076$ and SNR = 20 and 10. In the computation of H_{MAP} the regularization parameter is chosen relying on results obtained in the linearized case; we choose $\alpha = 0.5$ since it corresponds to the most accurate numerical solution. The poor gain in correspondence of SNR = 20 means that statistical information associated with a low amount of noise is not significant enough to make a considerable difference with respect to deterministic estimates in terms of accuracy. In the other cases statistical estimators are significantly more accurate and yield a gain up to the 25% in correspondence of low values of SNR.

4.4.4 Test case IV

We consider an axisymmetric formulation for the numerical solution of the 3-dimensional Poiseuille flow in a cylinder of length L =6, diameter D =3 and viscosity $\nu = 1$ in a 2-dimensional structured grid of dimension 80$\times$20. Data on the inflow boundary do not satisfy sufficient conditions and internal data are located on 5 internal slices with

SNR	$\overline{E}_{U,det}$	$\overline{E}_{U,MAP}$	γ
20	0.0396	0.0308	22%
10	0.1423	0.0978	31%

Table 4.4: Accuracy results for statistical and deterministic solutions for the axisymmetric case.

test case I			
SNR	α	$E_{U,MAP}$	λ_{MAX}
20	0.5	0.06003	0.09759
10	0.5	0.07754	0.1744

test case II			
SNR	α	$E_{U,MAP}$	λ_{MAX}
20	1.e-5	0.01720	0.3759
10	1.e-5	0.02565	0.7024

Table 4.5: Accuracy results and maximum deviation for different values of SNR.

10 data per slice. Here, the reference distance is $l = 1.5$. We perform interpolation and, in order to prevent potential ill-conditioning, we add a regularization term (or smoothness prior) with $\alpha =$ 1e-7. Results for SNR = 20 and 10 are reported in Table 4.4; in both cases we have a significant gain in accuracy. Also, the number of iterations, in average, is the same.

4.4.5 Spread estimators

Test case I We consider the square geometry $[0.5,\ 1.5] \times [0,\ 2]$ and the analytic solution (3.26); data on Γ_{in} satisfy conditions for optimality in Proposition 3.2.3. For this test case the computational grid is sufficiently small to allow explicit computation and storage of correlation matrices; matrix operations are performed in `Matlab`. In particular, for the computation of $\Sigma_{post}^{-1} = \Sigma_{pr} + \mathrm{Z}^{\mathrm{T}}\Sigma_{noise}^{-1}\mathrm{Z}$ and $\Sigma_U = \mathrm{T}\Sigma_{post}^{-1}\mathrm{T}^{\mathrm{T}}$ we rely on the conjugate gradient method for matrix inversion. For each sub matrix of Σ_U defined as in (4.28), corresponding to horizontal and vertical velocities on one DOF, say the j-th DOF, we compute the square root of the maximum eigenvalue, $\lambda_{max,\,j}$; as described in Section 4.2.3 this is the maximum deviation from the mean in a 60% confidence region. In Figure 4.3 (top left) we report the map of $\sqrt{\lambda_{max,\,j}}$ over the computational

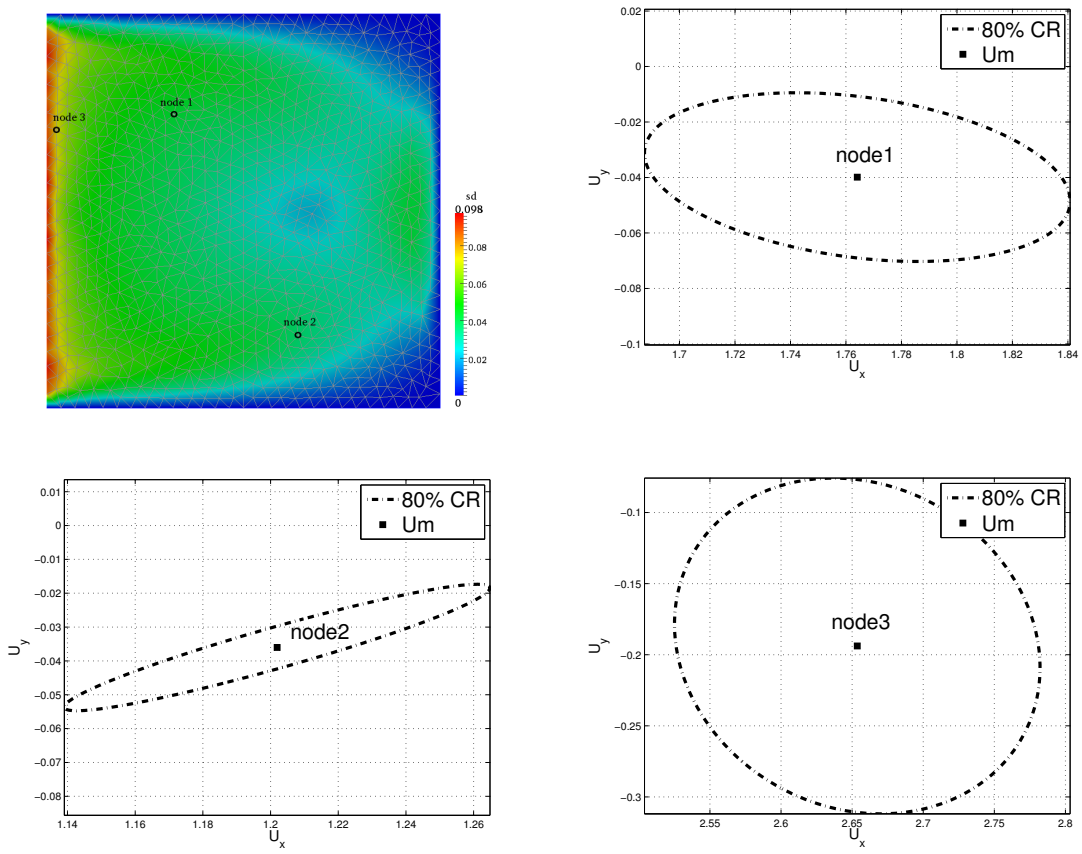

Figure 4.3: Standard deviation map (top left) and ellipses corresponding to node 1 (top right), 2 (bottom left) and 3 (bottom right).

grid for SNR = 20. We observe a peak on the inflow boundary, this is due to the fact that the noise of data on Γ_{in} has high influence on the solution, the result is a higher uncertainty for the velocity components. In correspondence of three areas featuring different values of deviation we compute a 80% confidence region corresponding to the set

$$(\mathbf{U}_j - U_j)^{\mathrm{T}} \Sigma_U^{-1} (\mathbf{U}_j - U_j) \leq \chi_2^2(20\%) \cong 3.219, \tag{4.31}$$

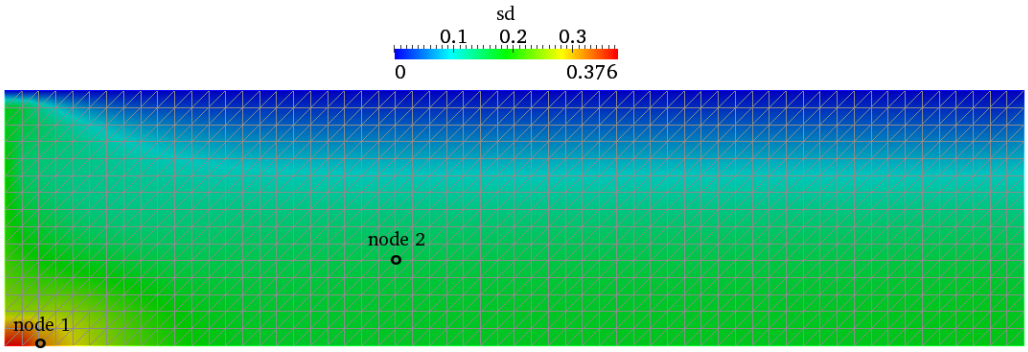

Figure 4.4: Standard deviation map.

where $\mathbf{U}_j$ corresponds to the vector of horizontal and vertical velocities on the j-th DOF and U_j is the corresponding mean value. Such ellipses are reported in Figure 4.3. Results for SNR = 20 and SNR = 10 are reported in Table 4.5 (left). Here $\lambda_{MAX} = max_j(\lambda_{max,j})$ is the maximum deviation over the computational grid.

Far from being realistic, this test case highlights the fact that Bayesian inversion is capable of reducing the standard deviation of the noise affecting observed measures, 0.1467 for SNR = 20 and 0.2953 for SNR = 10.

Test case II We consider the 3-dimensional axisymmetric formulation and data on Γ_{in} not satisfying conditions for optimality; thus, we perform interpolation. Recall that, in this case, $\Sigma_{noise} = \Pi\Sigma_{\varepsilon}\Pi^{\mathrm{T}}$, where Σ_{ε} is the correlation matrix for the measures. Matrices operations are treated as in the previous test case. In Figure 4.4 we report the map of $\sqrt{\lambda_{max,j}}$ in each DOF for SNR = 20. Here, the peak is located in the lower left corner. This result is reasonable and it is related to boundary conditions. On the wall and on the outflow section we prescribe exact boundary data; for this reason, we do not have uncertainty. As we move far from such boundaries, i.e. towards the axis of symmetry and the inflow section we have a higher deviation from the mean. This behavior is enhanced by the fact that the boundary condition on Γ_{in} is the control variable which

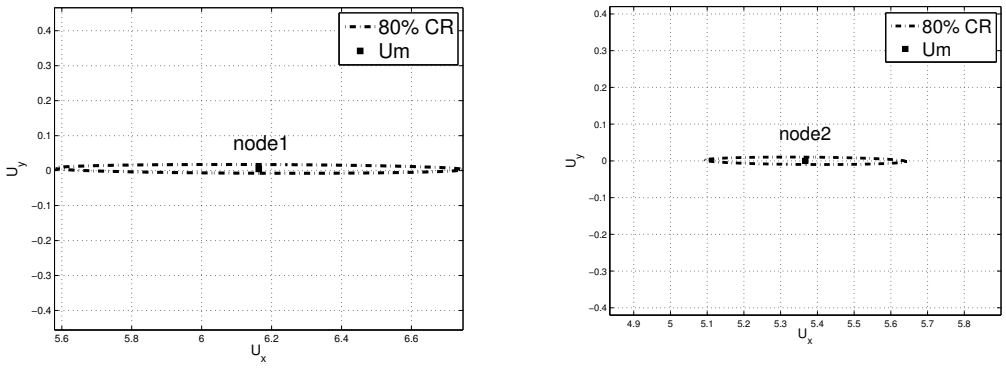

Figure 4.5: Ellipses corresponding to node 1 (left) and 2 (right).

SNR	n	$\overline{E}_{U,det}$	$\overline{E}_{U,ML}$	γ
20	20	0.05273	0.03617	31%

Table 4.6: Comparison results between deterministic and ML estimator: accuracy with respect to the reference solution.

is highly affected by the measurement noise. Nevertheless, we observe that except for the bottom left corner the deviation is lower that the one of the data, 0.325 for SNR = 20 and 0.65 for SNR = 10. As in Test case I, we compute the 80% confidence region in areas featuring different behavior. Results for SNR = 20 are reported in Figure 4.5; note that in this case we have a horizontal flow, this explains the low deviation from the mean for vertical components of the velocity.

4.4.6 Towards real geometries

In this section we consider a more complex geometry as done in Chapter 3, Section 3.4. We reproduce a 2-dimensional section of the carotid. We compare statistical and deterministic estimators and we compute confidence intervals for the velocity and for the WSS.

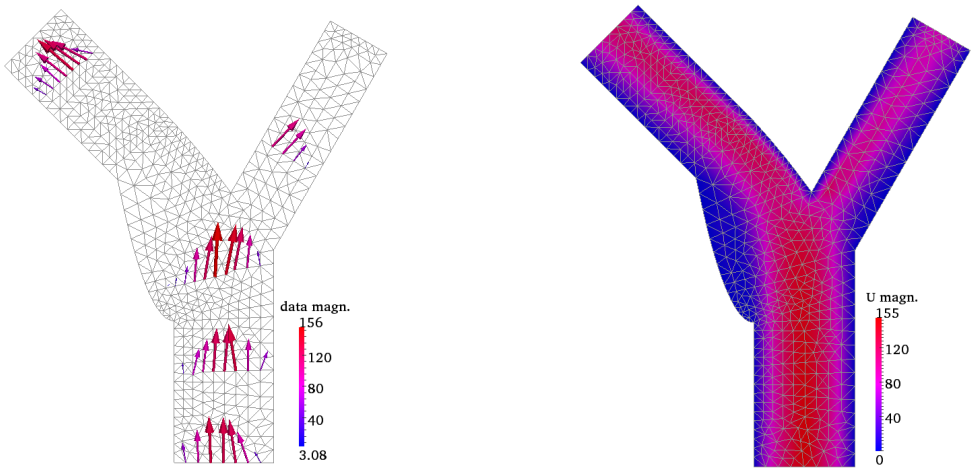

Figure 4.6: Data configuration and magnitude of the velocity field.

Data are located as reported in Figure 4.6 (left), internal data lie on four layers in correspondence of grid nodes. These are generated adding Gaussian noise to a reference solution $\mathbf{U}_{\mathrm{FE}}$, the numerical solution obtained solving, with FE, the forward problem on a very fine grid (see Section 3.4, test case I, for implementation details). The correlation matrix for the Gaussian noise is defined as in the previous test cases, i.e. as in equation (4.30). The indexes of accuracy are the average relative error $\overline{E}_U = \frac{1}{n}\sum_{i=1}^{n} E_{U,i}$ where $E_{U,i}$ is associated with the i-th realization and it is defined as $E_U = \frac{\|\mathbf{U}-\mathbf{U}_{\mathrm{FE}}\|_2}{\|\mathbf{U}_{\mathrm{FE}}\|_2}$, and the gain $\gamma = 1 - \frac{\overline{E}_{U,stat}}{\overline{E}_{U,det}}$.

In Table 4.6 we report comparison results between statistical and deterministic estimators; since data satisfy conditions for optimality we set the regularization parameter $\alpha = 0$, which corresponds to computing the ML estimator in the statistical formulation. These results show that also for more complex geometries statistical estimators are robust with respect to the noise and they are significantly more accurate than the deterministic ones. As en example, in Figure 4.6 we report the magnitude of the assimilated velocity field; in Figure 4.7 the difference between statistical and reference solution, and between deterministic and reference solution. It is interesting to note

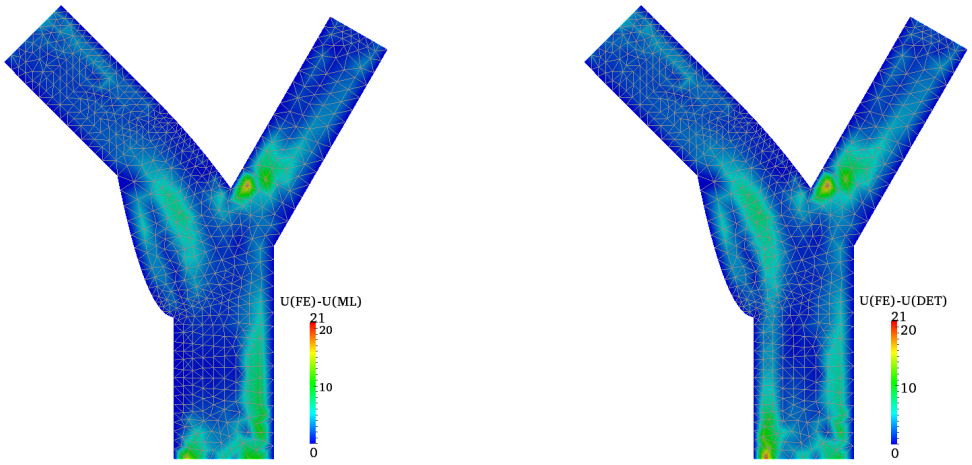

Figure 4.7: Comparison results between deterministic and ML estimator. Map of the difference between statistical and reference solution, and between deterministic and reference solution

that far from the inflow boundary the two estimators are very similar, while close to Γ_{in} the statistical solution is more accurate. This shows that the ML estimator is more robust with respect to the noise that significantly affects the numerical solution on Γ_{in}.

In view of the application to real cardiovascular problems we want to estimate the confidence intervals for the velocity. In Figure 4.8 we report the map of $\sqrt{\lambda_{max}}$, see Section 4.2.3, over the computational grid; consistently with previous results we observe that the standard deviation increases far from the wall since we work in a rigid assumption and we prescribe homogeneous Dirichlet conditions on the walls. Furthermore, since close to Γ_{in} the solution is more sensitive to the noise in this area we have the highest deviation from the mean.

The wall shear stress In medical practice other than estimating the flow and assessing its statistical properties it is fundamental to estimate other flow related variables as the WSS since, as a matter of fact, they are crucial for predicting the occurrence of diseases or even the rupture of a blood vessel. At the moment [10] the WSS is computed

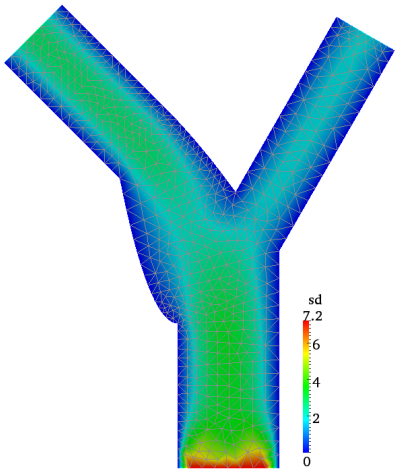

Figure 4.8: Standard deviation map.

using the observed velocity data (either projected onto the whole grid or collected on each node); these estimators are not accurate enough and are more sensitive to the presence of the noise. Using point and statistical estimators for the velocity we compute statistical parameters of the WSS distributions; also in this case we assume this random vector to be normally distributed, $\mathbf{WSS} \sim \mathcal{N}(WSS, \Sigma_{WSS})$, mean and correlation matrix are determined by the PDF of the velocity. In fact, velocity and WSS are related by the linear transformation

$$\mathbf{WSS} = \mathrm{T}_w \mathbf{U}; \tag{4.32}$$

where $\mathrm{T}_w \in \mathbb{R}^{N_u, N_w}$ maps the discretized velocity into the discretized WSS; N_w being the number of DOFs of the WSS. According to property **P1** in section 4.1.2, **WSS** has a Gaussian distribution with mean $WSS = \mathrm{T}_w U$ and covariance $\Sigma_w = \mathrm{T}_w \Sigma_U \mathrm{T}_w^{\mathrm{T}}$. Furthermore, according to **P2** the vector of horizontal and vertical components of the

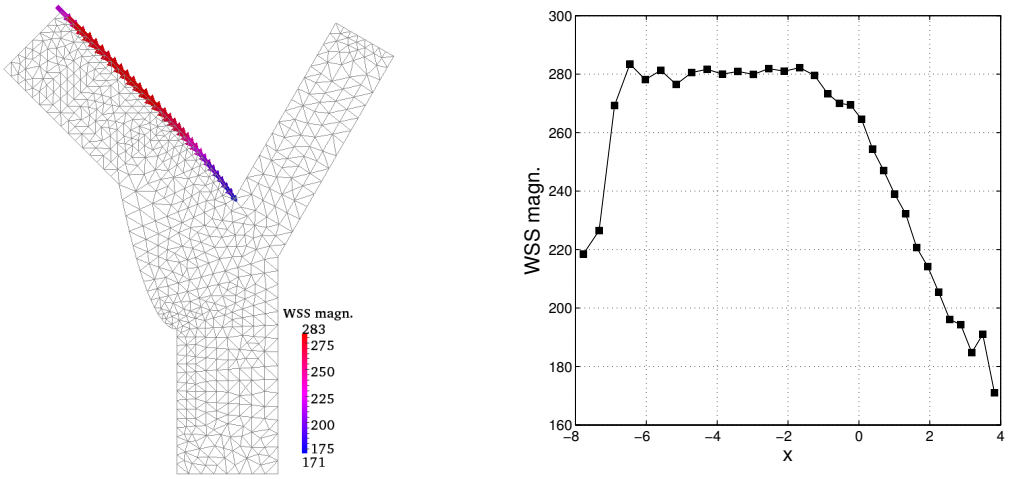

Figure 4.9: WSS on a selected wall; on the left the vector field, on the right the magnitude as a function of the x-coordinate.

WSS on each DOF is distributed as follows

$$\begin{bmatrix} \mathbf{WSS}_i \\ \mathbf{WSS}_{i+N_w/2} \end{bmatrix} \sim \mathcal{N}\left(\begin{bmatrix} WSS_i \\ WSS_{i+N_w/2} \end{bmatrix}, \begin{bmatrix} \Sigma_{WSS;i,i} & \Sigma_{WSS;i,i+N_u/2} \\ \Sigma_{WSS;i+N_u/2,i} & \Sigma_{WSS;i+N_u/2,i+N_u/2} \end{bmatrix} \right). \tag{4.33}$$

In Figure 4.9 (left) we report the WSS computed on the left inner wall of the bifurcation; the relative error, in norm l_2 with respect to the reference solution is of the order of the 15% with SNR = 20. On the right, the magnitude of the vector in each DOF of the selected boundary is displayed as a function of the horizontal coordinate. As we did for the velocity, we can compute in each DOF $\sqrt{\lambda_{max}}$, where λ_{max} is the maximum eigenvalue of the 2-dimensional correlation matrix in (4.33), this is a measure of the maximum variation from the mean in a confidence region of the 60%. In Figure 4.10 (left) we report on such selected wall the value of $\sqrt{\lambda_{max}}$ for each DOF; on the right we report the same quantity for a "non-assimilated" WSS. More specifically we assume $\mathbf{WSS} = \mathrm{T}_w \mathbf{U}_{obs}$, where $\mathbf{U}_{obs}$ is the vector of observed velocities. Thus, it features the

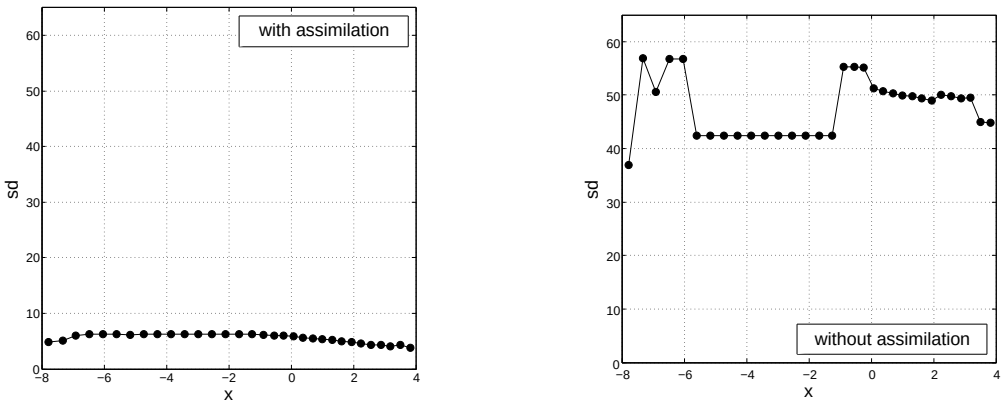

Figure 4.10: Standard deviation of the assimilated and non-assimilated WSS as a function of the x-coordinate.

correlation matrix

$$[\Sigma_{obs}]_{ij} = exp\left\{-\frac{1}{l^2}\|\mathbf{x}_i^m - \mathbf{x}_j^m\|_2^2\right\}; \tag{4.34}$$

where $\mathbf{x}_i^m$, $i = 1, \ldots N_u$, are observation sites (here corresponding to DOFs of the velocity). According to these relations, $\mathbf{WSS} \sim \mathcal{N}(\mathrm{T}_w U_{obs}, \Sigma_{obs})$. From the results we note that the maximum deviation from the mean is much higher than the assimilated one; note that the flat configuration of the non-assimilated WSS in the interval $(-6, -1)$ is due to the grid-structure, very regular in correspondence of that area. Even if the result is preliminary and depends on the data configuration, the huge reduction in the standard deviation obtained using DA, lead us to conclude that we can effectively filter the noise.

5 DA for the unsteady NSE

In previous chapters we focused our attention on the assimilation of data collected at the same time instant and we developed an assimilation procedure for steady phenomena. In the context of hemodynamics this is clearly limiting; during one heartbeat the flow dynamics might vary significantly. If we want to capture the whole behavior of blood circulation we need to account for snapshots of the blood velocity in different stages of the cardiac cycle. As an example, in the case study discussed in Chapter 1 (presented in [10] by Dr. Brummer and collaborators) using phase-velocity encoded MRIs of the aorta, 20 time points per cardiac cycle were collected on several internal slices of the vessel.

As anticipated in Chapter 1 there are plenty of methods to treat time dependent data. In this chapter we consider variational approaches inspired by the steady formulation presented in Chapter 3; in this context it is worth spending a few words on the issue of solving the adjoint problem (see Section 1.1.4 on variational approaches). In fact, the treatment of adjoint equations is one of the major issues in using control-based methods for unsteady problems. These methods are formulated as the minimization of the misfit between data and velocity subject to the state equations. When we solve this problem finding the stationary points of the Lagrangian functional we have to deal with a coupled system involving the state and adjoint equations and the optimality condition. The most important observation is that the adjoint equations are posed backward in time, while the state ones are forward in time. This means that, when discretizing the system, it is not possible to "march in time" [23]; thus, solutions to the optimality

system at all time levels are coupled to each other. This fact makes the monolithic solution to the system, the so called *one-shot method* [23], in general prohibitively expensive, even for simple differential equations.

In this chapter we first work on simple test cases where one-shot methods are still affordable and, then, we propose a variational method formulated so to circumvent the solution of the unsteady adjoint problem, we will refer to this method as *intermittent* DA meaning that the optimization is intermittent in time and, hence, local. In literature several strategies are available; the simplest is to introduce iterative methods for uncoupling the state and adjoint equations. In this case, given a guess for the control variable, state and adjoint are sequentially solved and used in the optimality equation to update the control variable. This is to be done until some criterion for the convergence is satisfied; this process might be very slow or even diverge. Other methods include sensitivity-based and adjoint-based optimization methods, see [23] for an extensive discussion.

This chapter is organized as follows. In Section 5.1 we treat the unsteady linearized NSE. For non-periodic problems we propose two variational formulations, one-shot and intermittent; while in the periodic case we consider a one-shot method. In Section 5.1.3 we show numerical results stressing consistency and accuracy of the proposed schemes. In Section 5.2 we present an intermittent algorithm for the non-periodic unsteady NSE and we propose a generalization to the periodic case. Also, on the basis of such algorithms, we propose a statistical approach to DA relying on schemes introduced in Chapter 4. In Section 5.2.1 we compare the performance of deterministic and statistical estimators and we test consistency ad accuracy of the periodic approach. Numerical results in this chapter are preliminary and represent a first attempt to the solution of this complex problem. The aim is to conduct a preliminary investigation which may guide the choice of effective methods.

5.1 The linearized problem

We consider the unsteady Stokes flow in Ω, a domain in $\mathbb{R}^d$ ($d = 2, 3$) featuring an inflow section Γ_{in}, an outflow section Γ_{out} and a wall Γ_{wall}. Variables of interest are velocity $\mathbf{u}(\mathbf{x}, t) \in L^2((t_0, T]; \mathbf{H}^1_{\Gamma_{wall}}(\Omega))$ and pressure $p(\mathbf{x}, t) \in L^2((t_0, T]; L^2(\Omega))$, which satisfy the unsteady Stokes equations. We assume to have $N_s \cdot N_t$ velocity measures $\mathbf{d}_n \in \mathbb{R}^{N_s}$ available at some sites $\mathbf{x}^m_{i,n} \in \Omega$ for $i = 1, ..., N_s$ at time t_n, $n = 1, ..., N_t$. We formulate the unsteady assimilation problem as a control problem of the form

$$
\begin{aligned}
&\min_{\mathbf{h}} \mathcal{J}(\mathbf{u}, \mathbf{h}) = dist\big(\mathbf{u}_n, \mathbf{d}_n; n = 1, ..., N_t\big) + \mathcal{R}(\mathbf{h}_n; n = 1, ..., N_t) \\
&\text{s.t.} \begin{cases}
\mathbf{u}_t - \nu \nabla \cdot (\nabla \mathbf{u} + \nabla \mathbf{u}^{\mathrm{T}}) + \nabla p = \mathbf{s} & \text{in } \Omega, \text{ for } t \in (t_0, T], \\
\nabla \cdot \mathbf{u} = 0 & \text{in } \Omega, \text{ for } t \in (t_0, T], \\
\mathbf{u} = \mathbf{0} & \text{on } \Gamma_{wall}, \text{ for } t \in (t_0, T], \\
-\nu (\nabla \mathbf{u} + \nabla \mathbf{u}^{\mathrm{T}})\mathbf{n} + p\,\mathbf{n} = \mathbf{h} & \text{on } \Gamma_{in}, \text{ for } t \in (t_0, T], \\
-\nu (\nabla \mathbf{u} + \nabla \mathbf{u}^{\mathrm{T}})\mathbf{n} + p\,\mathbf{n} = \mathbf{g} & \text{on } \Gamma_{out}, \text{ for } t \in (t_0, T], \\
\mathbf{u}(\mathbf{x}, t_0) = \mathbf{u}_0(\mathbf{x}) & \text{in } \Omega.
\end{cases}
\end{aligned}
\tag{5.1}
$$

Here $\mathbf{u}_n = \mathbf{u}(\mathbf{x}, t_n)$ and $\mathbf{h}_n = \mathbf{h}(\mathbf{x}, t_n)$; in this case, the distance function $dist(\cdot, \cdot)$ depends on velocity and data at measurement instants and will be specified later on. Other functions and parameters are defined as for the steady case. For the reasons specified in Chapter 3 we use the normal stress $\mathbf{h}$ as the control variable.

One of the major issues in dealing with time dependent phenomena is the prescription of the initial condition; in fact, in practical applications the velocity at time t_0 is not available. Thus, we proceed following two strategies. The first consists in using a reasonable and feasible guess on the initial data; the second in assuming periodicity in time, setting $\mathbf{u}_0 = \mathbf{u}(\mathbf{x}, \tau)$, τ being the period. The latter stems from the physics

of the problem; in fact, it is known that the cardiovascular system is characterized by periodic phenomena and in such cases τ is the the length of the cardiac cycle. Another possibility, often used in meteorology, is to include the initial condition in the set of control variables.

5.1.1 Non-periodic formulation

As in the steady case, we consider a DO technique (see Chapters 2 and 3); the space discretization is performed by means of the FE method and the time discretization by means of the backward Euler (BE) scheme [47]. Let $\mathrm{M}_{u,p} \in \mathbb{R}^{N_u+N_p,N_u+N_p}$ be the matrix that extends the velocity mass matrix, M, to the entire set of DOFs,

$$\mathrm{M}_{u,p} = \begin{bmatrix} \mathrm{M} & \mathrm{O} \\ \mathrm{O} & \mathrm{O} \end{bmatrix}. \tag{5.2}$$

In this context we assume the velocity mass matrix M to account for the time step, i.e.

$$[\mathrm{M}]_{ij} = \frac{1}{\Delta t} \int_{\Omega} \boldsymbol{\varphi}_i \boldsymbol{\varphi}_j \, \mathrm{d}\mathbf{x} \quad i,\, j = 1,\, ...,\, N_u; \tag{5.3}$$

where, $\boldsymbol{\varphi}$ is the Lagrangian FE basis function for the velocity. The space-time discretization of the constraints in (5.1), for all $n = 1,\, ...,\, N_f$ reads

$$\mathrm{S}\mathbf{V}_n + \mathrm{M}_{u,p}(\mathbf{V}_n - \mathbf{V}_{n-1}) = \mathrm{R}_{in}^{\mathrm{T}} \mathrm{M}_{in} \mathbf{H}_n + \mathbf{F}_n. \tag{5.4}$$

where, $N_f = \frac{T}{\Delta t}$, Δt being the time discretization step. $\mathbf{V}_n$ and $\mathbf{H}_n$ are the discretization of velocity and pressure and of normal stress at time t_n. Matrices S, R_{in} and M_{in} have been introduced in Section 3.2. For the sake of simplicity we assume that the set of measurement instants I_{meas} is contained in the set of time discretization instants I_{discr}, i.e. $I_{meas} = \{t_j\}_1^{N_t} \subseteq I_{discr} = \{t_n\}_1^{N_f}$; this assumption, in general, is also realis-

tic. In the solution of the non-periodic assimilation problem we consider two possible cases: $I_{meas} = I_{discr}$ and $I_{meas} \subset I_{discr}$.

Formulation I When discretization and measurement instants coincide we consider a one-shot method solved with a DO approach; here, the constraints are the state equations discretized in space and time. We formulate the problem as follows,

$$\begin{aligned} &\min_{\mathbf{H}_{n=1,\dots,N_f}} \sum_{n=1}^{N_f} \frac{1}{2}\|\mathrm{D}_n\mathbf{V}_n - \mathbf{d}_n\|_2^2 + \frac{\alpha}{2}\|\mathrm{L}\mathbf{H}_n\|_2^2 \\ &\text{s.t.} \quad (\mathrm{S} + \mathrm{M}_{u,p})\mathbf{V}_n = \mathrm{R}^{\mathrm{T}}\mathrm{M}_{in}\mathbf{H}_n + \mathrm{M}_{u,p}\mathbf{V}_{n-1} + \mathbf{F}_n, \quad \forall\, n = 1,\, ...,\, N_f. \end{aligned} \tag{5.5}$$

Here, the subscript n corresponds to the time instant t_n in I_{discr}. We rewrite (5.5) in a more compact form

$$\begin{aligned} &\min_{\mathbf{H}} \frac{1}{2}\|\overline{\mathrm{D}\mathbf{V}} - \overline{\mathbf{d}}\|_2^2 + \frac{\alpha}{2}\|\overline{\mathrm{L}\mathbf{H}}\|_2^2 \\ &\text{s.t.} \quad \overline{\mathrm{S}\mathbf{V}} = \overline{\mathrm{R}\mathbf{H}} + \overline{\mathbf{F}}, \end{aligned} \tag{5.6}$$

where

$$\overline{\mathrm{S}} = \begin{bmatrix} \mathrm{S} + \mathrm{M}_{u,p} & \mathrm{O} & ... & & \\ -\mathrm{M}_{u,p} & \mathrm{S} + \mathrm{M}_{u,p} & \mathrm{O} & ... & \\ ... & & & & \\ ... & & & & \\ & & ... & -\mathrm{M}_{u,p} & \mathrm{S} + \mathrm{M}_{u,p} \end{bmatrix}; \tag{5.7}$$

$$\overline{\mathrm{R}} = \begin{bmatrix} \mathrm{R}_{in}^{\mathrm{T}}\mathrm{M}_{in} & \mathrm{O} & ... & & \\ \mathrm{O} & \mathrm{R}_{in}^{\mathrm{T}}\mathrm{M}_{in} & \mathrm{O} & ... & \\ ... & & & & \\ ... & & & & \\ & & & ... & \mathrm{R}_{in}^{\mathrm{T}}\mathrm{M}_{in} \end{bmatrix}; \tag{5.8}$$

$$
\begin{aligned}
&\overline{\mathrm{D}} = diag\,(\mathrm{D}_1, ..., \mathrm{D}_{N_t})\,;\\
&\overline{\mathrm{L}} = diag\,(\mathrm{L}, ..., \mathrm{L})\,;\\
&\overline{\mathbf{d}} = [\mathbf{d}_1 \;\; \mathbf{d}_2 \;\; ... \;\; \mathbf{d}_{N_t}]^{\mathrm{T}}\,;\\
&\overline{\mathbf{V}} = [\mathbf{V}_1 \;\; \mathbf{V}_2 \;\; ... \;\; \mathbf{V}_{N_t}]^{\mathrm{T}}\,;\\
&\overline{\mathbf{H}} = [\mathbf{H}_1 \;\; \mathbf{H}_2 \;\; ... \;\; \mathbf{H}_{N_t}]^{\mathrm{T}}\,;\\
&\overline{\mathbf{F}} = [\mathbf{F}_1 + \mathrm{M}_{u,p}\mathbf{V}_0 \quad \mathbf{F}_2 \;\; ... \;\; \mathbf{F}_{N_t}]^{\mathrm{T}}\,.
\end{aligned}
\tag{5.9}
$$

Here, D_n is a selection matrix such that $\mathrm{D}_n\mathbf{V}_n$ corresponds to the evaluation of the velocity vector at time t_n on the measurement sites $\mathbf{x}_{i,n}^m$, for $i = 1, ..., N_s$; L is the discretization of the gradient.

Problem (5.6) is an algebraic optimization problem with linear constraints; it has the same form of problem (3.2) introduced in Chapter 3 for the steady case. For this reason, we solve it using the same approach, i.e. the reduced Hessian method. Matrix dimensions in this extended formulation might be large; nevertheless, $\overline{\mathrm{S}}$ is lower block triangular, with same diagonal and off-diagonal blocks. Thus, memory requirements and computational effort are affordable.

Formulation II When measurement instants are a subset of time discretization steps we refer to an intermittent assimilation technique consisting in two stages: assimilating and advancing in time. This formulation has affordable memory requirements and it is easy to be implemented. The following algorithm summarizes the two steps. For $n = 1, ..., N_f$, given a guess for velocity and pressure at time $t = t_0$, say $\mathbf{V}_0$

if $(t_n \in I_{meas})$ solve (with the reduced Hessian method):

$$
\begin{aligned}
&\min_{\mathbf{H}_n} \frac{1}{2}\|\mathrm{D}_n\mathbf{V}_n - \mathbf{d}_n\|_2^2 + \frac{\alpha}{2}\|\mathrm{L}\mathbf{H}_n\|_2^2\\
&\text{s.t.} \quad \mathrm{S}\mathbf{V}_n + \mathrm{M}_{u,p}(\mathbf{V}_n - \mathbf{V}_{n-1}) = \mathrm{R}_{in}^{\mathrm{T}}\mathrm{M}_{in}\mathbf{H}_n + \mathbf{F}_n;
\end{aligned}
\tag{5.10}
$$

else solve the unsteady Stokes problem (5.4) using suitable boundary conditions.

The choice of boundary conditions for the advancing stage depends on how much we trust available measures. We consider the following options at time $t_n \in I_{discr}$, such that $t_n \in [t_{j-1},\ t_j]$, where t_j and $t_{j-1} \in I_{meas}$, are two subsequent measurements instants.

1. *Dirichlet* with data $\Phi(\mathbf{d}_j, \mathbf{d}_{j-1}) = \frac{t_n - t_{j-1}}{t_j - t_{j-1}}\mathbf{d}_{j-1} + \frac{t_j - t_n}{t_j - t_{j-1}}\mathbf{d}_j$ on Γ_{in}.

2. *Neumann* with data $\mathbf{H}_{j-1}$, the value of the control variable resulting from the previous assimilation step.

The choice of 1. corresponds to assuming that data are not significantly affected by noise. On the other hand the choice of 2. corresponds to assuming that the normal stress does not vary considerably between two subsequent measurement instants. This assumption might be reasonable especially in applications where data are collected frequently.

Remark 8 The optimality result in Proposition 3.2.3, Chapter 3, is promptly extended to this unsteady formulation at each optimization step, i.e. equation (5.10). It is easy to show that Lemma 3.2.2 is applicable to this optimization problem. In fact, as stated in Remark 2, such lemma is not specific for the steady Stokes problem but for any PDE whose discretization matrix corresponding to a homogeneous Dirichlet problem on Γ_{in} is non-singular; which is the case for equation (5.10).

5.1.2 Periodic formulation

If a guess on the initial velocity is not available, we considere a periodicity constraint, in view of our application. For the sake of simplicity we assume $I_{meas} = I_{discr}$; thus, the formulation is a modified version of problem (5.6) with constraint

$$\overline{\mathrm{S}}_p\overline{\mathbf{V}} = \overline{\mathrm{R}\mathbf{H}} + \overline{\mathbf{F}}, \tag{5.11}$$

where

$$\overline{\mathrm{S}}_p = \begin{bmatrix} \mathrm{S}+\mathrm{M}_{u,p} & \mathrm{O} & \dots & & -\mathrm{M}_{u,p} \\ -\mathrm{M}_{u,p} & \mathrm{S}+\mathrm{M}_{u,p} & \mathrm{O} & \dots & \\ \dots & & & & \\ \dots & & & & \\ & & \dots & -\mathrm{M}_{u,p} & \mathrm{S}+\mathrm{M}_{u,p} \end{bmatrix}. \tag{5.12}$$

As opposed to $\overline{\mathrm{S}}$, this matrix is not block triangular; the system is coupled. This fact makes the numerical solution of the problem more challenging. In the following section we provide details for the choice of suitable preconditioners, which are mandatory for the numerical solution of the system, and we discuss difficulties caused by the complex structure of the problem.

Remark 9 Another possibility for forcing periodicity is to consider formulation (5.6) adding to the functional the penalizing term $\beta\|\mathbf{U}_0 - \mathbf{U}_\tau\|$, τ being the length of the period and β a penalizing parameter chosen a priori.

5.1.3 Numerical results

We present numerical results obtained for non-periodic and periodic problems. For Formulation I, we consider different choices of Δt; for Formulation II we compare different choices of boundary conditions on Γ_{in}. For the periodic case we discuss the choice of suitable preconditioners and we present comparison results.

Non-periodic case

We consider 2-dimensional rectangular geometries as in Figure 5.1, computational grids are generated with `FreeFem++`, see Section 2.2. We choose $\mathbf{s} = \mathbf{0}$, $\Omega = [0,\ 5] \times [-0.5,\ 0.5]$, $\mathbf{g} = \mathbf{0}$, $\mathbf{u}_0(\mathbf{x}) = \mathbf{0}$ and we assume that data are available on three internal layers $\{x = 1,\ x = 2.5,\ x = 4\}$ in correspondence of grid nodes.

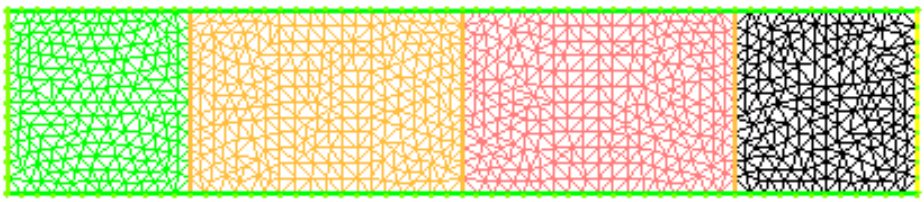

Figure 5.1: Rectangular triangulation on Ω.

Space discretization is performed by means of the FE method using compatible FE spaces P1bubble-P1 for velocity and pressure. For the time discretization we rely on the BE scheme.

For data generation and error analysis we consider a reference solution, say $\mathbf{U}_{\mathrm{FE}}$, as done in Section 3.4. This is a FE solution computed on a very fine grid (240×48 structured triangulation generated with `FreeFem++`) using $\Delta t = 0.02$ and FE spaces P1bubble-P1 for velocity and pressure. On Γ_{wall} we prescribe a homogeneous Dirichlet condition, on Γ_{out} a homogeneous Neumann condition and on Γ_{in} a time dependent Dirichlet condition given by $\mathbf{u}|_{\Gamma_{in}}(t) = [5t(1-4y^2)\ ,\ 0\ ]^{\mathrm{T}}|_{\Gamma_{in}}$. Data are generated adding uniform random noise to $\mathbf{U}_{\mathrm{FE}}$ with SNR = 100. The choice of such small amount of noise is due to the fact that, at this stage, our investigation is mainly focused on the consistency of the methods.

Error analysis The index of accuracy used in these test cases is the velocity relative error at time $T = t_{N_f}$ with respect to the reference solution $\mathbf{U}_{\mathrm{FE}}$; this is defined as $E_U(N_f) = \frac{\|\mathbf{U}_{N_f} - \mathbf{U}_{\mathrm{FE},N_f}\|_2}{\|\mathbf{U}_{\mathrm{FE},N_f}\|_2}$. The assimilation problem is solved in the time interval $[t_0, T] = [0, 1]$.

Concerning the choice of the regularization parameter α we utilize the DP method introduced in Chapter 3 (see Section 3.2.3) and the generalized cross validation (GCV) method. The main idea behind GCV is that if one data point is removed from the

set of observations, then a good regularized solution should predict that missing point considerably well [50].

More precisely, we let $\mathrm{G}(\alpha)$ be the so called *influence* matrix defined, in our case, as $\mathrm{G}(\alpha) = \overline{\mathrm{Z}}(\overline{\mathrm{Z}}^{\mathrm{T}}\overline{\mathrm{Z}} + N_s\alpha\overline{\mathrm{L}}^{\mathrm{T}}\overline{\mathrm{L}})^{-1}\overline{\mathrm{Z}}^{\mathrm{T}}$, where $\overline{\mathrm{Z}} = \overline{\mathrm{DS}}^{-1}\overline{\mathrm{R}}$. The GCV choice of α is the minimizer of the GCV function

$$\mathcal{G}(\alpha) = \frac{N_s^{-1}\|(\mathrm{I} - \mathrm{G}(\alpha))\overline{\mathbf{d}}\|_2^2}{N_s^{-1}tr(\mathrm{I} - \mathrm{G}(\alpha))}. \tag{5.13}$$

Here, I is the identity matrix and $tr(\,\cdot\,)$ is the trace operator. The function $\mathcal{G}$ can be expressed as the weighted sum of squared misfits between data and predicted velocity $\overline{\mathrm{D}}_k\overline{\mathbf{V}}_k\overline{\mathbf{d}}_k$, where $\overline{\mathbf{V}}_k$ is the regularized solution obtained leaving out the k-th data point (site), for $k = 1, ..., N_s$. Note that while DP requires the norm of the noise to be available, GCV does not.

However, values of the regularization parameter are quite low (see Table 5.1) and the smallest eigenvalue of the reduced Hessian is of the order of 10^{-2}; even though we did not prove an optimality result for Formulation I, this fact might be due to data location, which satisfies conditions of Proposition 3.2.3.

Accuracy results for Formulation I are shown in Table 5.1. Here, we report relative error $E_U(N_f)$ and optimal values of α (α_{DP} and α_{GCV} for DP and GCV respectively) for different choices of time steps. We consider Δt = 0.1 and 0.2, hence, $N_t = N_f$ = 5 and 10 respectively; recall that in this case $I_{meas} = I_{discr}$. In correspondence of DP solutions are slightly more accurate, which is consistent with the fact that exact information about the noise is used. As we decrease the time step (increase the number of data in the time interval) we obtain a better accuracy; the improvement is due both to the smaller time-step and to the higher number of data.

For Formulation II we consider Δt = 0.1 and N_t = 5; this corresponds to performing one advancing step between two consecutive measurement instants. Comparison

Δt	α_{DP}	α_{GCV}	$E_{U,DP}(N_f)$	$E_{U,GCV}(N_f)$
0.2	3.5918e-7	5.6266e-8	8.2962e-2	8.3021e-2
0.1	1.1391e-6	1e-9	5.4405e-2	6.3660e-2

Table 5.1: Relative errors and regularization parameters for Formulation I.

Advancing	$E_U(T)$
Dirichlet	5.7602e-2
Neumann	5.6641e-2

Table 5.2: Relative errors for Formulation II in correspondence of *Dirichlet* and *Neumann* boundary conditions.

results between options 1. and 2. for the boundary condition on Γ_{in} are reported in Table 5.2. Since solutions have the same accuracy, this test case does not provide enough evidence to discard one of the two approaches. Furthermore, the accuracy is of the same order of results obtained with Formulation I with $\Delta t = 0.1$; this fact suggests that accuracy might be mainly related to time discretization.

Clearly, this analysis is still preliminary, but it shows that these methods are consistent in case of a low amount of noise. For drawing reasonable conclusion and choosing the most efficient technique it is fundamental to conduct a deeper investigation of the sensitivity to the noise and to the time discretization step.

Time periodic solution

In this test case we use same computational grid and software as for the non-periodic case. The reference solution is given by the following analytic solution on Ω:

$$\mathbf{u}_{anl}(\mathbf{x},t) = \eta(1+\sin(100\pi t))[5t(1-4y^2)\ ,\ 0\ ]^{\mathrm{T}},\ \ \mathbf{x}\in\Omega,\ t>0. \tag{5.14}$$

Here $\eta = 0.01$, the period is $\tau = 0.02$ and the source term is defined as $\mathbf{s}(\mathbf{x},\, t) = 100\pi\eta\cos(100\pi t)[5t(1-4y^2)\ ,\ 0\ ]^{\mathrm{T}}$.

We want to stress important numerical issues concerning the solution of the linear system induced by necessary conditions for optimality; we recall that matrix $\overline{\mathrm{S}}_p$ has a complex structure; hence, the choice of an effective preconditioner is a non-trivial task. We consider two options: the first consists in computing the incomplete Cholesky (IC) factorization, it requires the explicit computation of the reduced Hessian and it is used only for comparison purposes. The other option does not require explicitly the matrix of the system and it is based on approximations of $\overline{\mathrm{S}}_p$ featuring a simpler structure. We propose two preconditioners: the first consists in using the non-periodic problem as a preconditioner for the periodic one. The second consists in building a block triangular matrix as follows. Let us rewrite matrix $\overline{\mathrm{S}}_p$ as

$$\overline{\mathrm{S}}_p = \begin{bmatrix} \overline{\mathrm{S}}_{1,1} & \overline{\mathrm{S}}_{1,2} \\ \overline{\mathrm{S}}_{2,1} & \overline{\mathrm{S}}_{2,2} \end{bmatrix}; \tag{5.15}$$

where the first block row corresponds to time steps from 1 to $N_f - 1$ and the second block row accounts for velocity and pressure at the last time step. Then, the solution of system in $\overline{\mathrm{S}}_p$ is equivalent to solving a system (with right hand side modified accordingly) in $\widetilde{\mathrm{S}}_p$ defined as

$$\widetilde{\mathrm{S}}_p = \begin{bmatrix} \overline{\mathrm{S}}_{1,1} & \overline{\mathrm{S}}_{1,2} \\ \mathrm{O} & \overline{\mathrm{S}}_{2,2} - \overline{\mathrm{S}}_{2,1}(\overline{\mathrm{S}}_{1,1})^{-1}\overline{\mathrm{S}}_{1,2} \end{bmatrix}. \tag{5.16}$$

Despite the block triangular structure, using (5.16) is still not affordable; in order to reduce the computational effort we approximate $\overline{\mathrm{S}}_{1,1}$, in that block, with $\widetilde{\mathrm{S}}_{1,1} = diag(\mathrm{M}_{u,p}, ..., \mathrm{M}_{u,p})$.

Error analysis and computational cost In this test case we use the following index of accuracy, the relative error in space and time with respect to the analytic solution

$$E_U = \sqrt{\frac{\sum_{n=1}^{N_f} \|\mathbf{U}_n - \mathbf{U}_{anl,n}\|^2}{\sum_{n=1}^{N_f} \|\mathbf{U}_{anl,n}\|^2}}; \tag{5.17}$$

where $\mathbf{U}_n$ and $\mathbf{U}_{anl,n}$ are the computed velocity and discretized analytic velocity at time t_n. We choose SNR = 100, $N_t = N_f = 5$ and $\Delta t = 0.004$, so to make the one-shot method affordable, as well as the Cholesky factorization. In Table 5.3 we report the relative errors in correspondence of the solution of a forward problem with exact initial condition obtained with a direct solver ($E_{U,ref}$, used as a reference value of accuracy) and the one obtained with the the preconditioned conjugate gradient (PCG) method ($E_{U,PCG}$). In solving with PCG we use three different preconditioners: the identity, the incomplete Cholesky factor and the preconditioner induced by the approximation of $\overline{\mathrm{S}}_p$ with $\overline{\mathrm{S}}$. $E_{U,PCG}$ refers to all of them since they deliver the same solution. In Table 5.4 we report CPU times for matrix assembling and solution of the linear system in correspondence of PCG with the identity, IC and $\overline{\mathrm{S}}$. The comparison between the second and the last column shows that the preconditioner $\overline{\mathrm{S}}$ does not bring a significant improvement.

For testing the preconditioner $\widetilde{\mathrm{S}}_p$ we consider the GMRES method. In Table 5.5 we report relative errors, number of iterations and CPU times using the non-preconditioned and preconditioned GMRES; in correspondence of different grids the methods deliver solutions with the same level of accuracy, which is mainly affected by time discretization. On the other hand, using the preconditioned GMRES method the number of iterations and the computational time is halved compared to the non-preconditioned case. However, performance is still not satisfactory and more investigation is required.

mesh	$E_{U,ref}$	$E_{U,PCG}$
(40× 10)	4.4e-2	8.03e-2
(60× 15)	4.2e-2	7.88e-2
(80× 20)	4.3e-2	7.74e-2

Table 5.3: Relative errors for the reference solution and the assimilated one.

stage	CG	PCG, IC	PCG, $\overline{\mathrm{S}}$
assembling	0	99	0
solving	3e+3	55	2e+3

Table 5.4: Computational times in seconds, in correspondence of a 80×20 triangulation.

5.2 Formulation for the nonlinear problem

We consider the same problem setting as in the linearized case and we add the nonlinear term to the momentum equation (5.1), which now reads

$$\mathbf{u}_t - \nu \nabla \cdot (\nabla \mathbf{u} + \nabla \mathbf{u}^{\mathrm{T}}) + (\mathbf{u} \cdot \nabla)\mathbf{u} + \nabla p = \mathbf{s} \quad \text{in } \Omega, \ \text{ for } \ t \in [t_0, \, T]. \tag{5.18}$$

We design a scheme for treating both periodic and non-periodic phenomena; for the latter we assume a feasible guess on $\mathbf{u}_0$ to be available. Our formulation is similar to the one introduced for the non-periodic linearized case and can be classified as intermittent DA. We consider a DO approach where space discretization is performed by means of the FE method and time discretization by means of a semi-implicit method [42], which reads as follows: for $n = 1, \, ..., \, N_f$

$$\mathrm{S}_{n-1}\mathbf{V}_n + \mathrm{M}_{u,p}(\mathbf{V}_n - \mathbf{V}_{n-1}) = \mathrm{R}_{in}^{\mathrm{T}}\mathrm{M}_{in}\mathbf{H}_n + \mathbf{F}_n. \tag{5.19}$$

Here,

$$\mathrm{S}_n = \begin{bmatrix} \mathrm{C} + \mathrm{A}_n & \mathrm{B}^{\mathrm{T}} \\ \mathrm{B} & \mathrm{O} \end{bmatrix}; \tag{5.20}$$

mesh	$E_{U,G}$	it$_G$	CPU$_G$	$E_{U,PG}$	it$_{PG}$	CPU$_{PG}$
(40×10)	8.22e-2	51	116	8.22e-2	32	86
(60×15)	7.95e-2	75	657	7.951e-2	38	394
(80×20)	7.76e-2	92	1984	7.761e-2	39	867

Table 5.5: Relative errors, number of iterations and CPU times for the non-preconditioned GMRES (G) and the preconditioned one (PG) with preconditioner $\widetilde{\mathrm{S}}_p$.

where A_n is the discrete advection operator associated with advection field $\mathbf{V}_n$, defined as in equation (3.4). Other matrices are defined as in the linearized case.

Non-periodic case In this case, even though not realistic, we assume that an initial velocity, $\mathbf{V}_0$, is available. The following formulation is based on the assumption that data are available at each time instant of the time discretization, i.e. $I_{meas} = I_{discr}$. Let $\mathbf{V}_0$ be the vector of velocity and pressure at time $t = t_0$, then for $n = 1, ..., N_f$ we solve

$$\begin{aligned} &\min_{\mathbf{H}_n} \ \frac{1}{2}\|\mathrm{D}_n\mathbf{V}_n - \mathbf{d}_n\|_2^2 + \frac{\alpha}{2}\|\mathrm{L}\mathbf{H}_n\|_2^2 \\ &\text{s.t.} \quad \mathrm{S}_{n-1}\mathbf{V}_n + \mathrm{M}_{u,p}(\mathbf{V}_n - \mathbf{V}_{n-1}) = \mathrm{R}_{in}^{\mathrm{T}}\mathrm{M}_{in}\mathbf{H}_n + \mathbf{F}_n. \end{aligned} \tag{5.21}$$

In our test cases we assume to have an analytic expression for velocity and pressure, say $\mathbf{V}_{anl}$, and we set $\mathbf{V}_0 = \mathbf{V}_{anl}$. This algorithm is formally similar to (3.28), in Section 3.3, which is designed for the steady case; hence, same numerical techniques are used for its numerical solution. Note that, with this approach we avoid the costly solution of the adjoint problem; nevertheless, the optimization in time is only local.

Periodic case We assume that the solution is periodic with period τ and that a guess for $\mathbf{V}_0$ is not available. We propose an algorithm based on the same iterative procedure

as for the non-periodic case: set $\mathbf{V}_0 = \mathbf{V}_{N_f} = \mathbf{0}$ and $N_f = \frac{\tau}{\Delta t}$, then

$$
\begin{aligned}
&\textbf{do} \\
&\quad \mathbf{V}_0 = \mathbf{V}_{N_f};\ n = 1; \\
&\quad \textbf{for}\ \ n = 1,\ ...,\ N_f,\ \ \text{solve} \\
&\qquad \min_{\mathbf{H}_n}\ \frac{1}{2}\|\mathrm{D}_n\mathbf{V}_n - \mathbf{d}_n\|_2^2 + \frac{\alpha}{2}\|\mathrm{L}\mathbf{H}_n\|_2^2 \\
&\qquad \text{s.t.}\quad \mathrm{S}_{n-1}\mathbf{V}_n + \mathrm{M}_{u,p}(\mathbf{V}_n - \mathbf{V}_{n-1}) = \mathrm{R}_{in}^{\mathrm{T}}\mathrm{M}_{in}\mathbf{H}_n + \mathbf{F}_n \\
&\textbf{while}\ (\|\mathbf{V}_0 - \mathbf{V}_{N_f}\|_2 < \delta)
\end{aligned}
\tag{5.22}
$$

This algorithm corresponds to solving repeatedly the non-periodic problem in $[0,\, \tau]$, each time improving the guess on $\mathbf{V}_0$ using $\mathbf{V}_{N_f}$, resulting from the previous simulation, until a convergence criterion is satisfied. As already stressed in Remark 9, another possible approach is to add the periodicity condition $\mathbf{V}_0 = \mathbf{V}_{N_f}$ to the set of constraints.

Remark 10 It is straightforward to generalize these algorithms to the case of $I_{meas} \subset I_{discr}$. One option is to perform interpolation of data in time in order to have approximated data at each step of the time discretization. This approach sounds promising on the basis of results obtained with interpolation in space, see Chapter 3, Section 3.2.2. A second option is to proceed as in Formulation II: adding advancing steps of the form (5.19) between two measurement instants, i.e. in $[t_{j-1},\, t_j]$, t_{j-1} and t_j being two consecutive measurement instants. The formulation would read as follows. For $n = 1,\ ...,\ N_f$, given a guess for velocity and pressure at time $t = t_{n-1}$, say $\mathbf{V}_{n-1}$

if $(t_n \in I_{meas})$ solve (with the reduced Hessian method):

$$
\begin{aligned}
&\min_{\mathbf{H}_n}\ \frac{1}{2}\|\mathrm{D}_n\mathbf{V}_n - \mathbf{d}_n\|_2^2 + \frac{\alpha}{2}\|\mathrm{L}\mathbf{H}_n\|_2^2 \\
&\text{s.t.}\quad \mathrm{S}_n\mathbf{V}_n + \mathrm{M}_{u,p}(\mathbf{V}_n - \mathbf{V}_{n-1}) = \mathrm{R}_{in}^{\mathrm{T}}\mathrm{M}_{in}\mathbf{H}_n + \mathbf{F}_n;
\end{aligned}
\tag{5.23}
$$

else solve the unsteady NSE using suitable boundary conditions.

Bayesian approach The formulation presented in this sections can be generalized to a Bayesian approach to unsteady DA. In fact, it is enough to compute either the MAP or ML estimator (see Chapter 4, Section 4.2.2), instead of the deterministic one, at each time step in (5.21). This corresponds to solving the following algorithm (for simplicity we report the non-periodic case only). Given a guess for the initial velocity $\mathbf{V}_0$, for $n = 1, ..., N_f$ compute the MAP estimator (as in equation (4.20)) solving

$$(\Sigma_{pr}^{-1} + \mathrm{Z}_n^{\mathrm{T}}\Sigma_{noise}^{-1}\mathrm{Z}_n)\mathbf{H}_{n,MAP} = \mathrm{Z}_n^{\mathrm{T}}\Sigma_{noise}^{-1}(\mathbf{d}_n - \mathbf{b}_n). \tag{5.24}$$

Here, $\mathbf{b}_n = (\mathrm{S}_{n-1} + \mathrm{M}_{u,p})^{-1}(\mathrm{M}_{u,p}\mathbf{V}_{n-1} + \mathbf{F}_n)$, $\mathrm{Z}_n = D_n(\mathrm{S}_{n-1} + \mathrm{M}_{u,p})^{-1}\mathrm{R}_{in}^{\mathrm{T}}\mathrm{M}_{in}$, Σ_{prior} and Σ_{noise} are the correlation matrices for the random variables for normal stress and measurement error. In the next section, deterministic and statistical estimators are compared.

5.2.1 Numerical results

In this section we consider the unsteady Navier-Stokes flow in a 3-dimensional cylindrical domain and we solve the problem using an axisymmetric formulation. The computational domain is a structured rectangular triangulation on the domain $[0,\ 1.5] \times [0,\ 6]$ corresponding to a section of a cylinder with radius 1.5 and height 6. Details on implementation and solvers can be found in Section 3.2.3.

For data generation and accuracy analysis we consider the Womersley flow [65] with period $\tau = 1$ and viscosity $\nu = 1$. We consider data on Γ_{in} not satisfying sufficient conditions for optimality and we perform interpolation; 55 data are equally distributed along 5 internal slices not corresponding to grid nodes. Measurement noise is assumed to be normally distributed with correlation matrix defined as in (4.30), see Section

SNR	$E_{U,det}$	$E_{U,\mathrm{ML}}$	γ
20	0.0935	0.0633	32%
10	0.1608	0.105	35%

Table 5.6: For different values fo SNR, we report comparison results for statistical and deterministic estimators.

4.4. The time discretization step is $\Delta t = 0.1$ and the computational grid is a 60×15 unstructured triangulation.

For testing the accuracy of the solution we consider the following indexes

$$\begin{aligned} E_{abs,n} &= \|\mathbf{U}_n - \mathbf{U}_{anl,n}\|_2; \\ E_U &= \sqrt{\frac{\sum_{n=1}^{N_f} \|\mathbf{U}_n - \mathbf{U}_{anl,n}\|_2}{\sum_{n=1}^{N_f} \|\mathbf{U}_{anl,n}\|_2}}; \end{aligned} \tag{5.25}$$

where $\mathbf{U}_n$ and $\mathbf{U}_{anl,n}$ are the computed velocity and discrete analytic velocity at time $t = t_n$.

Non-periodic solution In this test case we set $\mathbf{V}_0 = \mathbf{V}_{anl,0}$, the analytic solution at time $t = 0$, and we solve the problem in $[0, \tau]$ with $\tau = 1$. As an example, in Figure 5.2 we report data and assimilated velocity field for $t = 0$, 0.3, 0.7.

In Table 5.6 we report E_U for the deterministic solution and for the ML estimator in correspondence of SNR = 20 and 10; in the third column γ is defined as $1 - \frac{E_{U,\mathrm{ML}}}{E_{U,\mathrm{det}}}$. The choice of the ML estimator is due to the fact that, since we perform interpolation, the problem is well-posed and no regularization (or smoothness priors, see 4.2.2) is required. In Figure 5.3 we report $E_{abs,n}$ at each time step for both deterministic and statistical solutions. From these results we can infer that the additional information brought by the knowledge of the noise yields more accurate results. Furthermore, we observe that the statistical solution features a smoother error behavior.

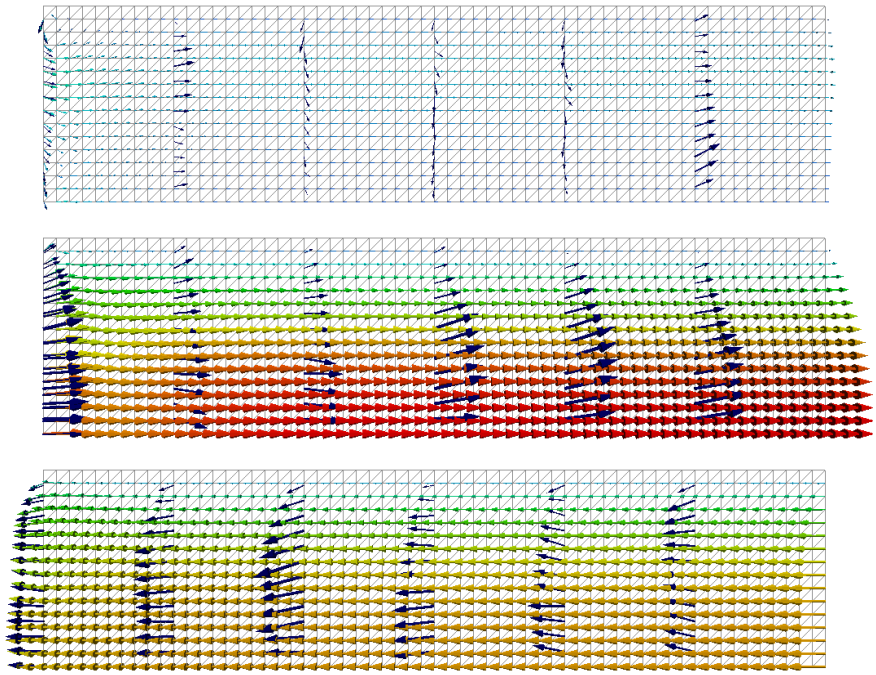

Figure 5.2: Assimilated velocity field and noisy data (SNR = 10) at time $t = 0, 0.3, 0.7$ of a Womersley simulation.

Periodic solution In this case we want to compare the solution obtained using $\mathbf{V}_0 = \mathbf{V}_{anl,0}$ and $\mathbf{V}_0 = \mathbf{0}$. In Table 5.7 we report E_τ obtained after 3 iterations of algorithm (5.22); recall that we set the initial velocity equal to the final velocity of the previous period. For the same simulations we report in Figure 5.4 for 3 subsequent iterations values of the absolute errors $E_{abs,0}$ and $E_{abs,anl}$ corresponding, respectively, to the solution obtained with $\mathbf{V}_0 = \mathbf{0}$ and $\mathbf{V}_0 = \mathbf{V}_{anl,0}$. This means that the assimilation is able to capture the solution in a very small amount of time (at most two iterations of algorithm (5.22)).

These results, although satisfactory and promising, are based on the assumption that $I_{meas} = I_{discr}$; this is definitely not realistic. Future work includes the implementation of the techniques proposed in Remark 10.

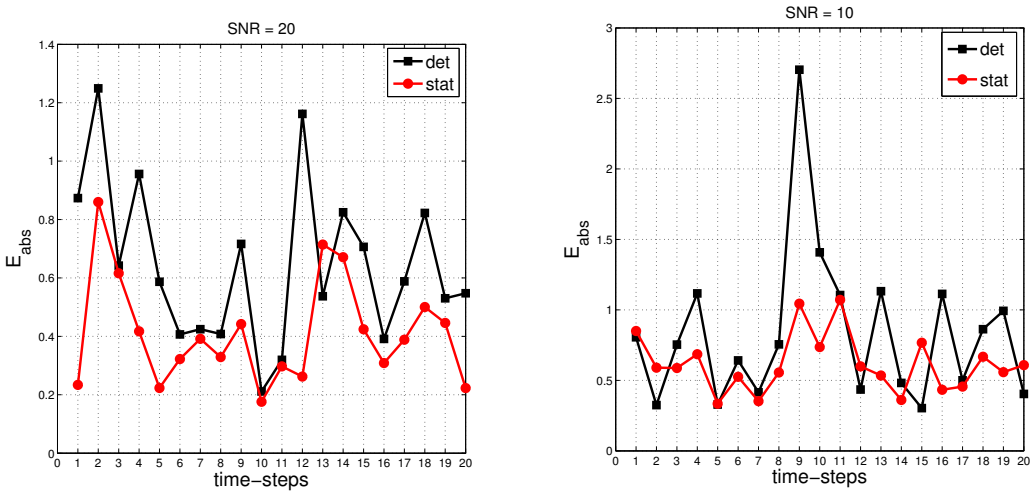

Figure 5.3: $E_{abs,n}$ for $n = 1, ..., N_f$ in $[0, 2\tau]$ for the deterministic and statistical solution for SNR = 20 and 10.

SNR	it	E_U, $\mathbf{V}_0 = \mathbf{0}$	E_U,$\mathbf{V}_0 = \mathbf{V}_{anl,0}$
20	1	0.1318	0.09985
	2	0.09456	0.09456
	3	0.09314	0.09314
10	1	0.1928	0.1711
	2	0.1533	0.1533
	3	0.1512	0.1512

Table 5.7: For different values of SNR we report accuracy results obtained comparing approach (5.22) with (5.21) using $\mathbf{V}_0 = \mathbf{V}_{anl,0}$.

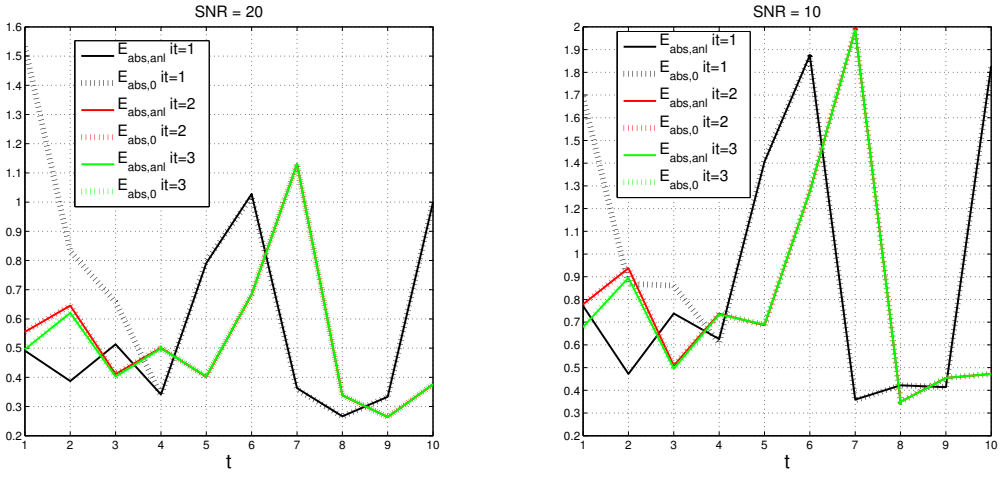

Figure 5.4: $E_{abs,n}$ for $n = 1, ..., N_f$ in $[0, \tau]$ for $\mathbf{V}_0 = \mathbf{0}$ and $\mathbf{V}_0 = \mathbf{V}_{anl,n}$ for SNR = 20 and 10.

6 Conclusion

Recent advances in measurement tools for the cardiovascular system and the establishment of numerical techniques for cardiovascular mathematics motivated in this work the design of a reliable and robust technique for the inclusion of velocity data into hemodynamics simulations. Our goal is the estimation of blood flow filtering the noise affecting the data and the quantification of the uncertainty and credibility of numerical results.

Current clinical methods for the estimation of such variable are based on simple interpolation techniques or manipulation of data [10] and they do not rely on any constitutive law for the phenomena of interest. Thus, results are not accurate and they might not even be feasible; for this reason they may fail in guiding clinical intervention. The added value of our technique is to force the numerical solution to satisfy the equations governing the system; in fact, our estimator is based on the solution of a control problem where the misfit between velocity data and numerical solution is minimized under the constraint of the fluid dynamics equations (the NSE).

Another important aspect that makes our technique valuable is the inclusion of the additional knowledge regarding the measurement process and the statistical features of the measurement noise. When data are characterized by high correlation (which is very likely in case of complex systems as the cardiovascular one) this factor cannot be neglected as it significantly determines the statistical properties of the flow.

Moreover, on the basis of the analysis of mathematical properties of the optimization problem we are able to establish conditions on the number and location of data

that ensure existence and uniqueness of the estimate. This result is the groundwork of a "regularization" technique to treat the case in which available data do not satisfy such conditions; based on data interpolation, this procedure proves to be competitive with current regularization techniques and it is parameter-free.

Our assimilation method is robust and consistent in case of noise-free data; its performance is not affected by the nature of the flow (low or high Reynolds number) and it works nicely combined with stabilization techniques for advection dominated phenomena.

The noise filtering properties Throughout this work we pointed out the filtering properties of this method. In this paragraph we would like to summarize this aspect in the case of 2-dimensional non-trivial geometries approximating vessels of interest.

In Chapter 3, Section 3.4, we tested the deterministic estimator on a 2-dimensional approximation of the carotid. Here the assimilated solution is compared to the one obtained from a forward simulation prescribing noisy velocity on the inflow boundary as Dirichlet condition and disregarding internal data. Our results are 50% more accurate than the non-assimilated ones. The same solutions are compared in the computation of the WSS; for decreasing values of SNR out estimator is up to the 50% more accurate than the forward simulation with respect to a reference solution.

For the same test case in Chapter 4, Section 4.4.6, comparison results show that statistical estimators are more accurate than deterministic ones in case of correlated data. In fact, the Bayesian estimation exploits the knowledge of the noise stochastic properties and yields a gain in accuracy of the 30% with respect to the deterministic estimates. Furthermore, the analysis of the standard deviation of the velocity reveals that, except for the area close to the inflow boundary, the deviation from the mean of the assimilated solution is at most half the one of the given data. This fact implies that the uncertainty of the WSS computed using the assimilated solution is lower than the

one obtained using given data only.

Future developments Although promising and potentially of great impact, DA in computational hemodynamics is still at its beginning stage and has some weaknesses. For the DA estimator to be applicable to 3-dimensional test cases with real geometries and data several computational issues have to be considered in order to improve the efficiency of the method.

As discussed in Chapter 2 and 3 the bottleneck of the optimization process is the solution of the state equation and its adjoint. Besides the PCD preconditioner, other effective preconditioners for the steady and unsteady problem should be considered. Among the others we mention the works by Benzi et al. [66, 67] and Elman et al. [58] for the steady case and the ones by Veneziani et al. [68, 69, 70, 71] and Cahouet-Chabard [72] for the unsteady one. For the solution of the nonlinear optimization problem we propose a nonlinear procedure that stems from the combination of the DA method for linear problems and fixed point iterative methods for the NSE. In literature there is plenty of methods for the solution of problems of this sort. For reasons related to the FE library, `lifeV`, that we utilize we plan to adopt the `NOX` package[1], which is part of Sandia's Trilinos project. `NOX` is short for Nonlinear Object-Oriented Solutions, and its objective is to enable the robust and efficient solution of nonlinear equations using globalized Newton methods such as line search and trust region methods. It can be easily customized and it is designed to work with any linear algebra package.

Another important issue is to be competitive with other assimilation approaches, such as the Kalman filter methods [32] which do not require the solution of the adjoint equation. A way to speed up the computation is to combine efficient optimization strategies with model reduction. In doing this it is important to find a good compromise between accuracy and efficiency; in medicine this is a delicate issue. On one hand

[1] http://trilinos.sandia.gov/packages/nox/

fast simulations allow fast clinical intervention, on the other hand, inaccurate results may fail in guiding correctly medical doctors' decisions. Several methods are available, among these we mention the reduced basis (RB) method for parameter-based reduction and the proper orthogonal decomposition [73, 74]. A very good review of the RB method can be found in [75] by Patera and Rozza focused on formulation, analysis, and computational procedures for reduced basis approximation and a posteriori error estimation for parametrized PDEs. Se [76] and [77] for applications of the RB method to Stokes and Navier-Stokes equations. Concerning the POD method we refer to [78, 79] for applications to fluid dynamics and to [80] for applications to PDE constrained optimization problems.

The author is currently working in collaboration with Prof. Haber (University of British Columbia, Vancouver, CA) and Dr. Horesh (IBM, T. J. Watson Research Center, Yorktown, NY) on the design of optimal reduced basis [81] obtained as the solution of an inverse problem. More specifically, the optimal basis is the control variable of a PDE constrained optimization problem where the misfit between reduced and non-reduced solution is minimized subject to the state and reduced-state equations. Our plan is to combine the DA method with this technique, now designed for elliptic PDEs only.

Concerning the unsteady formulation presented in Chapter 5 there are still many open issues which deserve further and deeper investigation. For the nonlinear problem we developed a DO iterative procedure based on the assimilation, at each time step, via solution of an optimization problem. This is limiting for two reasons: optimality in time is only local and the assumption of data availability at each time step is not feasible.

The first issue can be assessed exploiting different assimilation methods which are based on "global" optimization in time. In doing this we have to deal with the solution of the unsteady adjoint problem which may be highly computationally expensive as we already discussed in the introduction to Chapter 5. Additionally, we might also consider

an OD approach to be formulated in a way similar to the one presented in [38].

For the second issue, the generalization to sparse data in time can be managed by either interpolating the data in time or performing advancing steps between assimilation instants.

Furthermore, as we did for space discretization in the steady case, it is important to test the consistency and the sensitivity of the method with respect to the time step and for different time discretization schemes. In this work the choice of the BE method is dictated by its unconditional stability; an analysis of stability properties of the resulting assimilation scheme might allow the employment of more accurate and/or less expensive methods.

References

[1] B. EINARSSON. *Accuracy and reliability in scientific computing*. Society for Industrial Mathematics, 2005. 3

[2] R.W. WALTERS AND L. HUYSE. **Uncertainty analysis for fluid mechanics with applications**, 2002. 3

[3] L. FORMAGGIA, A. QUARTERONI, AND A. VENEZIANI, editors. *Cardiovascular Mathematics*. Springer, 2009. 3, 4, 15, 46, 72

[4] G.P. GALDI, R. RANNACHER, A.M. ROBERTSON, AND S. TUREK. *Hemodynamical Flows, Modeling, Analysis and Simulation*. Birkhauser, 2008. 3, 15

[5] C.A. TAYLOR, M.T. DRANEY, J.P. KU, D. PARKER, B.N. STEELE, K. WANG, AND C.K. ZARINS. **Predictive medicine: Computational techniques in therapeutic decision-making**. *Computer Aided Surgery*, **4**(5):231–247, 1999. 3, 4, 15

[6] L. GRINBERG, ANOR T., CHEEVER E., MARSDEN. J.P., AND G E KARNIADAKIS. **Simulation of the human intracranial arterial tree**. *Phil. Trans. R. Soc. A*, **367**:2371–2386, 2009. 3, 4

[7] A. QUARTERONI, L. FORMAGGIA, AND A. VENEZIANI. *Complex systems in Biomedicine*. Springer, 2006. 3, 4

[8] C. A. TAYLOR AND M.T. DRANEY. **Experimental and Computational Methods in Cardiovascular Fluid Mechanics**. *Ann Rev Fluid Mech*, **36**:197–231, 2004. 3, 4, 15

[9] C. A. TAYLOR, T. J. R. HUGHES, AND C. K. ZARINS. **Finite element modeling of blood flow in arteries**. *Comput. Methods Appl. Mech. Eng.*, **158**:155–196, 1998. 3, 15

[10] P.M. den Reijer, D. Sallee, P. van der Velden, E. Zaaijer, W.J. Parks, S. Ramamurthy, T. Robbie, G. Donati C., Lamphier, R. Beekman, and M. Brummer. **Hemodynamic predictors of aortic dilatation in bicuspid aortic valve by velocity-encoded cardiovascular magnetic resonance**. *Journal of Cardiovascular Magnetic Resonance*, **12**(1):4, 2010. 4, 33, 104, 109, 131

[11] J.J. Heys, T.A. Manteuffel, S.F. McCormick, M. Milano, J. Westerdale, and M. Belohlavek. **Weighted least-squares finite elements based on particle imaging velocimetry data**. *Journal of Computational Physics*, **229**(1):107–118, 2010. 4, 15, 23, 30, 34

[12] J. Blum, F.X. Le Dimet, and I.M. Navon. *Data Assimilation for Geophysical Fluids*, **XIV** of *Handbook of numerical analysis*, chapter 9. Elsevier, 2005. 4, 5, 7

[13] B. Wang, X. Zou, and J. Zhu. **Data assimilation and its applications**. *Proceedings of the National Academy of Sciences of the United States of America*, **97**(21):11143–11144, October 2000. 6

[14] H. Panofsky. **Objective weather map analysis**. *Journal of Meteorology*, 1949. 6

[15] P. Bergthórsson and B. R. Döös. **Numerical objective weather map analysis**. *Tellus*, **7**:329–340, 1955. 6

[16] E. Kalnay. *Atmospheric Modeling, Data Assimilation and Predictability*. Cambridge University Press, 2003. 7

[17] E. M. Kalman. **A New Approach to Linear Filtering and Prediction Problems**. *Transactions of the ASME–Journal of Basic Engineering*, **82**(Series D):35–45, 1960. 7

[18] S. J. Julier and J. K. Uhlmann. **A New Extension of the Kalman Filter to Nonlinear Systems**. pages 182–193, 1997. 9

[19] S. Julier, J. Uhlmann, and H. Durrant-Whyte. **A new approach for filtering nonlinear systems**. pages 1628–1632, 1995. 9

[20] H. C. Davies and R. E. Turner. **Updating prediction models by dynamical relaxation: an examination of the technique**. *Quarterly Journal of the Royal Meteorological Society*, **103**(436):225–245, 1977. 9

[21] G. J. HALTINER AND R. T. WILLIAMS. **Numerical Prediction and Dynamic Meteorology**. 1980. 9

[22] X. ZOU, I. M. NAVON, AND F. X. LEDIMET. **An Optimal Nudging Data Assimilation Scheme Using Parameter Estimation**. *Quarterly Journal of the Royal Meteorological Society*, **118**:1163–1186, 1992. 10

[23] M. D. GUNZBURGER. *Perspectives in Flow Control and Optimization*. Society for Industrial Mathematics, December 2002. 11, 12, 13, 26, 62, 109, 110

[24] M.D. GUNZBURGER. **Sensitivities, adjoints and flow optimization**. *International Journal for Numerical Methods in Fluids*, **31**(1):53–78, 1999. 11

[25] M.D. GUNZBURGER, L.S. HOU, AND T.P. SVOBODNY. **Analysis and finite element approximation of optimal control problems for the stationary Navier-Stokes equations with Dirichlet controls**. *Modélisation mathématique et analyse numérique*, **25**(6):711–748, 1991. 11

[26] M.D. GUNZBURGER, S.L. HOU, AND T.P. SVOBODNY. **Analysis and finite element approximation of optimal control problems for the stationary Navier-Stokes equations with distributed and Neumann controls**. *Mathematics of Computation*, **57**(195):123–151, 1991. 11

[27] M. HINZE AND K. KUNISCH. **Second order methods for boundary control of the instationary Navier-Stokes system**. *ZAMM - Journal of Applied Mathematics and Mechanics*, **84**(3):171–187, 2004. 11

[28] M. HINZE. **Optimal and instantaneous control of the instationary Navier-Stokes equations**, 2000. 11

[29] S. SCOTT COLLIS, K. GHAYOUR, M. HEINKENSCHLOSS, M. ULBRICH, AND S. ULBRICH. **Optimal control of unsteady compressible viscous flows**. *International Journal for Numerical Methods in Fluids*, **40**(11):1401–1429, 2002. 11

[30] E. HABER, U. M. ASCHER, AND D. OLDENBURG. **On optimization techniques for solving nonlinear inverse problems**. *Inverse Problems*, **16**(5):1263–1280, 2000. 12, 13, 29, 36

[31] P. MOIREAU AND D. CHAPELLE. **Reduced-order Unscented Kalman Filtering with application to parameter identification in large-dimensional systems.** *ESAIM: Control, Optimisation and Calculus of Variations*, **17**:380–405, 2011. 15, 16

[32] C. BERTOGLIO, P. MOIREAU, AND J. F. GERBEAU. **Sequential parameter estimation for fluid-structure problems. Application to hemodynamics**. Technical Report 7657, 2011. 15, 17, 133

[33] R.P. DWIGHT. **Bayesian inference for data assimilation using Least-Squares Finite Element methods**. In *IOP Conference Series: Materials Science and Engineering*, **10**, page 012224. IOP Publishing, 2010. 15, 16

[34] P. B. BOCHEV. **Analysis of Least-Squares Finite Element Methods for the Navier-Stokes Equations**. *SIAM Journal on Numerical Analysis*, **34**(5):pp. 1817–1844, 1997. 15, 16

[35] P.B. BOCHEV AND M.D. GUNZBURGER. **Accuracy of least-squares methods for the Navier-Stokes equations**. *Computers & Fluids*, **22**(4-5):549–563, 1993. 15, 16

[36] M. D. GUNZBURGER AND P. B. BOCHEV. *Least-Squares Finite Element Methods*. Springer, 2009. 15, 16

[37] D. BEDIVAN AND G. J. FIX. **Least-Squares methods for optimal shape design problems**. *Computers and mathematics with applications*, **30**:17–25, 1995. 16

[38] M. PEREGO, A. VENEZIANI, AND C. VERGARA. **A Variational Approach for Estimating the Compliance of the Cardiovascular Tissue: An Inverse Fluid-Structure Interaction Problem**. **33**(3):1181–1211, 2011. 17, 135

[39] M. D'ELIA AND A. VENEZIANI. **Methods for assimilating blood velocity measures in hemodynamics simulations: Preliminary results**. *Procedia Computer Science*, **1**(1):1225–1233, May 2010. 18, 21, 25, 46

[40] M. D'ELIA, M. PEREGO, AND A. VENEZIANI. **A Variational Data Assimilation Procedure for the Incompressible Navier-Stokes Equations in Hemodynamics**. *Journal of Scientific Computing*, 2011. 18, 43

[41] M. D'ELIA AND A. VENEZIANI. **A Data Assimilation technique for including noisy measurements of the velocity field into Navier-Stokes simulations**. *Proceedings of V European Conference on Computational Fluid Dynamics, ECCOMAS*, June 2010. 18, 43

[42] A. QUARTERONI AND A. VALLI. *Numerical Approximation of Partial Differential Equations*. Springer-Verlag, 1994. 24, 27, 32, 47, 51, 59, 63, 66, 122

[43] A. QUARTERONI. *Numerical Models for Differential Problems*. Modeling, Simulation and Applications. Springer, Heidelberg, DE, 2009. 24

[44] A. VENEZIANI AND C. VERGARA. **An approximate method for solving incompressible Navier-Stokes problem with flow rate conditions**. *Comp Meth Appl Mech Engr*, **196**(9-12):1685–1700, 2007. 25

[45] J. NOCEDAL AND S. WRIGHT. *Numerical Optimization*. Springer, April 2000. 29, 49, 65

[46] E. BURMAN AND P. HANSBO. **Edge stabilization for the generalized Stokes problem: A continuous interior penalty method**. *Computer Methods in Applied Mechanics and Engineering*, **195**(19-22):2393–2410, April 2006. 30

[47] A. QUARTERONI, R. SACCO, AND F. SALERI. *Numerical mathematics*. Springer, 2000. 33, 112

[48] J. G. HEYWOOD, R. RANNACHER, AND S. TUREK. **Artificial boundaries and flux pressure conditions for the incompressible Navier-Stokes equations**. *International Journal for Numerical Methods in Fluids*, **22**(5):325–352, 1996. 46

[49] A. VENEZIANI. *Mathematical and numerical modeling of blood flow problems*. PhD thesis, Politecnico di Milano, 1998. 46

[50] P. C. HANSEN. *Rank-deficient and discrete ill-posed problems: numerical aspects of linear inversion*. Society for Industrial and Applied Mathematics, Philadelphia, PA, USA, 1998. 46, 47, 54, 56, 60, 61, 118

[51] T. J. RIVLIN. *An Introduction to the Approximation of Functions*. Courier Dover Publications, 2003. 55

[52] H. A. VAN DER VORST AND C. VUIK. **GMRESR: a family of nested GMRES methods**. *Numerical Linear Algebra with Applications*, **1**(4):369–386, 1994. 56, 94

[53] C. VUIK. **New insights in GMRES-like methods with variable preconditioners**. *J. Comput. Appl. Math.*, **61**:189–204, July 1995. 56, 94

[54] V. SIMONCINI AND D. B. SZYLD. **Theory of Inexact Krylov Subspace Methods and Applications to Scientific Computing**. *SIAM Journal on Scientific Computing*, **25**:454–477, 2003. 56

[55] X. DU, E. HABER, M. KARAMPATAKI, AND D. B. SZYLD. **Varying Iteration Accuracy Using Inexact Conjugate Gradients in Control Problems governed by PDE's**. Technical Report 08-06-27, Department of Mathematics, Temple University, JUN 2008. 56

[56] D. KAY, D. LOGHIN, AND A. WATHEN. **A Preconditioner for the Steady-State Navier–Stokes Equations**. *SIAM J. Sci. Comput.*, **24**:237–256, January 2002. 57, 94

[57] D. SILVESTER, H. ELMAN, D. KAY, AND A. WATHEN. **Efficient preconditioning of the linearized Navier-Stokes equations for incompressible flow**. *Journal of Computational and Applied Mathematics*, **128**(1-2):261 – 279, 2001. 57, 94

[58] H. C. ELMAN, D. J. SILVESTER, AND A. J. WATHEN. *Finite Elements and Fast Iterative Solvers: With Applications in Incompressible Fluid Dynamics*. Oxford Science Publications, 2005. 57, 58, 133

[59] J. L. LIONS. **On the controllability of distributed systems**. *PNAS*, **94**:4828–4835, 1997. 62

[60] A. VENEZIANI AND C. VERGARA. **An approximate method for solving incompressible Navier-Stokes problems with flow rate conditions**. *Computer Methods in Applied Mechanics and Engineering*, **196**(9-12):1685 – 1700, 2007. 63, 76

[61] M. D'ELIA AND A. VENEZIANI. **Uncertainty quantification for data assimilation in hemodynamics**. In preparation, 2011. 79

[62] R. A. JOHNSON AND D. W. WICHERN. *Applied multivariate statistical analysis*. Prentice-Hall, Inc., Upper Saddle River, NJ, USA, 1988. 81, 83

[63] J. KAIPIO AND E. SOMERSALO. *Statistical and Computational Inverse Problems*. Springer, 2005. 83, 84, 85, 89, 92

[64] R. P. CHRISTIAN. *The Bayesian Choice: From Decision-Theoretic Foundations to Computational Implementation*. Springer Texts in Statistics. Springer Verlag, New York, 2nd edition, June 2007. 88

[65] J. R. WOMERSLEY. **Method for the calculation of velocity, rate of flow and viscous drag in arteries when the pressure gradient is known.** *The Journal of physiology*, **127**(3):553–563, March 1955. 125

[66] M. BENZI, G. H. GOLUB, AND J. LIESEN. **Numerical solution of saddle point problems**. *Acta Numerica*, **14**:1–137, 2005. 133

[67] M. BENZI, M. A. OLSHANSKII, AND Z. WANG. **Modified augmented Lagrangian preconditioners for the incompressible Navier-Stokes equations**. *International Journal for Numerical Methods in Fluids*, **66**(4):486–508, 2011. 133

[68] A. GAUTHIER, F. SALERI, AND A. VENEZIANI. **A fast preconditioner for the incompressible Navier–Stokes Equations**. *Computing and Visualization in Science*, **6**(2):105–112, 2004. 133

[69] A. QUARTERONI, F. SALERI, AND A. VENEZIANI. **Analysis of the Yosida method for the incompressible Navier-Stokes equations* 1**. *Journal des Mathématiques Pures et Appliqués*, **78**(5):473–503, 1999. 133

[70] F. SALERI AND A. VENEZIANI. **Pressure correction algebraic splitting methods for the incompressible Navier-Stokes equations**. *SIAM journal on numerical analysis*, **43**(1):174–194, 2006. 133

[71] A. VENEZIANI. **Block factorized preconditioners for high-order accurate in time approximation of the Navier-Stokes equations**. *Numerical Methods for Partial Differential Equations*, **19**(4):487–510, 2003. 133

[72] J CAHOUET AND J. P. CHABARD. **Some fast 3D finite element solvers for the generalized Stokes problem**. *International Journal for Numerical Methods in Fluids*, 1988. 133

[73] M. RATHINAM AND L. R. PETZOLD. **A New Look at Proper Orthogonal Decomposition**. *SIAM Journal on Numerical Analysis*, **41**(5):pp. 1893–1925, 2004. 134

[74] K. WILLCOX AND J. PERAIRE. **Balanced model reduction via the proper orthogonal decomposition**. *AIAA Journal*, pages 2323–2330, 2002. 134

[75] A. T. PATERA AND G. ROZZA. *Reduced Basis Approximation and A Posteriori Error Estimation for Parametrized Partial Differential Equations*. MIT-Pappalardo Graduate Monographs in Mechanical Engineering. MIT, Massachusetts Institute of Technology, Cambridge, MA, US, 2007. 134

[76] J. S. PETERSON. **The reduced basis method for incompressible viscous flow calculations**. *SIAM J. Sci. Stat. Comput.*, **10**:777–786, July 1989. 134

[77] G. ROZZA AND K. VEROY. **On the stability of the reduced basis method for Stokes equations in parametrized domains**. *Computer Methods in Applied Mechanics and Engineering*, **196**(7):1244 – 1260, 2007. 134

[78] K. KUNISCH AND S. VOLKWEIN. **Galerkin Proper Orthogonal Decomposition Methods for a General Equation in Fluid Dynamics**. *SIAM Journal on Numerical Analysis*, **40**(2):pp. 492–515, 2003. 134

[79] S. S. RAVINDRAN. **A reduced-order approach for optimal control of fluids using proper orthogonal decomposition**. *International Journal for Numerical Methods in Fluids*, **34**(5):425–448, 2000. 134

[80] M. FAHL AND E. W. SACHS. **Reduced Order Modelling Approaches to PDE-Constrained Optimization Based on Proper Orthogonal Decomposition**. **30**:268–280, 2003. 134

[81] M. D'ELIA, E. HABER, AND L. HORESH. **Design of Proper Orthogonal Decomposition basis by means of nonlinear inversion**. In preparation, 2011. 134